De-novo design and characterization of peptides containing conformationally constrained α,β-dehydrophenylalanine residue

Thesis Submitted for the Award of the Degree of
Doctor of Philosophy
to
Jawaharlal Nehru University
New Delhi, India.

By

Aseem Mishra

Malaria Research Group
International Centre for Genetic Engineering and Biotechnology
New Delhi, India
2008

Certificate

This is to certify that the research work described in this thesis entitled "De-novo design and characterization of peptides containing conformationally constrained α,β- dehydrophenylalanine residue" has been carried out in the Malaria Research Group, International Centre for Genetic Engineering and Biotechnology, New Delhi, India. This work is original and no part has been submitted for the award of any other degree or diploma to any other university.

Prof. V. S. Chauhan
Guide and Head,
Malaria Research Group,
I.C.G.E.B.
New Delhi -110067
India.

Prof. V. S. Chauhan
Director,
I.C.G.E.B.
New Delhi -110067
India.

Declaration

I declare that the research work described in this thesis entitled "De-novo design and characterization of peptides containing conformationally constrained α,β- dehydrophenylalanine residue" has been carried out by me under the supervision of Prof.V.S.Chauhan, Head, Malaria Research Group, International Centre for Genetic Engineering and Biotechnology, New Delhi, India. This work is original and no part has been submitted for the award of any other degree or diploma to any other university.
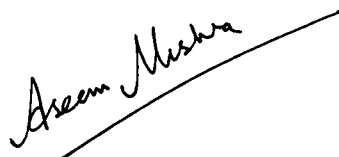
Aseem Mishra
Graduate Student,
Malaria Research Group,
I.C.G.E.B., New Delhi -110067
India

Acknowledgement

Acknowledgement

It is not customary to do so, but I would start by thanking my family for being the greatest support during my graduate study. In particular, it has been due to my elder brother ('Bhaina' as I call him) that I could achieve this goal. My mother and father have always been the guiding factors. The love and support of my younger brother, Raja, and my grandparents, 'Aja' and 'Aai' was a driving force. My sister, Palo, has been the most important lady in my life after my mother. She was the support that kept me going on even during the most difficult time of my life.

I have been fortunate to have Prof. Virander Singh Chauhan as my mentor. He has not just been a supervisor to my thesis but has also taught me the essence of doing science. He has always been enthusiastic and encouraging about science, despite his busy administrative responsibilities. Words can never describe my gratitude for him. I would just like to say that it's not every day that you meet someone like him in your life.

Dr. Atanu Basu, National Institute of Virology, Pune, has been equally important for me. He has been a great teacher and a friend. I cherish all the time I have spent in his lab doing electron microscopy. He is known in the scientific circle to be one of the best electron microscopist of the country and I have had the privilege of being his student. Mrs. Shobha has also been of great help during my work at NIV. She was always ready with reagents and coated grids whenever I needed them.

I worked for a year with Dr. R.Natesh learning protein structural biology. Very frankly, I spent some of the best time of my career under his mentorship. He is an excellent teacher, patient with his students and ever encouraging. I look forward to be working with him in future.

I also wish to thank Dr. B.L.V.Prasad, National Chemical Laboratory, Pune, for his support and guidance. He is a very nice

man with great knowledge and understanding. I also wish to thank Dr. S.P.Lochab, Dr. Ravi Kumar and Dr.Ambuj Tripathy, Inter University Accelarator Centre, New Delhi for supporting me to use facilities at IUAC. Special thanks to Dr. Ambuj Tripathy for all the AFM imaging I did in his lab. I would also like to thank Prof.H.B.Bohidhar for his suggestions on light scattering studies.

I also wish to thank my teachers, Prof. G.B.N.Chainy and Prof. S.P.Adhikary for training me during my post-graduation studies. And also Luna mam, Kajari mam, and Anita mam, who have not only been good teachers but also good friends. I can never forget all the fun-time the students used to have with them. It's very rare that a student and a teacher share such a relationship. My sincere gratitude to Devaki mam and Benudhar sir for being great teachers. I also wish to thank all my school teachers. I have always strongly believed that good teachers shape a man's character. And I feel myself privileged to have always had best people as my teachers.

I would also thank Mr. Alok Sharma for being a great friend and a guide. I owe my knowledge on HPLC and spectrophotometers to him. He has been instrumental in reviving in me the love for machines. Mr. Joby John has also been of utmost help when machine would break down or we had to repair small gadgets in the lab.

I also wish to extend my gratitude to Richa, Prasad, Madhurima, Mayank, Pratibha, Rawat, and Murliji for helping me in various ways. Richa has always pampered me like a little brother. Madhurima has been an excellent person, always jovial and fun-loving.

The entire credit goes to Ajayji for my being able to finish my thesis early. He was there always with whatever help possible. Any work given to him was always done before asking him the second time. I am not exaggerating, but he is the only indispensible person in the lab. I can recall atleast 5 incidents when his technical expertise helped us save a lot of money and time. He has

repaired things when trained engineers failed. He has helped me a lot on both the fronts, professional as well as personal.

I have had two very important ladies whom I want to thank for all their love and support. Madhvi 'didi' as I call her has been the one who taught me everything I needed to learn. Jyoti, the little sister, who has also been my junior since my M.Sc. days, has had the maximal contribution to all the work I have done during my thesis. She has advanced the research in the group to levels none of us had imagined four years back. She has been a meticulous worker, an intelligent mind and above all good company. She has complemented me all through.

I am blessed to have Sumona as a friend, batchmate and as my soul mate. She was always there for me, even during times when I behaved very irrationally. More importantly I wish to thank her family and my 'would be' in-laws. 'Mamoni' and 'Baudi' have always been very sweet and caring. 'Dadamoni' was always there as an elder brother. And 'Aanu' for being a very good friend. 'Dida' was too very sweet and so was everyone else in her family. They have been a lot of support in difficult times and always a guiding factor.

I have always treasured the company of Sarika and Aparna. They have always been the 'best of friends', that's all that I can say for them. The company of Shaheena and Ashwani, brilliant students of my junior batch, was always enjoyable. Paresh, Akash, Shivani and Harshesh have also been excellent company. Infact, I re-lived my graduation days with them. Maryam has been a 'phenomemon' in the lab. And an enjoyable company too. Vaishnavi has also been a great junior and friend.

My seniors, Kannan, Mridul, Nurul, Dharmendra, Kartik, Moin and Dhiraj have been great people. Though they were 4 years senior to me and were on the verge of their thesis submission when I joined ICGEB, their company made me feel at home. They have been very good friends and have always helped me with their

valuable suggestions. Pradipto 'dada' and Shubhra 'baudi' have been like family.

Srikrishna has been my room-mate for the last one and half year. Though I had rarely interacted with him before that, he has since then become a really great friend. He has taken care of me as an elder brother all through. I must say, I have been fortunate to have his company. Shrawan joined ICGEB early this year has somehow become an integral part of my life. In a very short time, he has become one of my best friends. The friendship of Srikrishna and Shrawan are very dear to me. The love and guidance of Jiban 'bhaina' is also greatly treasured. He has been an ideal for me.

Jasmita has always been of great help with all her computational expertise. Yogavel has helped me on many occasions with all the diffraction experiments and structural computation studies. And of course, Dr. Amit Sharma for allowing me to use all his facilities without any hicupps.

I would like to present 'all' my batchmates with the biggest bouquet of thanks for making this period of my life memorable. I can never forget all the outings, tea-time gossips and get-togethers that we had together. And not to forget the 'Feb 14 cake-cutting' ceremonies, the fun-n-food village trip, and the movie 'Kaal'.

All other people, Pinky, Asrar, Krishna, Jagdish, Naveen, Ravi, Nidhi, Harshal, Indresh, Priyank, Praveen, Arun, Mudasir, Reshma, Urvashi, and all those who have helped me directly or indirectly during my journey. Among all, Praveen always made the lab feel alive with his energy and funny remarks. Arun, I am sure, would one day become a leading personality of the country. He has a rare mix of talent, intelligence, hard-work and most importantly humility. I wish him all the luck for his future. My friends, Shweta, Khirod, Anando, Bhumesh sir, Prerna, Pranjal, Vikas also deserves special thanks.

My friends from my graduation and post-graduation days, Amresh and his wife Rolly, Bighneshwar ('Amu' as we used to call him), Sakti and his family, my late friend Lt.Col. Sandeep Pradhan, Madhu, Gitanjali ('Lee'), Priyankar, Abhishek, Dhananjay, Umakant and Binay ('Binu bhai') deserve lot more thanks. I am privileged to still have my school-mates, Anubhuti, Rakshan, Sharad, Vishwas and Asuri Krishna, as my friends, though many of us haven't seen each other since the last 14 years. I would also like to thank Manjit Mishra for helping me get rid of the greatest human phobia - 'stage fright' and also teaching me to work as a team.

I do not have a dedication page in my thesis for the reason that I dedicate my thesis and my success to all these people.

Aseem Mishra

25th Dec'08

New Delhi

Table of Contents

Introduction

& Objectives

Proteins (derived from the greek word *'Proteios'*, that means *'first rank'*) are involved in virtually every biological process. Their functions range from catalysis of chemical reactions to maintenance of the electrochemical potential across cell membranes. They are synthesized on ribosomes as linear chains of amino acids in a specific order as dictated by the information encoded within the cellular DNA. The linear chain of proteins folds into unique native three dimensional structures that is characteristic for each protein and is strongly dependent on its linear sequence. The phenomenon of folding involves a multitude of complex molecular recognition that depends on the cooperative action of many relatively weak nonbonding interactions. As the number of possible conformations for a polypeptide chain is astronomically large, a systematic search for the native (lowest energy) structure would require an almost infinite length of time. However, in real terms, this never happens. Proteins fold into their native structure on relatively fast time-scales traversing a defined trajectory of events. This has been termed as the *'Levinthal's paradox'* and has been the central dogma of the complex problem of protein folding. Significant progress has been made, of late, towards solving this paradox and understanding the mechanism of folding. This has come about through advances in experimental strategies for following the folding reactions of proteins using state-of-the-art techniques and theoretical approaches that simulate the folding process with simplified models. However, biologically relevant proteins are generally large in size and hence not always amenable to thorough investigation. This has fuelled the design of small peptide fragments that can be successfully used as smaller model systems to address the larger problem of protein folding.

'De novo' design has, thus, emerged as an attractive approach for a systematic investigation of the structure-function relationship in proteins. It is a hierarchic approach towards the construction of novel mini proteins with predetermined three-dimensional structure and function. The process involves the design of a linear chain of peptide with the desired tertiary structures stabilized by hydrophobic, ionic and

hydrogen bonding interactions, placed at appropriate positions, to achieve a unique function.

De novo design has also been successfully applied to the study of peptides. In short, **'peptides'** are smaller fragments of proteins consisting of less than 30 residues. Thus, proteins could be considered as a number of covalently connected peptide sub-domains that although highly flexible and disordered, cooperatively assemble into a well-defined three-dimensional (3D) structure. Interestingly, proteins are constructed only from a limited number of secondary structure elements, such as strands, helices and turns, assembled using loosely structured loops and stabilized by tertiary and quaternary associations. These secondary structures act as loci for intermolecular, long range and non-covalent interactions to overcome the unfavorable conformational entropy associated folding to adopt a functional 3D structure. However, polypeptides composed of 30 amino acids or less generally adopt an ensemble of energetically similar conformations in aqueous solutions. However, for proper function the peptides should adopt only a specific three dimensional structure. Nature uses several such constraints such as incorporation of cyclic amino acid residues (proline), disulfide bonds, etc. Although the use of constraints could highly reduce the number of conformational degrees of freedom in a peptide, molecular motions would exist due to the inherent flexibility in the molecules. These motions may include librations around peptide bonds, rotations of side chains and more global conformational rearrangements. Peptide design, thus, has been a challenging task.

There have been a variety of strategies for protein and peptide design that have led to the structural characterization of mini-proteins comprising 40 residues or less with a compact folded structure. Most design strategies relied on information from the rich database of solved protein structures or the redesign of naturally occurring motifs in peptides and proteins. The strategies that have been commonly utilized are

the design of amphipathic molecules that aggregate into controlled assemblies by patterning of polar/non-polar residues, introduction of ligands for metal mediated assembly, introduction of disulfide bonds that permit covalent tethering of individual molecules and covalent assembly of polypeptide chains on a suitable template TASP.

A conceptually different approach has been the introduction of stereo-chemical control over protein folding. It is widely known that for folding, two requirements must be met by the linear chain of the protein or peptide: one thermodynamic and one kinetic. The thermodynamic requirement is that the molecules should adopt a unique folded conformation (the native state) which is stable under physiological conditions. The kinetic requirement is that the denatured polypeptide chain can fold into the native conformation within a reasonable time. But a small polypeptide chain could theoretically adopt many conformations. In model designed compounds, the process of folding can be facilitated by introduction of stereo-chemical control over peptide folding. This could be done by the incorporation of conformation-restricting residues for constructing stable structures. These essential basic modules could then be connected covalently to get the desired folding. This strategy of protein mimicry has been known as 'Meccano (or Lego) set' approach. Such a strategy dictates the use of amino acids with restricted access to conformational space such as α,β-**dehydrophenylalanine (ΔPhe),** α-aminoisobutyric acid (Aib), D-Pro, α,α-dialkylated glycines Deg (diethyl glycine), Dpg (dipropyl glycine), Dbg (dibutylglycine) and a variety of synthetically designed residues. Among all, ΔPhe has been subjected to an extensive characterization due to its unique molecular structure, optical properties that aid easy characterization and also the ease of chemical synthesis.

On the other side, there has been a considerable interest on organic molecule based assembling systems from the perspective of new generation biosensors, biocatalysts, novel materials, and more importantly as tunable and biocompatible drug delivery agents. Recent studies have generated a tremendous excitement especially in the

area of peptide based self-assembling systems, not only as novel, biocompatible nano-materials but also as models for investigation of processes like aggregation.

Thus, the principles of *de novo* peptide design that has been traditionally utilized for investigating structural preferences of peptide molecules, could very well be applied for the rational design of peptide based novel self-assembling systems.

Objective 1:

The primary focus of the thesis has been the **"design of small peptides (dipeptides) containing conformation constraining residue α,β-dehydrophenylalanine (ΔPhe) amino acid that could self-assemble into distinct nano-structures in an aqueous environment."**

Studies indicated that in dipeptides containing with the motif H-Xaa-ΔPhe-OH, the nature of the N-terminus residue (Xaa) affected the assembly behavior. For example, dipeptides with Xaa having no or small side-chain like Gly and Ala, respectively, did not self-assemble at the concentrations tested or the time-scale of the investigation. However, residues with larger hydrophobic side-chains resulted in self-assembly of the dipeptides into structures of varied morphologies. Interestingly, the dipeptide with Xaa as Phenylalanine (Phe), self-assembled into distinct nanotubes with average diameter of 27nm and length in microns. The nanotubes were stable to pH conditions and resisted proteolytic degradation. We also found that dipeptides with Xaa as Ser (-OH group) or Gln ($-CONH_2$) did not assemble. Of interest was the observation that charged amphiphilic dipeptides with Xaa as Glu (-COOH) or Lys ($-NH_2$) self-assembled into vesicular structures. The necessity of the aromaticity for self-assembly in the model dipeptide H-Phe-Phe-OH was also explored. This was done by selective substitution of Phe by Cyclohexylalanine (Cha) having a side-chain with a non-aromatic and saturated ring structure. As opposed to the proposed idea that homo aromatic dipeptides formed the fundamental units of self-assembly,

results suggested that residues containing non-aromatic ring structures could very well be used for generating peptide based self-assembling structures. From the above studies, a few design rules that dictated the phenomenon of self-assembly in dipeptides and the morphology of the resultant self-assembled structures could be elucidated.

Further, nano-structures generated from the self-assembly of dipeptides could entrap small drug molecules like amodiaquin, doxorubicin, mitoxantrone, vitamins, peptides and proteins to varying degrees. It was also observed that the morphology of the self-assembled vesicles changed depending on their ionization status occurring at the different pH conditions. The change in shape was also associated with the release of the entrapped drug making the dipeptide systems amenable for triggered drug release applications.

Objective 2:

The work in the thesis also aimed at "**investigating structural similarilties between the fibrils formed by a small aromatic dipeptide (Phe-ΔPhe) and generic amyloid fibrils.**"

The results suggested that the structure and fibriilization of the dipeptide, Phe-ΔPhe, mimicked the amyloids. The kinetic studies suggested a primarily heterogenous nucleation mediated fibrillization pathway. The effect of non-assembling dipeptides on the fibrillization of Phe-ΔPhe was also investigated. The results suggested that soluble dipeptide Ser-ΔPhe could exert potential anti-fibrillization activity against Phe-ΔPhe alongwith other peptide fragments derived from Aβ and hIAPP.

In brief, the thesis describes the self-assembly behavior of ΔPhe containing model peptides and their potential applications.

Chapter 1

Review of literature

1.1 Self-assembling peptides

Self-assembly has been broadly defined as the autonomous organization of components into patterns or structures without human intervention. Self-assembling processes are commonly observed throughout nature and involve components from the molecular (crystals) to the planetary (weather systems) scales. The structures in self-assembly are organized into higher levels of order and stabilized through many different kinds of interactions. The concepts of self-assembly have been used in many disciplines albeit with a different flavor and emphasis in each. There have been several reasons for interest in self-assembly [1, 2]. First, humans are attracted by the appearance of order from disorder. Second, components of living cells self-assemble, and thus, study of self-assembly would enable better understanding of life. The cell offers countless examples of functional self-assembly that stimulate the design of non-living systems. Third, self-assembly is one of the few practical strategies for generating ensembles of functional nanostructures. Fourthly, self-assembly is common to many dynamic, multi-component systems, from smart materials and self-healing structures to netted sensors and computer networks. Finally, the phenomenon of self-assembly connects the reductionist approach to complexity and emergence [3]. Despite a lot of interest and research, the field "self-assembly" has not been formalized as a subject. For this reason, the definition of the term has been highly elastic. Processes ranging from the non-covalent association of organic molecules in solution to the growth of semiconductor quantum dots on solid substrates have been called self-assembly. However, a process of generating higher order structures from pre-existing components (separate or distinct parts of a disordered structure), in a reversible and controlled fashion by appropriate design of the components is believed to be truly synonymous with "self-assembly"[18].

Self-assembly has been broadly classified into two kinds: static and dynamic. Static self-assembly (S) (Figure1- 1) involves systems that are at global or local equilibrium and do not dissipate energy [4, 5].

(a)
Hydrophilic
Single molecule
(β-strand conformation)
Hydrophobic
β-sheet tape

(b)
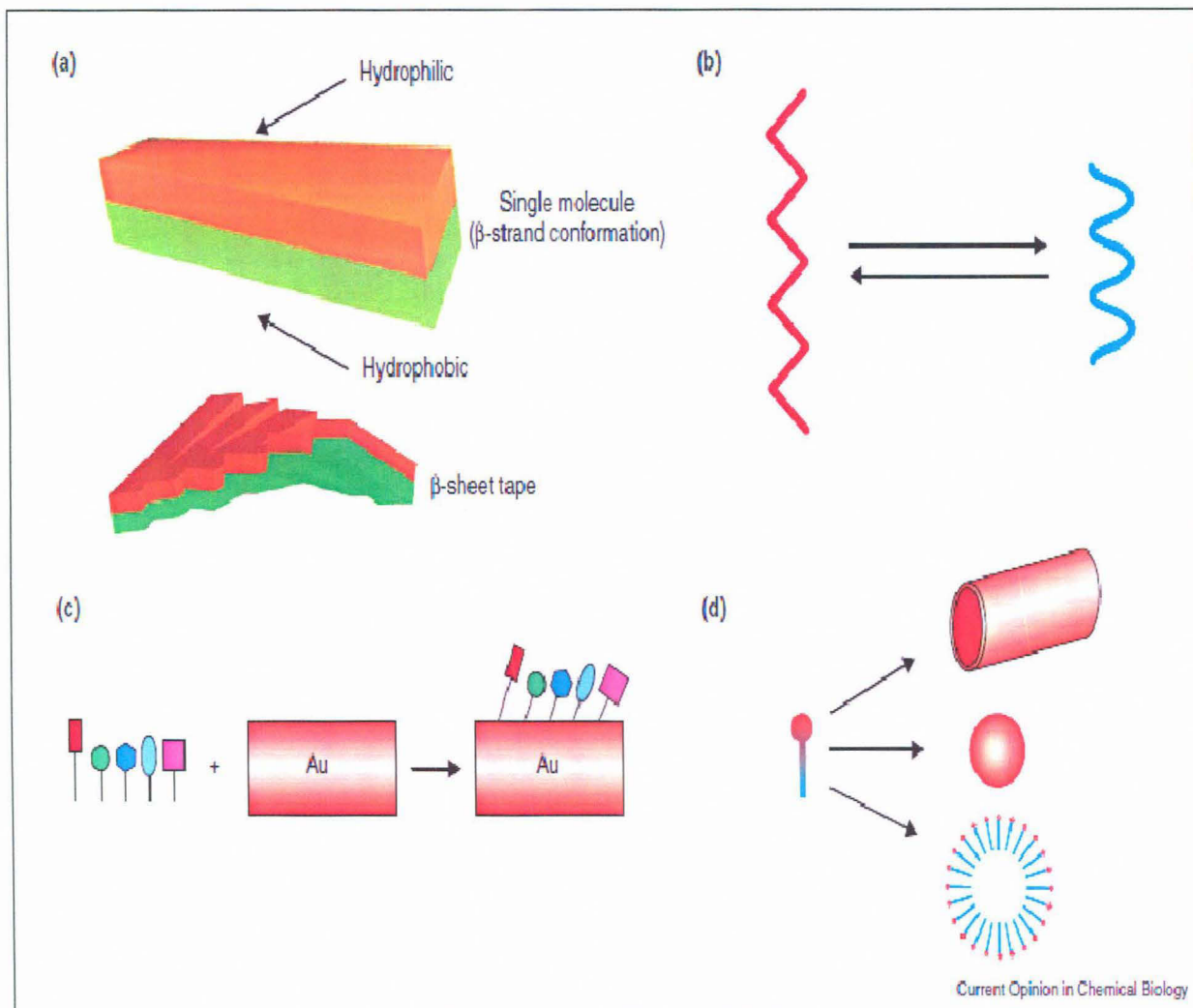
(c)
Au → Au

(d)

Current Opinion in Chemical Biology

Figure 1-1: Various types of self-assembling peptide systems. (a) Amphiphilic peptides in β-strand conformation self-assembling into twisted tapes. (b) Helical dipolar peptides undergoing a conformational change between α-helix and β-sheet like a molecular switch. (c) Surface-binding peptides forming mono-layers covalently bound to a surface. (d) Surfactant-like peptides can forming vesicles and nanotubes.

(*Image from Current Opinion in Chemical Biology 2002, 6:865–871)

In static self-assembly, formation of the ordered structure requires energy but once formed, it is stable. Most research in self-assembly has focused on this static type. In dynamic self-assembly (D) (Figure1- 2), structures or pattern formation occur only if

the system is dissipating energy. The patterns formed by competition between reaction and diffusion in oscillating chemical reactions [6, 7] are simple examples; biological cells are much more complex ones. There are two further variants of self-assembly. In templated self-assembly (T), interactions between the components and their environment determine the resulting structures. Crystallization on surfaces that determine the morphology of the crystal is one example [8-10]. The other form is the phenomenon governing biological self-assembly (B) and the resultant variety and complexity of the functions that it produces. The information coded in individual components in form of shape, surface properties, charge, polarizability, magnetic dipole and mass determine the interactions among them and reflect on the shape and properties of the self-assemblies. The study of dynamic self-assembly is in its infancy and not a lot is truly understood. Therefore, the design of components that organize themselves into desired patterns and functions is the key to applications of self-assembly and the also primary focus of the thesis.

1.2 Self-Assembly in Designed Systems

The difficulty of studying self-assembly in living cells (and in many nonliving systems) has been the impracticality of changing many of the parameters that determine the behavior of the system. Therefore, it has been difficult to test hypotheses relating structures and properties of these components and the aggregates that they form. Thus, it would be desirable to have available a set of self-assembling components in which the parameters could be changed easily for investigating the processes by which components self-assemble into defined geometrical structures [11, 12]. Towards this end, many self-assembling systems have already been designed and investigated. These include a myriad of inorganic systems like nanosphere, nanorods and nanotubes made from carbon, metals and/or semi-conductors [13-17]. But there has been a relatively recent fascination in organic systems that self-assembled into geometric structures for the simple reason that such structures could in some way mimic living systems.
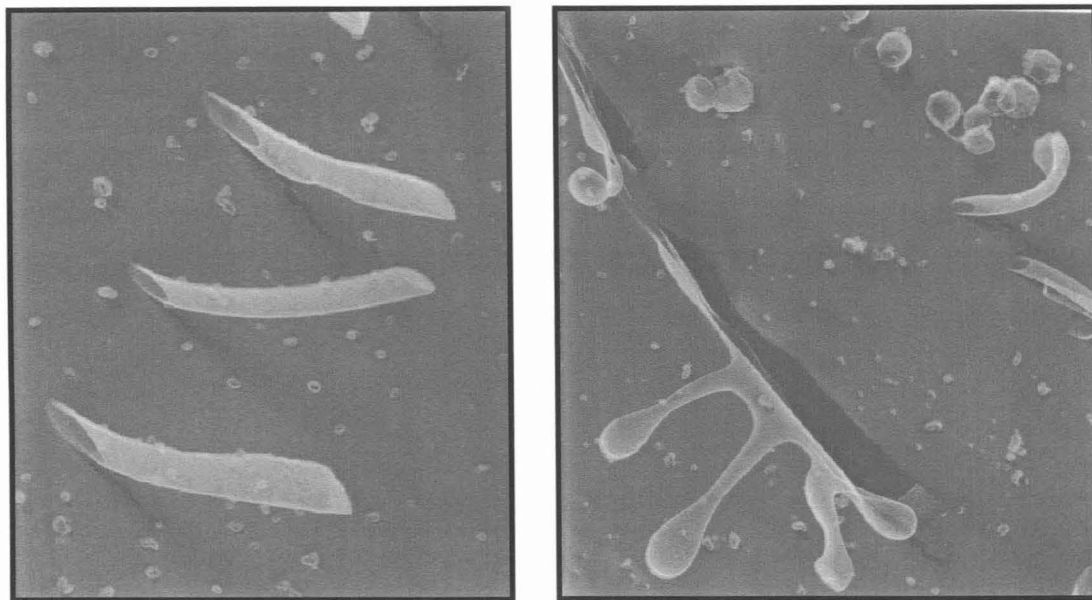
Figure 1-2: Transmission electron microscope images of nanotube and vesicle structures formed by V6D. The sample was flash frozen in liquid propane (–180°C) and surface-coated with a thin layer of platinum and carbon, yielding a replica. This technique preserved the structures formed in solution.

Organic polymers, carbohydrates, nucleic acids, proteins and also peptides have already been used for the design of self-assembling systems in order to investigate the phenomenon more closely and/or to use them for applications ranging from devices to delivery systems [18 and references therein]. However, their relative instability within living systems and their deleterious effects have limited their potential applications. However, a still newer focus has been on the development of small peptide based self-assembling systems. The interest in design of peptide based nanostructures started with the observation that many soluble cellular proteins could undergo self-assembly that led to the formation of well ordered tubular deposits as in neurodegenerative diseases such as Alzheimer's, Parkinson's and prions [19-21]. Though such assemblies exhibited disastrous consequences on normal cellular physiology, they have been shown to have potential applications as novel

nano-materials [19-21]. This led to a focussed and concentrated effort on the study of self-assembling peptides[22-24] to generate pH responsive hydrogels [25, 26], nanotubes from cyclic and linear peptides [27-29], fibres fron β-sheet forming peptides[30,31], and also biomimetic peptides that formed complexes with heme [32,33], metals and semiconducting materials [34, 35]. The results of these collective efforts has led to the emergence of the new field of molecular self-assembly for fabricating nanostructured materials.

1.3 Self-assembled nanostructures from amphiphilic peptides

Amphiphiles (amphis: both and philia: love) are broadly defined as chemical structures with a hydrophobic and a separated polar region. Such structures have been shown to self-assemble into distinct morphologies such as micelles, vesicles or tubules in aqueous environment [31, 36-38] with the assembly driven by hydrophobic effect that sequesters the nonpolar region of each polymer molecule away from water and thus, towards one another. The dimension and shape of the supramolecular structures formed from such assemblies depend on different factors, such as the geometry of the polar head group and the shape of each molecule [36-38]. In biology, the most common example of such amphiphilic molecule is the phospholipid which is the predominant constituent of the cell membrane that encapsulates and protects the cytoplasm from the environment. The formations of ordered and reproducible structures from amphiphilic molecules are common in biology. But, there has been a tremendous challenge for material scientists and has therefore stimulated the discovery and development of novel materials based on amphiphilic biomolecules (Figure1-1). Many simple self-assembling amphiphilic peptides have been designed that consisted exclusively of L-amino acids [31, 36-39]. One subset of such molecules are surfactant like peptides that consisted of a polar region made up of charged amino acids and a non-polar region made up of four or more consecutive hydrophobic amino-acids. The peptide V_6D (composed of six consecutive hydrophobic valine residues from the N-terminus followed by the negatively charged

aspartic acid) self-assembled into a mixture of tubular and vesicular structures in aqueous solution [37] (Figure1-2). A few large polypeptides with alternating segments of polar and non-polar regions as a diblock co-polymer have also been shown to self-assemble into pH responsive hydrogels [25, 26, 36]. Hydrophilic peptides linked to long alkyl chains could also self-assemble into tubular structures [40, 41]. The incorporation of a phosphorylated serine in the said peptide sequence facilitated bio-mineralization of hydroxy-apatitite, and thus generating an environment conducive for growth of osteoblasts. Subsequent functionalization of the peptide with cell adhesion motif RGD resulted in enhanced cell growth [41], of osteoblast. In another interesting design, a peptide with repeated segments of R-A-D-A (a positively charged amphiphilic segment followed by a negatively charged amphiphilic segment) and a related variant were used for the fabrication of hydrogels [36]. The matrix consisted of interwoven nano-fibers with diameter of 10-20nm and pore size of about 50-200nm (Figure1-3). The hydrogel matrix was used for culturing neuronal cells that formed active connections: an important step in neuronal repair. The hydrogel was also tested for its ability to anchor mammalian cells and support cell proliferation, differentiation and the direction of cell growth for potential applications in biosensor devices [36]. Bovine chondrocytes have been shown to express large amounts of collagen and glycosaminoglycans during their growth and differentiation within the peptide scaffold [42]. Besides the applications of amphiphilic peptides in generation of biocompatible materials, they have also served as scaffolds for metallization and fabrication of nanoscale devices [24, 28]. An interesting class of amphiphilic molecules is bola-amphiphiles. Unlike linear amphiphiles containing one polar and one hydrophobic region, bola-amphiphiles are characterized by two hydrophilic head groups connected by a hydrophobic linker. Depending on the head group functionality, they exhibit self-assembly by hydrogen bonding, hydrophobic effect and electrostatic interaction. A peptide bola-amphiphile, bis(N-aamido-glycylglycine)-1,7-heptane dicarboxylate, assembled into a nanotube via networked 3D hydrogen bonds between amide and carboxylic acid groups [43-45]. Such peptide nanotube have

also been functionalized with DNA, synthetic peptides, proteins, porphyrins, and azobenzenes, via hydrogen bonding [46-49] molecules onto the nanotube surfaces via non-covalent bonding [46]. Functionalization with antibodies enabled the nanotubes to smartly navigate to antigen-marked surfaces [50]. The amenability to functionalization also made the peptide nanotubes as templates for growing metals and semiconductors in controlled morphologies [51-54]. Importantly, the functionalization of bola-amphiphile based nanotubes had no effect on its structure and stability. Though amphiphilic peptides pose enormous opportunities for design of novel bio-inspired materials, there is a considerable lack of understanding of underlying principles that govern the phenomenon of self-assembly. The molecular structure of the nano-assemblies has been difficult to obtain because they were not amenable to high resolution X-ray diffraction nor solution NMR studies.
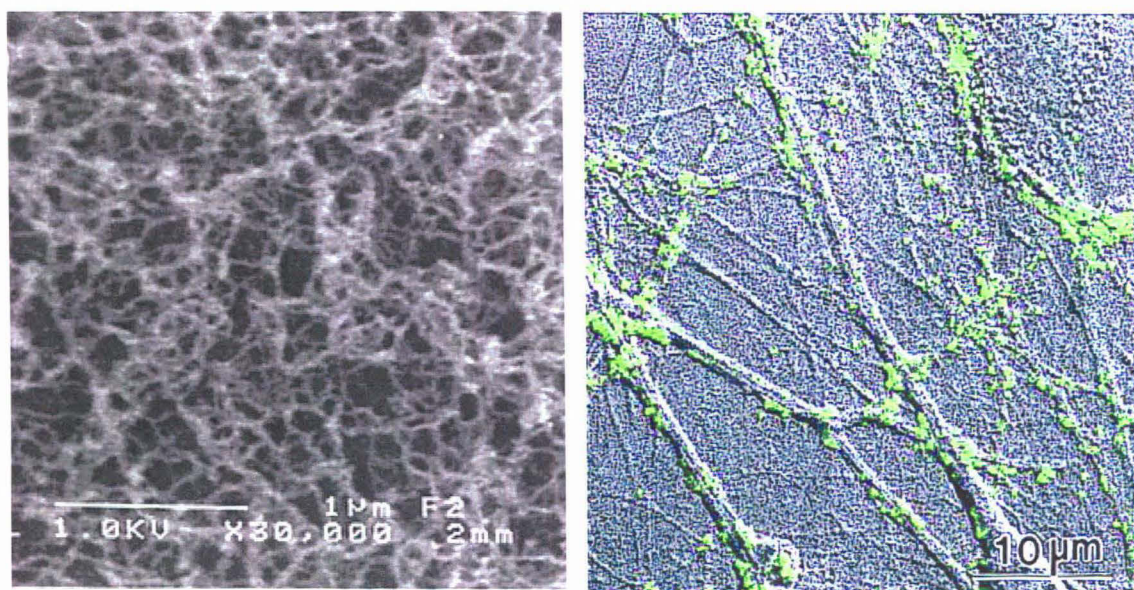

Figure 1-3: The SEM image of the self-asembled RADA peptide showing the fibrous network of structures (left). The matrix consist of interwoven nano-fibers with diameter of 10-20nm and pore size of about 50-200nm. The matrix was used for culturing neuronal cells (right) that exhibited extensive neurite growth with active axonal connections.

Theoretical models of self-assembled peptide structures have been investigated to some extent by molecular, semi-continuum or fully continuum models depending on the level of scalings involved [55, 57, 58]. Moreover, the precise mechanism of nucleation and growth of the nano-structures from the free monomer is still unclear [55-58], and thus design rules for directing the molecules to assemble into micelles, vesicles, fibers or tubes need to be further explored.

1.4 Nanotubes from rationally designed peptides

As discussed earlier, all forms of assembled structures could be obtained from amphiphilic peptide structures influenced by the design of the peptide or the condition of assembly. However, considerable advances have been made in the specific design of nanotubular structures with controllable features. There have been two basic strategies for the design of peptide based nanotubes. The first involved the use of 'linear peptide' sequences and the other utilized stacking of 'cyclic peptide' monomers for the generation of self assembled nanotubes.

There have been various approaches for the design of linear peptide based nanotubes (Figure 1-4). Peptide combinatorial library involving polar (His, Lys, Asn, Asp, Gln, Glu) and non-polar (Leu, Ile, Val, Phe, Met) amino acid residues have been used for the de-novo design of sequences that assembled into nanotubes with their dimension highly dependent on the peptide sequence [59]. In a different design, the peptide monomers contained 'sticky-end' residues [43, 60, 61] that could selectively bind to complementary residues based on their charge, polarity and hydrophobicity. The position of the sticky ends in the linear peptide monomers determined the morphology of the assembled structures. For example, when the stiff and straight peptide monomers (peptides ABABAB and CDCDCD in Figure 1-4b) incorporated the sticky end sequences, they assembled into straight peptide nanotubes. However, kinked and wavy peptide nanotubes could be obtained by mixing a small flexible peptide monomer (peptide CC in Figure1-4c) with a straight peptide monomer AA.
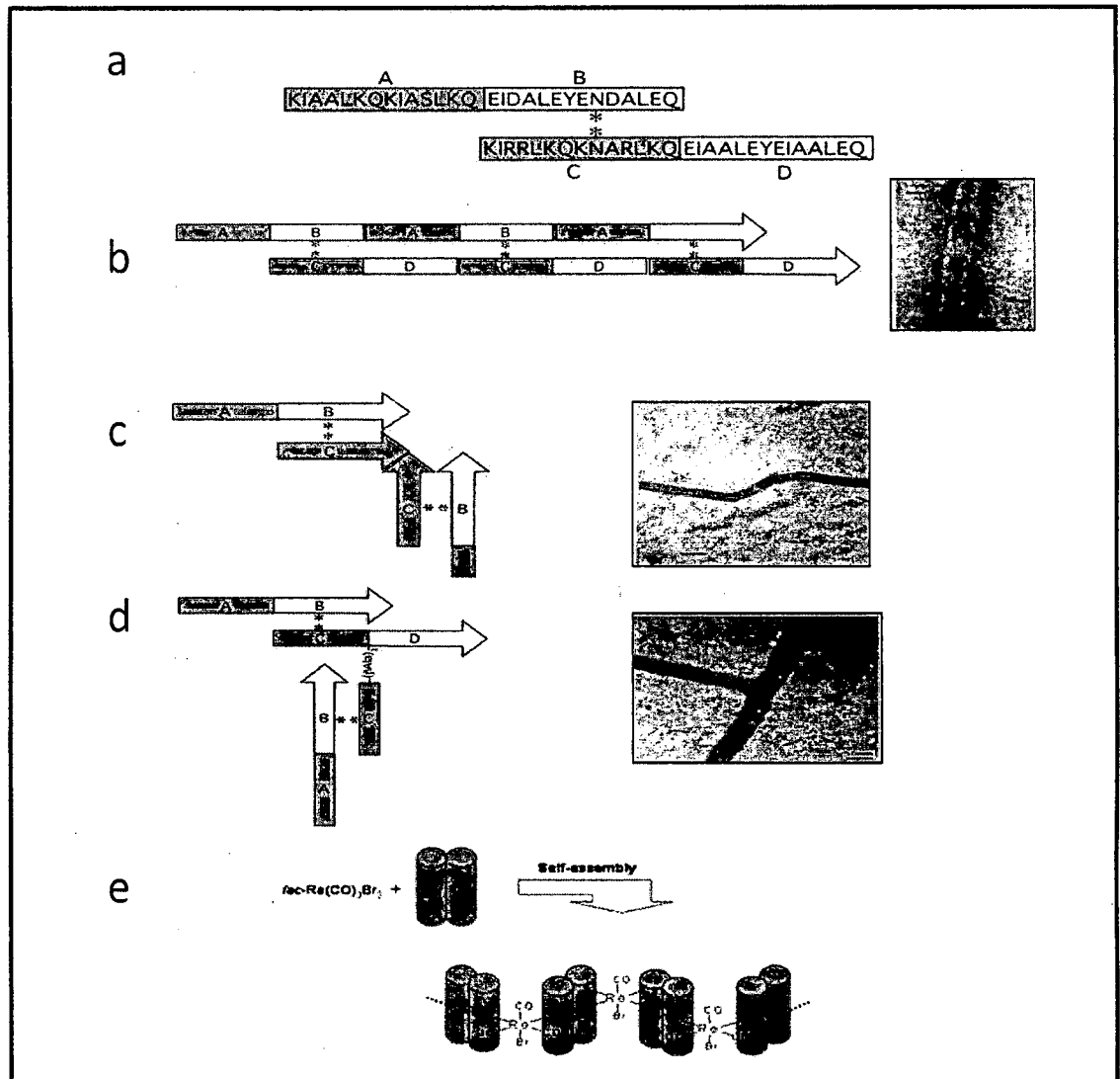
Figure 1-4: Schematic principle and TEM images of morphology controlled peptide nanotubes assemblies. (a) The sequences of standard self-assembling fibers. Block A complements block D, and block B complements block C. This dimerization creates the sticky ends in the nanotubes. b) Straight nanotubes formation, c) kinked nanotubes formation, and d) branched nanotubes formation. e) Peptide assemblies mediated via an octahedral rhenium complex between peptide monomers.

(*Image taken from **Advanced Materials 2005, 17:2037-2050**)

Instead when a T-shaped peptide monomer, CDC (Figure 1-4d), was mixed with the straight peptide monomer AB, they assembled into branched peptide nanotubes [60]. The advantage of this technique was that by placing the sticky ends at proper positions is the peptide monomer one could obtain a predictable nanotube structure. In another approach, linear peptides were assembled into nanotubes by utilization of highly directional metal-ligand interactions instead of sticky-end interactions [61]. In this case the designed polypeptide monomers bridged by Re ions causing them to assemble into nanotubes. This strategy offered a highly desirable feature i.e. precise control of the nanotube length by regulating the number of cross linking ions. However, nanotubes assembled from linear peptides generally not offer rationale control of features like diameter and surface properties of the tubes. The earliest propositions that peptide nanotubes could self-assemble by stacking cyclic peptides monomers came from Hassal (1972) [62] and DeSantis (1974) [67]. This led to an increasing focus on cyclic peptide based nanotubes that were inspired by natural design of cyclic antibiotics that created pores in the bacterial membrane (Figure1-5). Later, the assembly of nanotubes in many designed cyclic peptides was experimentally demonstrated [63-66]. Nanotubes could be assembled from monomers with alternating D,L-α-amino acids, β-amino acids, alternating α,β-amino acids, alternating α,γ-amino acids, and oligoureas. Heterocyclic alterations between α and ϵ-amino acids in a cyclic peptide was also demonstrated to form open ended, hollow tubular structure [67-70]. One of the characteristic features of cyclic peptide based nanotubes has been their precise diameter control, determined by chain length, side-chain size, peptide monomer bond angle, and stereochemistry of the amino acids [67-70]. The number and sequence of the amino acids defined the surface properties in-side and outside the nanotubes. This feature enabled the nanotubes to possess distinctive properties on the inner and outer surfaces. While the amino acid sequence of the cyclic peptide controlled the internal diameter of the peptide nanotubes, the control was limited to a narrow range of size.
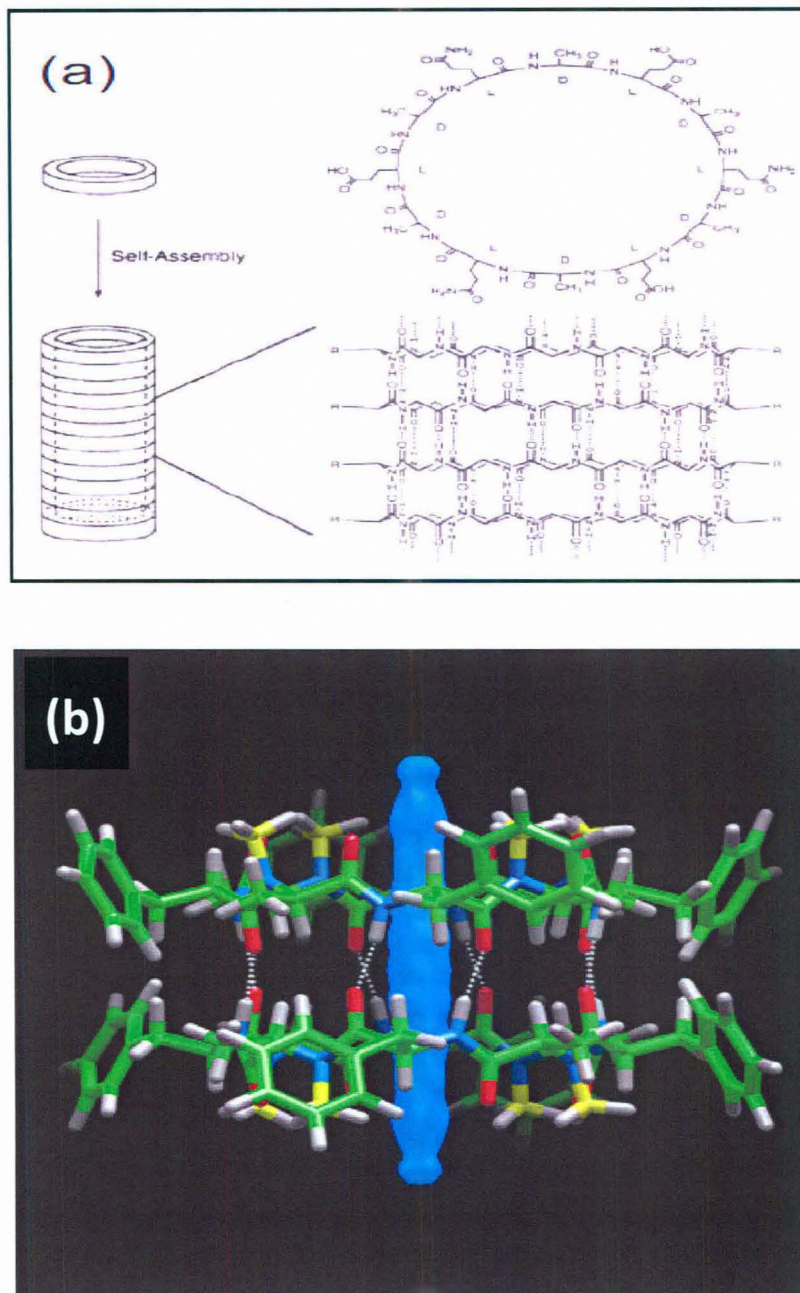
Figure 1-5: (a) Self-assembled nanotubes from cyclic peptides stabilized by back-bone hydrogen bonding interaction. (b) Crystal structure of cyclo-[(L-Phe-D-N-Me-Ala)4] including modelled partially ordered water centered in the cyclic peptide

(*Image taken from **Advanced Materials 2005, 17:2037-2050**)

For example, cyclic D,L-peptide monomers could be sequenced only between 9 and 13 Å in diameter to maintain a stable cyclic structure [70]. To produce large diameter peptide nanotubes, either the ring diameters of the cyclic peptide monomers should be larger or the nanotubes should be bundled [71]. Another important feature of the hydrogen bond-driven nanotubes self-assemblies was their sensitivity to external conditions, such as pH and solvent because the protonation states of peptide monomers influenced the intermolecular hydrogen bonds in self-assembled peptide structures [66-71]. Moreover, the optimization of experimental conditions to grow nanotubes from cyclic peptide monomers has been more straight-forward than the methods for obtaining nanotubes from linear peptide monomers [27, 66-71]. However, to achieve a wide range of peptide-nanotube sizes, it might be more advantageous to assemble them from linear peptide monomers [27].

Dendritic peptide monomers have also been reported to form peptide nanotubes [72,73] by self-assembly of the dendrons to form pseudo cyclic structures by hydrogen bonding of the narrow ends of the peptides and the spreading out of the dendritic parts. The cyclic part of the dendritic peptides stacked to form nanotubes via hydrogen bonding, as in previously described true cyclic peptides [72]. This strategy enabled the diameter control of the peptide nanotube (between 1 to 24Å) by appropriate choice of the amino acid composition. Nanotube assembly from dendritic peptides could also be controlled by pH and choice of complementary sequences [73].

All of the above described strategies utilized large polypeptide sequences with the use of either purely L- amino acids, D-amino acids or both. However, the associated expense and complexity of synthesis of large linear peptides, cyclic and dendritic structures has strongly limited the applicability of such peptides for practical use. Moroever, the proteolytic instability of large peptides have also been a major concern. Of late, it has been demonstrated that even very small peptides

(dipeptides) could self-assemble into distinct nanostructures in aqueous medium [74-106], thereby reducing the difficulty and cost of synthesis.

1.5 Dipeptides as self-assembling systems

Amyloid fibrils are believed to be the hallmark of diverse groups of diseases of unrelated origin, including Alzheimer's disease, type II diabetes, and prion diseases. Despite their formation by a diverse and structurally unrelated group of proteins, all amyloid fibrils share similar biophysical and structural properties. On the basis of both experiments, theory and the well-known role of aromatic stacking in the formation of chemical and biochemical supra-molecular structures [76, 77, 137-149], it has been suggested that the interaction between the aromatic residues of the core region play a crucial role in the process of molecular recognition and self-assembly resulting in the formation of amyloid fibrils. In this context, the self-assembly behavior of the diphenylalanine core motif of Aβ was investigated [76, 113, 125] and it was found that the short aromatic dipeptide with a free N- and C- terminus exhibited a rapid assembly into ordered semi-crystalline structures that appeared to be hollow tubular structures. The diameter of the tubes was in the range of 100nm with persistent length of over a micron. The structures were similar to nanotubes formed from larger linear and surfactant peptides (discussed in previous sections). However, the observed dimensions varied significantly from the cyclic peptide based nanotubes. Interestingly, the nanotube structures showed many properties of amyloids like congo-red staining and a β-sheet like molecular structure. Studies also showed that the tubes were extremely rigid with an averaged point stiffness of 160 N/m and an estimated Young's modulus of ~19 GPa, which was much higher than that of other biological nano-structures (Young's modulus of microtubules is on the order of 1 GPa) making them useful for applications ranging from drug-delivery to material sciences [85]. Later studies also proved that they could have novel electrochemical biosensing capabilities. Voltammetric and time-based amperometric techniques demonstrated the ability of the peptide nanotubes to improve the

electrochemical parameters of graphite electrodes [84]. Further investigation revealed that the amine- and carboxyl-modified dipeptides could also self-assemble into amyloid like structures. However, modification of the N-terminus with aromatic groups such as Fmoc- or Cbz- enhanced fibril formation. It was also shown that other aromatic structure containing dipeptides like di-D-1-napthylalanine and di-D-2-napthylalanine also assembled into tubular structures of 10nm and 50nm respectively. Two fluorinated diphenylalanine peptides, di-para-fluoro-Phe and di-pentafluoro-Phe, also assembled into tubular structures with different diameters and lengths. Substitution of fluorine with iodine in the halogenated dipeptide also resulted in tube formation. Interestingly, di-para-nitro-Phe and di-4-phenyl-Phe dipeptides assembled into spherical and thin symmetrical square plates, respectively. It was also observed that the aromatic dipeptide, diphenylglycine, self-assembled into well ordered closed-caged nanospheres [78].

There is very little information on the molecular structure of the dipeptides. Infra-red and circular dichroism spectroscopy of the different model dipeptides suggested that self-assembly did not require a specific kind of molecular conformation. Infra-red signatures of β-sheet, anti parallel β-sheet, α-helix and β-turns have been obtained for the different dipeptides [88]. Circular dichroism spectrum of the Phe-Phe dipeptide exhibited a positive band at 197nm and another at 220nm [87]. However, other dipeptides have not been subjected to conformation analysis using CD spectroscopy.

There has also been considerable investigation of structure and assembly pattern of dipeptides in solid-state [107-136]. The formation of hydrophilic nanotubes by supramolecular aggregation of small peptide molecules have been demonstrated in the crystals of dipeptides constructed of amino-acids with large hydrophobic side-chains [125]. The nanotubes had a hydrophilic inner surface with ability to entrap solvents. The monomers were arranged in a helical pattern in the nanotube and were stabilized by a network of head-to-tail hydrogen bonding interactions. The typical van der Waals' diameter of the channel ranged from a rectangular 2.5 x 6.0 Å

for Leu-Leu, Leu-Phe and Ile-Leu, to circular channels with diameter at 10 Å for Phe-Phe. All peptide molecules which formed this type of nanotube occurred in an unique conformation that placed both side chains on the same side of the plane defined by the peptide bond. The crystal structure of the dipeptide Ala-Val also exhibited a stable peptide nanotube system with the hydrophobic channels acting as supramolecular hosts for organic solvent molecules [122]. The pores could entrap small molecules like acetonitrile, methanol and acetone. Alcohols larger than methanol could also be trapped, but induced a change in shape and size of the pores. Another dipeptide Leu-Ala crystallized with the occurrence of cyclic water pentamers forming colums in the crystal [136]. Cocrystallized acetonitrile solvent molecules were located inside channels in the crystal structure of L-leucyl–L-serine which could be replaced by I_2 molecules with full retention of the peptide scaffold [113]. The monohydrates of the four polar dipeptides L-seryl-L-asparagine, L-seryl-L-tyrosine, L-tryptophanyl-L-serine and L-tyrosyl-L-tryptophan were also dominated by extensive hydrogen-bonding networks that include cocrystallized solvent water [107]. Template-directed supramolecular assembly of a new type of nanoporous peptide-based material has been observed in the crystal structure of L-Leu-L-Ile wherein the presence of D-Leu in the crystallization mixture resulted in the dipeptide to assemble with hydrophilic, water-filled channels with an irregular cross section of approximately 5.5 x 3.5 Å [108]. Another interesting arrangement has been observed in the crystal structure of L-Phenylalanyl-L-isoleucine wherein hydrophobic and hydrophilic layers are formed with channels of water molecules at the layer interface [115]. Thus, dipeptides could serve as a unique class of compounds for the design of novel biocompatible nanostructures.

1.6 De novo design

De novo design has been an attractive and fairly successful approach to investigate the structure-function relationship in peptides and proteins. However, the accessibility of the constituent amino-acids in small peptides to a relatively large

conformational space has made peptide design a challenging task. However, stereo-chemical control over peptide folding can be achieved by the incorporation of conformation restricting residues and aid construction of conformationally stable structures. This strategy involved the use of amino-acids with restricted access to conformational space such as, α,β-dehydrophenylalanine (ΔPhe), α-aminoisobutyric acid (Aib), D-Pro, α,α-dialkylated glycines Deg (diethyl glycine), Dpg (dipropyl glycine), Dbg (dibutylglycine) and a variety of synthetically designed residues [136-142]. Among all, ΔPhe has been subjected to extensive characterization due to its unique molecular structure, optical properties that aid easy characterization and also the ease of chemical synthesis.

As discussed in preceding sections, *de novo* design principles have also been applied repeatedly for investigating aggregation and self-assembling behavior in peptides. Many interesting and functional nano-structures have been generated using different design rules. However, the conformation restricting non-protein amino acids have never been used for the design of stable peptide based self-assemblies.

1.7 α, β-dehydrophenylalanine (ΔPhe)

α, β-unsaturated (or dehydro) amino acids have been frequently found in naturally occurring peptides of microbial origin [143-146] and in some proteins, e.g. histidine ammonia lyase from bacterial and mammalian sources and phenylalanine ammonia lyase from plants [147]. They are also constituents of a separate class of polycyclic peptide antibiotics, lantibiotics [148] such as nisin, epidermin, subtilin, etc. [147]. Nisin and subtilin contain both dehydroalanine (ΔAla) and dehydrobutyrine (ΔAbu). A recent study suggested that nisin, well known as a food preservative, latched to a molecule known as lipid-II on bacterial cell membrane and killed the host by punching a hole in the membrane [149]. Dehydroleucine (ΔLeu) and dehydrophenylalanine (ΔPhe) are present in albonoursin [150] while dehydrovaline (ΔVal) is found in penicillin [151] and cephalosporin [152]. Dehydrotryptophan (ΔTrp) is
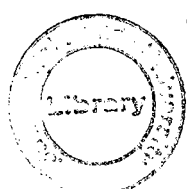
contained in neochinulins (growth inhibitor) [153] and dehydrophenylalanine is found in tentoxin (phytotoxic) [154]. In some cases, dehydroalanine residues form a part of the active site in the protein and lack of these residues result in certain diseases [155]. Peptides containing α, β-dehydroresidues are synthesized in the ribosome via a precursor protein followed by enzymatic modifications [146]. The presence of α,β-dehydro residues in peptides confer altered bioactivity as well as increased resistance to enzymatic degradation [156]. Dehydroresidues have been introduced in several bioactive sequences in order to obtain highly active agonist and antagonist analogs, and this modification has become one of the most promising methods to study structure-function relationships in biologically active peptides [157- 164]. α,β-dehydroamino acid analogs of some peptide hormones, dehydroangiotensin [165, 166], dehydrobradkynin [167] dehydrodermorphin [168-171], dehydrosomatostatin [172], dehydrosubstance P fragments [173], dehydroenkephalin [157-161,164] and dehydrogramicidin S have been synthesized and their biological activity reported.

α, β-dehydroamino acids are represented by the symbol Δ and are characterized by a double bond between Cα and Cβ atoms. The presence of three functional groups at position Cα of an unsaturated residue: the amino group, the carboxyl group, and the C=C double bond have considerable chemical, physicochemical and stereochemical consequences. The presence of a sp2 hybridized carbon atom in the backbone, the altered electronic distribution (conjugation) caused by the α-β π-system and the change in the side chain rotamer populations, all contribute to significantly to the behavior of a peptide chain. The conformational flexibility of both, the dehydropeptide backbone as well as the specific side chain of the dehydroresidues is restricted on account of the double bond between Cα and Cβ atoms. Although conjugation prefers extended conformation of the dehydroresidues, the bulkiness of the side-chain plays a deciding role in its overall conformation.

α, β-dehydrophenylalnaine (ΔPhe) (Figure1-6) is structural analog of the naturally occurring amino acid phenylalanine, with a double bond between the Cα and Cβ

atoms. There are two isomeric forms of ΔPhe, the Z-isomer (Δ^ZPhe) and the E-isomer (Δ^EPhe) [147]. In the former the C=O group occurs in trans- position with respect to the phenyl group while in the latter it is in the cis position. Most of the conformational studies have been carried out on Δ^ZPhe because of all chemical synthesis procedures result exclusively in the Δ^ZPhe. The values of average bond lengths and angles of Δ^ZPhe residue calculated from crystal structures have been presented in Table 1-1.

The shortening of N-Cα, Cα-C', Cβ-Cγ single bond lengths and elongation of C'=O double bond in ΔPhe occurs due to partial conjugation of Cα = Cβ double bond and the peptide bond. In the saturated Phe amino acid, the distances are, N-Cα=1.45Å, Cα-C'= 1.53Å, C'=O=1.20Å [174]. The steric clash between Cδ1H and NH of ΔPhe residue results in opening up of the bond angles Cα-Cβ-Cγ and N-Cα-Cβ which assume values of ~130° and 125°, respectively, thus deviating from the ideal trigonal value of 120° [136-137,175]. From simple model building studies it has been observed that the most favorable conformation of ΔPhe residues were (ϕ,ψ) ~ (60º, 30º), (-60º, -30º), (-60º, 150º) and (60º, -150º).

1.8 Theoretical studies on conformational properties of ΔPhe

Theoretical investigations on the conformation of several model dehydropeptides have been carried out, [176] including several diamides and triamides and have provided a characteristic conformer pattern that was determined by conjugation effects in the peptide backbone and steric effects of the Z and E substituents. The introduction of larger Z or E substituents compensated the conjugation influence to a certain amount and changes selectively the torsion angles ϕ and ψ [176, 177, 178, 180, 181, 182, 183]
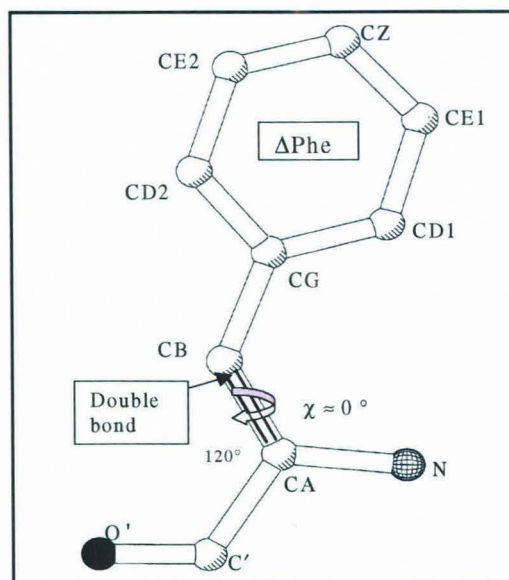
Figure 1-6: Schematic representation of the molecular structure of α,β-dehydrophenylalanine (ΔPhe)

Table 1-1: Table of geometrical parameters for ΔPhe

Bond lengths (Å)		Bond angles (°)	
$N_2\text{-}C_2{}^{\alpha}$	1.425	$C_1{}'\text{-}N_2\text{-}C_2{}^{\alpha}$	121.4
$C_2{}^{\alpha}\text{-}C_2{}'$	1.504	$N_2\text{-}C_2{}^{\alpha}\text{-}C_2{}'$	116.5
$C_2{}^{\alpha}\text{=}C_2{}^{\beta}$	1.329	$N_2\text{-}C_2{}^{\alpha}\text{-}C_2{}^{\beta}$	124.5
$C_2{}'\text{=}O_2$	1.237	$C_2{}^{\beta}\text{-}C_2{}^{\alpha}\text{-}C_2{}'$	118.4
$C^{\beta}\text{-}C^{\gamma}$	1.460	$C_2{}^{\alpha}\text{-}C_2{}^{\beta}\text{-}C_2{}^{\gamma}$	130.8

Theoretical conformational energy calculations have shown that there were six energy minima for ΔPhe [179], but all of them have not been observed experimentally. In experimentally determined structures of small peptide units, ΔPhe in the Yaa position favored the βII turn in agreement with the theoretical studies. Calculations for ΔZPhe in the Xaa position showed βII′ and βI turns were most stable and energetically equivalent. In larger peptide sequences, ΔZPhe has been frequently found as a part of 3_{10} helices. Figure1-7 depicts the Ramachandran plot for For-ΔZPhe-NH2 that was calculated using the modified CHARMm 23.1 force field. This two-dimensional (φ,ψ) plot results from a three-dimensional conformational analysis additionally considering the phenyl ring rotation angle, i.e. each (φ,ψ) grid point corresponded to the optimum χ2 torsion angle. There was a satisfactory agreement between theoretical and experimental values, especially the region around φ= -60° and ψ= -30°, which was frequently found in crystal structures of longer peptides with ΔZPhe.

1.9 Crystal and molecular structural studies

1.9.1 Crystal structure of ΔPhe containing small peptides

Approximately 49 crystal structures of peptides containing α, β-dehydrophenylalanine have been reported. The ΔPhe residue adopted a conformation corresponding to one of the three sets of φ, ψ torsion angles: i.e. −60°, 140°; 80°, 0°; -60°, -30° or their enantiomers [136, 137]. They were accommodated at both (i+1, i+2) positions of type I and type II β-turns in small peptides and helical conformation in larger peptides. In most small tripeptides, the ΔPhe residue was found to induce a β-turn structure, itself occupying the (i+2) position of the turn [184-189]. In these structures, the φ,ψ values of ΔPhe were near 80° and 0°, respectively, which were close to the values assigned to a type II β-turn (φi+1= -60°, ψi+1= 120°, φi+2= 80°, ψi+2 = 0°). The turn was usually stabilized by an intramolecular 1←4 hydrogen bond. In dipeptide derivatives containing a ΔPhe residue where 1←4

intramolecular hydrogen bond was not possible, the ΔPhe assumed φ,ψ angles in the

vicinity of −60° and 120°, respectively, typical of the torsion angles of the residue at
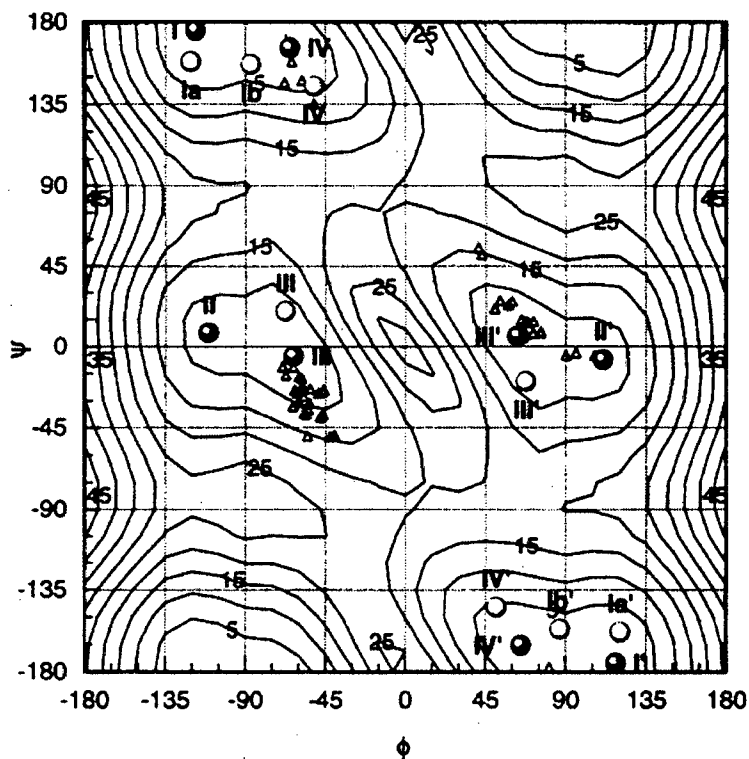
(i+1) position of type II β-turn [190, 191].

Figure 1-7: Force field (modified CHARMm 23.1) Ramachandran plot for For-Δ^{Z}Phe-NH$_2$ and conformers found at the molecular mechanics (black) and HF/6-31G* (white) levels and (φ, ψ) torsion angles determined for Δ^{Z}Phe residues in crystal structures (triangles).

The nature of the amino acid residues flanking a ΔPhe residue in a peptide has been observed to significantly influence its φ,ψ angles. A comparison of torsion angles revealed that the bulky phenylalanine residue exerted the maximum steric effect [185], while glycine with no side chain imposed minimum constraints [187] and represents a structure closest to an ideal type II β-turn. The branched β-carbon residues such as Val and Ile appeared to have strong conformational preferences.

When these amino acids flanked a ΔPhe residue, a distorted β-turn [186] or an S-shaped conformation [192,193] or even unfolded conformations [194] resulted.

In longer peptides (larger than tripeptides) containing ΔPhe residues, 3_{10} helical conformations were stabilized. In peptides with a single ΔPhe, Boc Leu-ΔPhe-Ala-Leu-OCH_3 [195] and Boc Leu-Phe-Ala-ΔPhe-Leu-OCH_3 [196], 3_{10}-helices were favored. In peptides containing two or more ΔPhe residues separated by one or two saturated amino acids, 3_{10} helical structures were preferred, usually with an unwinding at the C-terminus [197, 198]. The helices were well formed and intramolecular hydrogen bonds were also well aligned. Several peptides with alternating ΔPhe residues that stabilize a 3_{10}-helix, have been referred in the literature [199-202]. The structure of a hexapeptide, Boc-Val-ΔPhe-Leu-Ala-ΔPhe-Ala-OCH_3 [203] and the helical hairpin [204] solved in our laboratory further validated the proposition that two ΔPhe residues interspersed by two saturated residues favor the formation of a 3_{10}-helix. It seemed from these studies that in peptides containing $-\Delta$Phe-X-ΔPhe- or -ΔPhe-X-X-ΔPhe-motifs, there was a tendency to form 3_{10} helical structure, irrespective of the nature of residue X. A nonapeptide containing three ΔPhe residues, Boc-Val-ΔPhe-Phe-Ala-Phe-ΔPhe-Val-ΔPhe-Gly-OCH_3 stabilized three full turns of a right-handed 3_{10}-helix in the crystal structure (Figure1-8a) [205].

When ΔPhe residues were placed consecutively at (i+1) and (i+2) positions in tri and tetra peptides, they adopt positive and negative torsion angles alternately, thereby leading to an S-shaped structure. However, the torsion angle values of ΔPhe residue were centered around + 60°, + 30°, thus reducing the ϕ, ψ space to a single region [206, 207]. In the crystal structure of the peptide Boc-Ala-ΔPhe-ΔPhe-$NHCH_3$ [208] two independent molecules were found in the crystallographic unit, a right-handed and a left-handed 3_{10}-helix. However, a heptapeptide containing three Val residues interspersed by two consecutive ΔPhe stabilized a 3_{10}-helix [209]. A tetrapeptide with Ile at the C-terminus, Boc Val-ΔPhe-ΔPhe-Ile-OCH_3 and a pentapeptide with Leu at the N-terminus and Phe at C-terminus, Boc-Leu-ΔPhe-ΔPhe-Ala-Phe-$NHCH_3$ [210] gave

rise to a right handed 3_{10}-helical conformation suggesting that consecutive ΔPhe containing peptides possessing bulky L-residues may favor formation of a right-handed 3_{10}-helix.

Several interesting observations have been made with peptides containing three consecutive ΔPhe residues. Boc-Val-ΔPhe-ΔPhe-ΔPhe-Val-OCH$_3$ [211] and Boc-Ala-ΔPhe-ΔPhe-ΔPhe-NHCH$_3$ [212] showed a left-handed 3_{10}-helical conformation. In both cases however, the terminal L-amino acids were not a part of the helix and a type II β-bend is observed at the N-terminus. From model building studies, it can be seen that if a type II β-bend were followed by a helix, the helix would tend to be left-handed because of unfavorable steric interactions. Recent crystallographic studies on a decapeptide, Boc-L-Ala- (ΔPhe)$_4$-L-Ala- (ΔPhe)$_3$-Gly-OCH$_3$ [213], revealed the presence of two conformers (i) a slightly distorted right-handed 3_{10} helix, and (ii) a left-handed 3_{10} helix, per asymmetric unit.

The molecular structure of the pentapeptide Boc-Val-ΔPhe-Ala-Leu-Gly-OCH$_3$ exhibited a α-helical structure. This has been the only example of a ΔPhe containing peptide depicting a α-helix (Figure1-8c). Another pentapeptide, Boc-Pro-ΔPhe-Ala-ΔPhe-Ala-OCH3 [214] formed a flat β-bend ribbon conformation. The octapeptide Boc-Val-ΔPhe-Phe-Ala-Leu-Ala-ΔPhe-Leu-OH [215] was characterized by a right-handed 3_{10}-helix at the N-terminus and a π-turn at the C-terminus. The ΔPhe$_7$ residue in the sequence adopted a left-handed helical conformation and facilitated a 1←6 hydrogen bond (Figure1-8d). Another octapeptide Ac-ΔPhe-Val-ΔPhe-Phe-Ala-Val-ΔPhe-Gly-OMe [216] folded into (i) an N-terminal right-handed 3_{10}-helical pentapeptide segment, (ii) Val$_6$ assumed non-helical dihedral angles, $\phi = -123.81°$, ψ = 18.76° signaling helix termination and (iii) a C-terminal incipient left-handed 3_{10}-helix comprising ΔPhe$_7$-Gly$_8$-OCH$_3$(Figure1-8c). The structure also showed a water-mediated π-turn [217].

1.9.2 Occurrence of Super secondary structures in ΔPhe containing peptide

Dehydrophenylalanine zippers have been observed in the decapeptide Boc-Ala-(ΔPhe)$_4$-Ala- (ΔPhe)$_3$-Gly-OCH$_3$ [213] that crystallized with two conformers per asymmetric unit - a right-handed 3$_{10}$-helix and a left-handed 3$_{10}$ helix, both antiparallel to each other with a 15° angle between the two helical axes (Figure 1-8b). A remarkable feature of the structure was that the two antiparallel ambidextrous helices were held together by symmetrically placed aromatic backbone C-H⋯O interactions distributed all along the helical axis. The C-H (phenyl)⋯O (carbonyl) hydrogen bonds were observed between Cδ2(ΔPhe^2), Cδ2(ΔPhe^5), Cδ2(ΔPhe^8) of one helix to O8′(Y), O5′(Y), O2′(Y) of the other and vice versa. The hydrogen bonds represented an amazing regularity and provided maximum possible hydrogen bonding between the two helices. Further, ΔPhe with its planar aromatic side chain stacked against another ΔPhe from the adjacent shape- complement helix leading to two 'extended phenyl embrace' arrangements at the helix-helix interior. An α, β-dehydrophenylalanine containing 21-residue apolar peptide, Ac-Gly-ΔPhe-D-Ala-ΔPhe-ΔPhe-D-Ala-ΔPhe-ΔPhe-L-Ala-(Gly)$_4$-ΔPhe-L-Ala-L-Leu-ΔPhe-L-Ala-L-Leu-ΔPhe -L-Ala-NHCH3 [204] was designed to mimic the helical hairpin motif by using a simple geometric design strategy. The segment from ΔPhe^2 to ΔPhe^8 was characterized by left-handed 3$_{10}$-helix stabilized by appropriate intramolecular NH⋯O hydrogen bonds. The segment ΔPhe^8-L-Ala^9-Gly^{10}-Gly^{11} caused chain reversal by adopting a type I β-turn. The segment from Gly^{12} to Ala^{21} folded into a right-handed 3$_{10}$ helix, containing seven consecutive overlapping type III β-bends stabilized by appropriate 1←4 intramolecular NH...O hydrogen bonds. The protuberant ΔPhe side chains from the shape-complement helices exhibit parallel stacking: ΔPhe^8 stacked against ΔPhe^{14} and ΔPhe^5 against ΔPhe^{17}. This arrangement resulted in interactions between the two conjugated π systems, supported by C-H⋯O interactions providing a wedge into groove kind of arrangement. The above

structures highlight the important role of weak interactions (C-H···O, π-π stacking, NH···π) in the association of secondary structural elements.
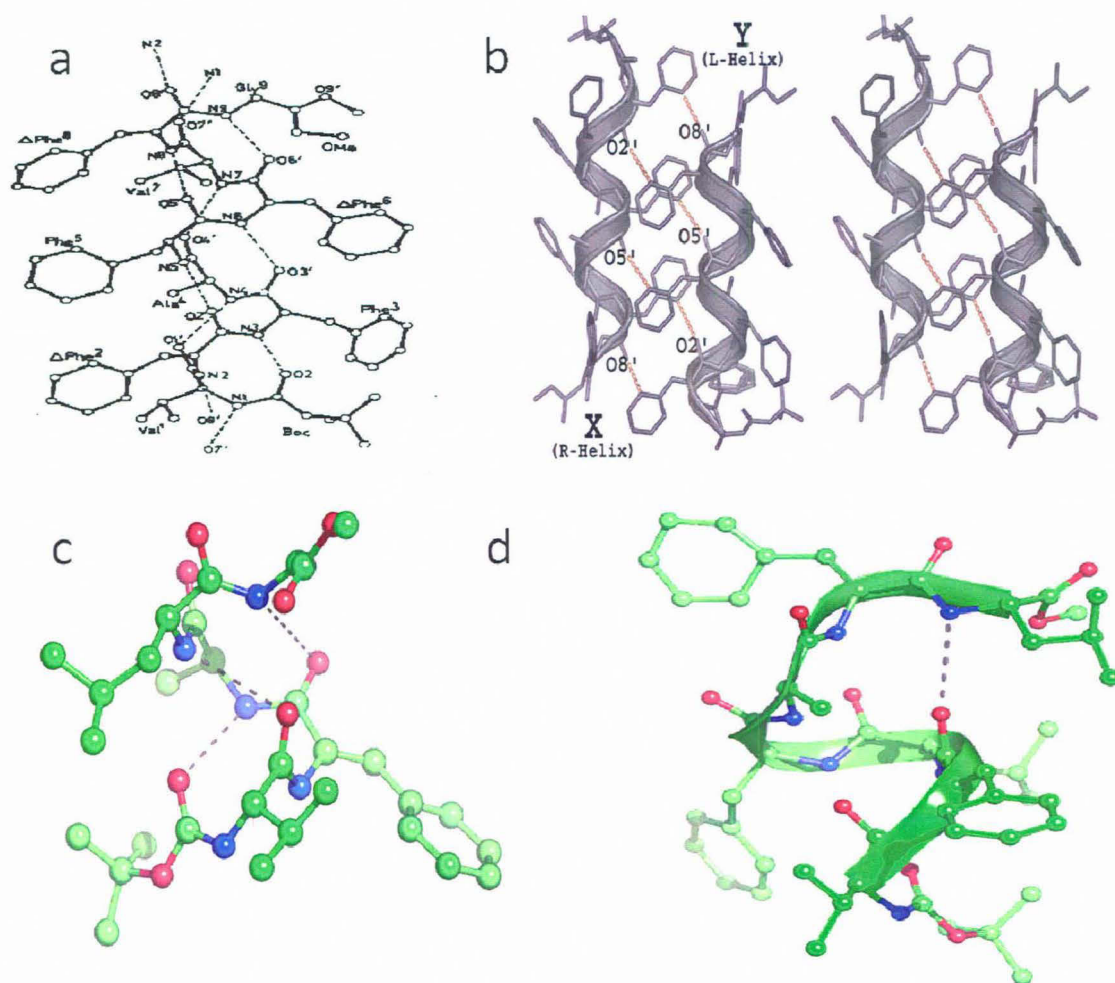

Figure 1-8: (a) A nonapeptide containing three ΔPhe residues, Boc-Val-ΔPhe-Phe-Ala-Phe-ΔPhe-Val-ΔPhe-Gly-OCH3 exhibiting a right-handed 3_{10}-helix in the crystal structure. (b) Stereo diagram depicting helix-helix recognition. The two molecules X and Y are antiparallel and interact with each other through interdigitation of ΔPhe side chains. (c) The molecular structure of the pentapeptide Boc-Val-ΔPhe-Ala-Leu-Gly-OCH$_3$ exhibiting a α-helical structure. (d) The octapeptide Boc-Val-ΔPhe-Phe-Ala-Leu-Ala-ΔPhe-Leu-OH [215] was characterized by a right-handed 310-helix at the N-terminus and a π-turn at the C-terminus. The ΔPhe7 residue in the sequence adopted a left-handed helical conformation and facilitated a 1←6 hydrogen bond.

1.10 Solution conformational studies

1.10.1 Absorption spectra

The absorption spectrum of peptides containing ΔPhe is characterized by an intense absorption band at about 280 nm that has been assigned to a charge-transfer electronic transition from the electron donating styryl groups to the electron-accepting carbonyl group. A weaker band occurs at 300 nm that corresponds to the benzene moeity. The chromophoric system of the ΔPhe residue is essentially the cinnamic moiety C_6H_5-C=C-C=O. The molar extinction coefficient of the peptides containing one ΔPhe residue is ~19,000 $mol^{-1}cm^{-1}$ [206] in methanol. The peptides containing two ΔPhe residues show an analogous band, centered on the same wavelength, but the intensity of the band is approximately twice that of the mono-unsaturated ones.

1.10.2 Circular dichroism (CD) studies

The ΔPhe containing peptides exhibit different CD profiles depending on the chain length, position and number of dehydroresidues. CD spectra of a few tripeptides containing ΔPhe at i+2 position exhibited broad negative bands centered at 280 nm, in correspondence with the main absorption maximum of the dehydro chromophore. On the basis of NMR and crystal structure of these peptides, this band has been attributed to type II β-bend [218]. The varying intensities of the CD bands were indicative of the varying propensity of the peptide to form a β-bend. The coexistence of folded and disordered conformers in solution is confirmed by the solvent dependence of the intensity of CD bands that generally decrease from apolar to polar solvents. Peptides containing two or more ΔPhe residues show a couplet of intense bands with opposite signs at 300 and 270 nm and a crossover point at ~285 nm. This CD pattern is typical of exciton splitting due to dipole-dipole interactions between the ΔPhe chromophores and is a strong indication that the two ΔPhe residues were placed in a mutual fixed disposition within the molecule, generally a

3_{10} helix [208, 219, 220]. The (-+) sign of the couplet corresponds to a 3_{10} helix with a right handed screw sense while (+-) couplet is assigned to the helix with a left handed screw sense. For a 'perfect' 3_{10}-helix containing three resides per turn, the transition moments would have a parallel arrangement along the helix and would not show any exciton couplet. However, all of them show prominent exciton couplets leading to the conclusion that the peptides contain non-integral number of residues per turn. Such 3_{10} helices have been reported in a number of crystal structures [221] and also evidenced theoretically.

CD has also been widely used to establish the screw sense of ΔPhe containing peptides in various solvents. For the decapeptide that assumed a 3_{10} conformation, CD studies exhibited a striking feature. A negative CD couplet, typical of a right-handed 3_{10} helix was observed in dichloromethane, hexafluoro-2-propanol and chloroform (Figure1-9). However, a positive CD couplet (+-) characteristic of the left-handed screw sense of the helix was observed in DMF and 80 % methanol. CD of the decapeptide in chloroform with increasing concentration of methanol is indicative of the equilibrium shifting towards the left-handed conformer. Addition of methanol gradually destabilizes the right-handed form and at a concentration 60:40 (chloroform: methanol), almost equal proportions of the two conformers were present. Similar effects of solvent dependence on helix handedness have also been reported by other workers [222]. The prominent band at 320 nm has been attributed to the weak electronic transition along the short axis of the benzene ring. This couplet, with a negative band at 290 nm, overlapping with the previous negative band, and a positive band at 320 nm or vice versa, might arise due to dipole-dipole interaction between transition moments polarized along the short axis of the benzene ring [213].

1.10.3. Conformation of ΔPhe containing peptides by NMR

Extensive 1D and 2D NMR studies have been carried out on ΔPhe containing peptides to elucidate their conformation. The β-turn conformation with ΔPhe as

$(i+2)^{th}$ residue of the turn in a number of tripeptides was initially derived from NMR and IR studies [223-227]. Studies were usually carried out in solvents like $CDCl_3$ and $(CD_3)_2SO$. The presence of intramolecularly hydrogen-bonded NH in these peptides has been identified using solvent and temperature dependent NMR studies. This was supported by IR studies carried out in solution at different concentrations of the peptide. In $(CD_3)_2SO$ solutions, solvation destabilized the β-turn conformation resulting in partially extended conformations.
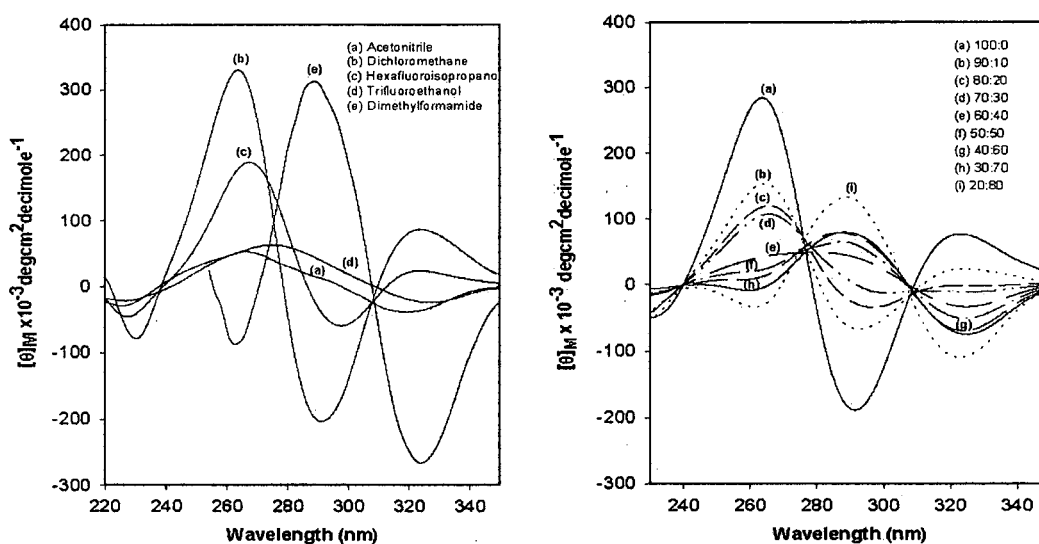
Figure 1-9: CD of the decapeptide depicting chloroform-methanol titrations. Ratios represent   concentration of chloroform to methanol

1H and 13C NMR experiments have been carried out on some cyclic pentapeptides [228, 229]. Results suggested that ΔPhe could be accommodated at β and γ-turn positions in these cyclic pentapeptides. In the peptide cyclo (Gly-Pro-ΔPhe-DAla-Pro), Gly-Pro-ΔPhe-DAla exhibited a type II β-turn with ΔPhe at (i+2) position and the fragment DAla-Pro-Gly forms a γ-turn. In cyclo (ΔPhe-Pro-Gly-DAla-Pro), the ΔPhe occupies the ith position of a β-turn and also position i+2 of a γ-turn. Yet another peptide cyclo (Gly-Gly-ΔPhe-DAla-Pro) contains only one proline and consequently had more potential conformations. However in this peptide ΔPhe was found to occur

in the i+1 position of the γ-turn. NMR studies on larger peptides containing ΔPhe at alternate positions revealed the presence of 3_{10} helical structures [230]. For example, Ac-ΔPhe-Ala-ΔPhe-NHCH$_3$ [201, 219], Ac-ΔPhe-Val-ΔPhe-NHCH$_3$ [200] and Boc-Gly-ΔPhe-Leu-ΔPhe-Ala-NHCH$_3$ [230] adopted 3_{10} helical structures in both solution and solid states. NOE studies on another peptide containing -ΔPhe-X-X-ΔPhe- moiety, Boc-Phe-ΔPhe-Val-Phe-ΔPhe-Val-OCH$_3$ suggested a significant solvent-dependent conformational variability with a 3_{10} helical conformation stabilized in CDCl$_3$. In (CD$_3$)$_2$SO, the peptide favored an extended conformation. Another peptide of this class Boc-Val-ΔPhe-Leu-Ala-ΔPhe-Ala-OCH$_3$, formed a 3_{10} helix in CDCl$_3$ but was largely extended in (CD$_3$)$_2$SO [203]. Detailed 2D NMR studies on the octapeptide Ac-ΔPhe-Val-ΔPhe-Phe-Ala-Val-ΔPhe-Gly-OCH$_3$ [196] showed a 3_{10} helical conformation at the N-terminus tetrapeptide fragment Ac-ΔPhe-Val-ΔPhe-Phe-OH. However, the NOEs at the C-terminal segment Ala-Val-ΔPhe-Gly-OH suggested a turn conformation. NMR data on a heptapeptide, Boc-Gly-ΔPhe-Ala-Phe-Leu-ΔPhe-Ala-NHCH$_3$ [231] and an octapeptide Boc-Val-ΔPhe-Phe-Ala-Leu-Ala-ΔPhe-Leu-OCH$_3$ [230] containing three and four spacer residues between ΔPhe, respectively, were found compatible with a succession of i←i+4 hydrogen bond suggesting an α-helical structure. These examples suggest that ΔPhe residues could be utilized for the generation of various kinds of conformations in a peptide.

1.11 Conclusion

In view of the unique conformational properties of ΔPhe and the recent focus on the design of nano-particles from small peptide, the work in the thesis explored the possibility of using ΔPhe as a model conformation restricting amino acid for the design of dipeptide based self-assembling nanostructures.

Chapter 2

Self-assembly of α,β-dehydrophenylalanine (ΔPhe) containing dipeptides into nanostructures.

2.1 Introduction

Molecular self-assembly, by which well-defined higher order structures result from spontaneous association of the components of the system by non-covalent forces, has emerged as an attractive tool for design and fabrication of nanostructures with novel properties [233, 234]. Characterization of supramolecular assemblies involving small biomolecules has also generated a lot of interest for they offer a large variety of variations through chemical modifications. Numerous reports of organic and inorganic tubular assemblies of carbon [235, 236], boron nitrite [237], zeolites [238, 239], and carbohydrate based nanotubes [240], have catapulted the research in this vast area of material science research. Of particular interest have been the peptide based nanostructures because they offer easy but many opportunities for chemical variations, and hence control, in designing molecular assemblies which have been successfully demonstrated to be good models for ion channels and membrane pores [241, 242, 243, 244]. Existence of pores filled with co-crystallized solvent molecules in the crystal structure of many dipeptides with two hydrophobic residues have been particularly well characterized and has opened possibilities for the development of such structures as biosensors, biocatalysts and specific molecular recognition platforms [245-248, 111, 113, 122, 125]. Recent demonstration of well-ordered and discrete peptide nanotubes by self-assembly of the diphenylalanine core recognition motif of Alzheimer's β-amyloid polypeptide has further highlighted the potential use of peptide-based structures for design of folded and self-organized structures [76, 87, 111].

In the following work, the self-assembly process in dipeptides incorporating a noncoded, achiral amino acid i.e. α,β-dehydrophenylalanine residue (ΔPhe) has been investigated. ΔPhe is an analog of the naturally occurring phenylalanine amino acid, but with a double bond between C^α and C^β atoms. Introduction of ΔPhe in peptide sequences has been known to induce conformational constraint, both in the peptide backbone as well as the side chain, and to provide the peptide with increased resistance to enzymatic degradation [156-161, 186, 187, 192-226, 230]. The studies describe the

synthesis, characterization and self-assembly of the dipeptide, Phe-ΔPhe, into distinct tubular structures which were stable at broad range of pH conditions and treatment of proteases. However, substitution of N-terminal Phe by other hydrophobic residues did not result in self-assembly of tubes under identical solvent conditions. The importance of aromatic interactions in the self-assembly of dipeptides into nanotubes was also investigated by the selective substitution of phenylalanine residue by a structurally analogous residue, cyclohexylalanine, that lacked aromaticity. The studies helped in deciphering few rules governing the rational design of dipeptide based nanostuctures.

2.2 Materials and Methods

2.2.1 Peptide synthesis: Dipeptides were synthesized as described below:

(a) **H-Phe-ΔPhe-OH**

Boc-Phe-OH (Novabiochem) (1.32g, 5mM) was dissolved in dry tetrahydrofuran (Sigma-Aldrich) and the resulting solution stirred in an ice-salt bath at -15°C. N-methyl morpholine (Sigma) (0.65ml, 5mM) was added to the solution followed by isobutyl chloro-formate (Sigma) (0.7ml, 5mM). After 10min, a pre-cooled aqueous solution of DL-threo-β-phenylserine (Sigma-Aldrich) (1g, 5.5mM) and sodium hydroxide (0.22g, 5.5mM) was added and mixture stirred overnight at room temperature. The reaction mixture was concentrated *in vacuo*, acidified with citric acid to pH 3.0 and extracted with ethyl acetate (Spectrochem) (3×20ml). The ethyl acetate layer was washed with water (2×15ml), with saturated sodium chloride (1×20ml), dried over anhydrous sodium sulfate and evaporated to yield Boc-Phe-DL-threo-β-phenylserine as an oily compound (2.2g, ~100%). The compound, Boc-Phe-DL-threo-β-phenylserine, was then mixed with anhydrous sodium acetate (0.53g, 6.5mM) in freshly distilled acetic anhydride (50ml) and stirred for 36hrs at room temperature. The thick

slurry obtained was poured over crushed ice and stirred till the oily suspension gave rise to a yellow colored solid. The precipitate was filtered, washed with 5% $NaHCO_3$, cold water and dried under vacuum. The resulting azalactone, Boc-Phe-ΔPhe-Azl (1.7g, 4.8mM), was dissolved in methanol, treated with 1.5 equivalents of 1N NaOH solution and stirred at room temperature for 3-4hrs. The mixture was then partially evaporated to remove methanol, acidified with citric acid to pH 3.0 and extracted with ethyl acetate (3×30ml), the combined ethyl acetate extract was washed with water (2×20ml), dried over anhydrous sodium sulphate and evaporated to yield Boc-Phe-ΔPhe-OH (1.8g, 4.5mM) as a white solid. Deprotection at the α-amino group was achieved by treatment with 98% formic acid (30ml) for 3hrs or 50% Trifluoro-acetic acid (TFA): Dichloromethane (DCM) for 1hr at room temperature. The reaction mixture was evaporated to dryness and the residue was precipitated with anhydrous diethyl ether (50ml). The resulting precipitate was filtered, washed several times with dry ether and subsequently lyophilized from 10% acetic acid-water (20ml) to yield the final compound H-Phe-ΔPhe-OH as white powder. Overall yield (1.2g, 82.6%); R_f = 0.18 ($CHCl_3$-MeOH, 9:1).

The peptide was purified on a preparative reverse phase C_{18} column (Deltapak, C_{18}, 15μ, I.D. 300×19mm) using acetonitrile-water linear gradient 5-45% acetonitrile (0.1%TFA)/water (0.1% TFA) at a flow rate of 4ml/min over 25min. The purified peptide was reinjected into an analytical reverse phase C_{18} column (Phenomenex, C18, 5μ, I.D. 250×4.6mm) using a acetonitrile-water linear gradient 5-45% acetonitrile (0.1%TFA)/water (0.1% TFA) at a flow rate of 1ml/min over 25min and was found to be 98% pure with retention time of 15min. The purified peptide was analyzed by mass spectroscopy (Applied Biosystems QStar (Q-TOF)) Observed Mass- 310.32 Da, Expected Mass- 310 Da.

(b) **H-Gly-ΔPhe-OH**

The peptide was synthesized as described above starting with Boc-Gly-OH. Overall yield (0.88g, 40%); R_f = 0.1(CHCl₃-MeOH, 9:1); The peptide was purified as described above. The purified peptide was reinjected into an analytical reverse phase C_{18} column (Phenomenex, C18, 5μ, I.D. 250×4.6mm) using a acetonitrile-water linear gradient 5-45% acetonitrile (0.1%TFA)/water (0.1% TFA) at a flow rate of 1ml/min over 25min and analyzed by mass spectroscopy. Retention Time- 9min; Observed Mass-220.3 Da, Expected Mass-220 Da.

(c) **H-Ala-ΔPhe-OH**

The peptide was synthesized as described above starting with Boc-Ala-OH. Overall yield (1.35g, 58%); R_f = 0.1(CHCl₃-MeOH, 9:1); The peptide was purified as described above. The purified peptide was reinjected into an analytical reverse phase C_{18} column (Phenomenex, C18, 5μ, I.D. 250×4.6mm) using a acetonitrile-water linear gradient 5-45% acetonitrile (0.1%TFA)/water (0.1% TFA) at a flow rate of 1ml/min over 25min and analyzed by mass spectroscopy. Retention Time- 11min; Observed Mass-234.6 Da, Expected Mass-234 Da.

(d) **H-Val-ΔPhe-OH**

The peptide was synthesized as described above starting with Boc-Val-OH. Overall yield (1.51g, 58%); R_f = 0.1(CHCl₃-MeOH, 9:1); The peptide was purified as described above. The purified peptide was reinjected into an analytical reverse phase C_{18} column (Phenomenex, C18, 5μ, I.D. 250×4.6mm) using a acetonitrile-water linear gradient 5-45% acetonitrile (0.1%TFA)/water (0.1% TFA) at a flow rate of 1ml/min over 25min and

analyzed by mass spectroscopy. Retention Time- 12.5min; Observed Mass-262.4 Da, Expected Mass-262 Da.

(e) H-Leu-ΔPhe-OH

The peptide was synthesized as described above starting with Boc-Leu-OH. Overall yield (1.07g, 39%); R_f = 0.1(CHCl$_3$-MeOH, 9:1); The peptide was purified as described above. The purified peptide was reinjected into an analytical reverse phase C$_{18}$ column (Phenomenex, C18, 5μ, I.D. 250×4.6mm) using a acetonitrile-water linear gradient 5-45% acetonitrile (0.1%TFA)/water (0.1% TFA) at a flow rate of 1ml/min over 25min and analyzed by mass spectroscopy. Retention Time- 14min; Observed Mass-276.23 Da, Expected Mass-276 Da.

(f) H-Ile-ΔPhe-OH

The peptide was synthesized as described above starting with Boc-Ile-OH. Overall yield (1.1g, 42%); R_f = 0.13(CHCl$_3$-MeOH, 9:1); The peptide was purified as described above. The purified peptide was reinjected into an analytical reverse phase C$_{18}$ column (Phenomenex, C18, 5μ, I.D. 250×4.6mm) using a acetonitrile-water linear gradient 5-45% acetonitrile (0.1%TFA)/water (0.1% TFA) at a flow rate of 1ml/min over 25min and analyzed by mass spectroscopy. Retention Time- 14min; Observed Mass-276.23 Da, Expected Mass-276 Da.

(g) H-Phe-Phe-OH

Boc-Phe-OH (Novabiochem) (1.32g, 5mM) was dissolved in dry tetrahydrofuran (Sigma-Aldrich) and the resulting solution stirred in an ice-salt bath at -15°C. N-methyl morpholine (Sigma) (0.65ml, 5mM) was added to the solution followed by isobutyl chloro-formate (Sigma) (0.7ml, 5mM). After 10min, a pre-cooled aqueous solution of H-Phe-OH (Sigma-Aldrich)

(0.9g, 5.5mM) and sodium hydroxide (0.22g, 5.5mM) was added and mixture stirred overnight at room temperature. The reaction mixture was concentrated *in vacuo*, acidified with citric acid to pH 3.0 and extracted with ethyl acetate (Spectrochem) (3×20ml). The ethyl acetate layer was washed with water (2×15ml), with saturated sodium chloride (1×20ml), dried over anhydrous sodium sulfate and evaporated to yield Boc-Phe-Phe-OH dipeptide (1.9g, ~95%). Deprotection at the α-amino group was achieved by treatment with 98% formic acid (30ml) for 3hrs or 50% Trifluoro-acetic acid (TFA): Dichloromethane (DCM) for 1hr at room temperature. The reaction mixture was evaporated to dryness and the residue was precipitated with anhydrous diethyl ether (50ml). The resulting precipitate was filtered, washed several times with dry ether and subsequently lyophilized from 10% acetic acid-water (20ml) to yield the final compound H-Phe-Phe-OH as white powder. Overall yield (1.38g, 89%); $R_f = 0.17$ ($CHCl_3$-MeOH, 9:1).

The peptide was purified on a preparative reverse phase C_{18} column (Deltapak, C_{18}, 15μ, I.D. 300×19mm) using acetonitrile-water linear gradient 5-45% acetonitrile (0.1%TFA)/water (0.1% TFA) at a flow rate of 4ml/min over 25min. The purified peptide was reinjected into an analytical reverse phase C_{18} column (Phenomenex, C18, 5μ, I.D. 250×4.6mm) using a acetonitrile-water linear gradient 5-45% acetonitrile (0.1%TFA)/water (0.1% TFA) at a flow rate of 1ml/min over 25min and was found to be 98% pure with retention time of 15min. The purified peptide was analyzed by mass spectroscopy (Applied Biosystems QStar (Q-TOF)) Observed Mass- 312.2 Da, Expected Mass- 312 Da.

(h) **H-Cha-Phe-OH**

The peptide was synthesized as described above starting with Boc-Cha-OH (1.5g, 5mM) and coupling it to sodiated H-Phe-OH (0.9g, 5.5mM). Overall

yield (1.1g, 35%); R_f = 0.17(CHCl$_3$-MeOH, 9:1); The peptide was purified as described above. The purified peptide was reinjected into an analytical reverse phase C$_{18}$ column (Phenomenex, C18, 5μ, I.D. 250×4.6mm) using a acetonitrile-water linear gradient 5-45% acetonitrile (0.1%TFA)/water (0.1% TFA) at a flow rate of 1ml/min over 25min and analyzed by mass spectroscopy. Retention Time- 19min; Observed Mass- 318.23 Da, Expected Mass-318 Da.

(i) **H-Cha-Cha-OH**

The peptide was synthesized as described above by Boc-Cha-OH (1.5g, 5mM) and coupling it to sodiated H-Cha-OH (0.94g, 5.5mM). Overall yield (1.2g, 39%); R_f = 0.19(CHCl$_3$-MeOH, 9:1); The peptide was purified as described above. The purified peptide was reinjected into an analytical reverse phase C$_{18}$ column (Phenomenex, C18, 5μ, I.D. 250×4.6mm) using a acetonitrile-water linear gradient 5-45% acetonitrile (0.1%TFA)/water (0.1% TFA) at a flow rate of 1ml/min over 25min and analyzed by mass spectroscopy. Retention Time- 25min; Observed Mass- 324.8 Da, Expected Mass-324 Da.

(j) **H-Phe-Cha-OH**

The peptide was synthesized as described above starting with Boc-Phe-OH (1.32g, 5mM) and coupling it to sodiated H-Cha-OH (0.94g, 5.5mM). Overall yield (1.3g, 42%); R_f = 0.17(CHCl$_3$-MeOH, 9:1); The peptide was purified as described above. The purified peptide was reinjected into an analytical reverse phase C$_{18}$ column (Phenomenex, C18, 5μ, I.D. 250×4.6mm) using a acetonitrile-water linear gradient 5-45% acetonitrile (0.1%TFA)/water (0.1% TFA) at a flow rate of 1ml/min over 25min and analyzed by mass spectroscopy. Retention Time- 19min; Observed Mass- 318.23 Da, Expected Mass- 318 Da.

2.2.2 Assembly of dipeptides: A stock solution of the dipeptides was prepared by dissolving 1 mg of the peptides in 50μl of 1,1,1,3,3,3-Hexafluoro-2-propanol (HFIP). In some cases mild sonication or heating was necessary to dissolve the peptides. Assembly was initiated by addition of double distilled water (1ml) to the stock solution. The samples were aged 24-48 hrs before experiments.

2.2.3 Scanning Electron Microscopy: The peptide stock solution was diluted to a final concentration range of 0.5mg/ml in ddH_2O and aged for one day. A 20μL of the aged sample was dried at room temperature on a microscopic glass cover slip followed by gold coating in a gold chamber for a minute. The images were taken using a JSM JEOL 6300 SEM.

2.2.4 Transmission Electron microscopy: The peptides stock solutions were diluted to final concentration of 1 mg/ml in ddH_2O. The grid was stained with 1% uranyl acetate in water. Samples were viewed with a Phillips Technai 120KV low dose electron microscope.

2.2.5 Circular Dichroism Spectrometry: All spectra were recorded on a JASCO-810 polarimeter equipped with a Peltier type thermostat and purged continuously with dry N_2 gas at 10 LPM during data acquisition. Data was collected in a quartz cuvette with path length of 1cm between 190nm to 300nm at scan speed of 25nm/min and response time of 16sec. The average of 50 scans was used for analysis of the spectrum. The CD spectra were converted to molar ellipticity. The concentration of the peptide was estimated by UV spectrometry with ε_{205} = 5167 per peptide bond [256]

2.2.6 Fourier Transform Infra Red Spectrometry: Spectra were collected on a Perkin Elmer Spectrum BX-II FTIR spectrometer. The assembled peptide samples. were spotted on a CaF_2 window and air-dried at 99% relative humidity. The samples were then rehydrated with D_2O for 30min before collecting the spectra. Each spectrum was average of 1000 collections at a resolution of $4cm^{-1}$ in the spectral range of

$1400cm^{-1}$ to $1900cm^{-1}$. The FTIR spectra were smoothed with smoothing length of 20. Subsequently, the second order derivative spectra were calculated with 13 data points. The spectral processing was done with *Spectrum*™ supplied by Perkin Elmer. To monitor the HD exchange, the tubes were collected by centrifugation and washed with water twice. After drying under vacuum, the tubes were rehydrated with D_2O and the spectra were collected at intervals of 1 min. Each spectrum was average of 10 collections at a resolution of $4cm^{-1}$ in the spectral range of $1400cm^{-1}$ to $1900cm^{-1}$. The area under the Amide II peak was plotted against time to observe the kinetics of deuteration.

2.2.7 X-ray crystallography: The peptide, Phe-ΔPhe, was crystallized by controlled slow evaporation of peptide in acetic acid-water mixture. Plate like crystals, suitable for x-ray diffraction, appeared within 3-4 days. X-ray diffraction data was collected on a Bruker AXS SMART APEX CCD diffractometer with MoKα radiation (α=0.71073Å). The structure solution was obtained using direct methods employed in SHELXS. The structure was refined to an R-factor of 3.74%. Acetic acid molecules were located in the electron density map. (CCDC 298818).

2.3 Results and Discussion

2.3.1 Self-assembly of diphenylalanine dipeptide

Alzheimer's disease has been characterized by heavy deposition of insoluble plaques composed primarily of Aβ$_{(1-42)}$. Fragmentation based approach to delineation of the core sequence responsible for aggregation resulted in the identification of a hepta peptide sequence, KLVFFAE, as the core determinant for fibrillogenesis. The fibril formed by the peptide showed all characteristics features of amyloid fibrils formed by Aβ$_{(1-42)}$. The peptide assembled into tubular structure with a β-sheet signature as evidenced from TEM and FTIR studies.

Interestingly, the central portion of this sequence, i.e. the diphenylalanine motif was observed to be sufficient for assembly into nanotubular structures as in amyloids

(Figure 2-1). This resulted in the first report of dipeptide based self assembled nanotubes. TEM images revealed a light shell and the dark center suggesting hollow tubular structures filled with the negative stain, uranyl acetate. Energy-dispersive x-ray analysis (EDX) indicated the presence of uranium within the assembled structures. The nano-tubular structures had average diameter between 100-150nm with length over microns (Figure 2-2). The nanotubes were highly ordered and without the usual branching and curving typical of amyloid fibrils. The tubular structures formed by the dipeptides also showed green-gold birefringence upon staining with Congo red dye, which was consistent with an organization that may be similar to that of amyloid structures. FTIR studies suggested a β-sheet structure due to the appearance of $1630cm^{-1}$ peak. However, the CD spectrum did not show any existence of β-sheet [87].
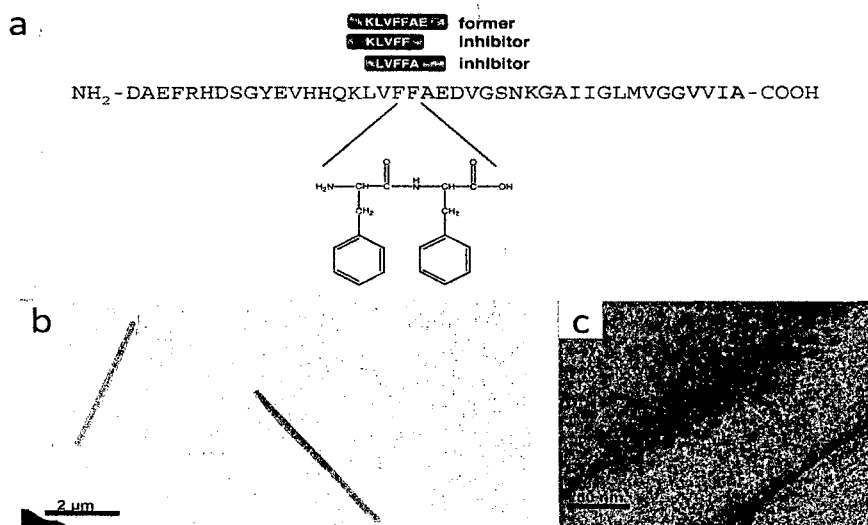
Figure 2-1: Self-assembly of well-ordered and elongated peptide nanotubes by a molecular recognition motif derived from the ß-amyloid polypeptide. (A) The central aromatic core of the ß-amyloid polypeptide is involved in the molecular recognition process that leads to the formation of amyloid fibrils. Various fragments of the core form amyloid fibrils or inhibit their formation. (B) TEM images of the negatively stained nanotubes formed by the diphenylalanine peptide. (C) HR-TEM images of negatively stained peptide nanotubes, visualized by field emission gun microscope.

(*Excerpted from *Science* 25 April 2003:Vol. 300. no. 5619, pp. 625 – 627)
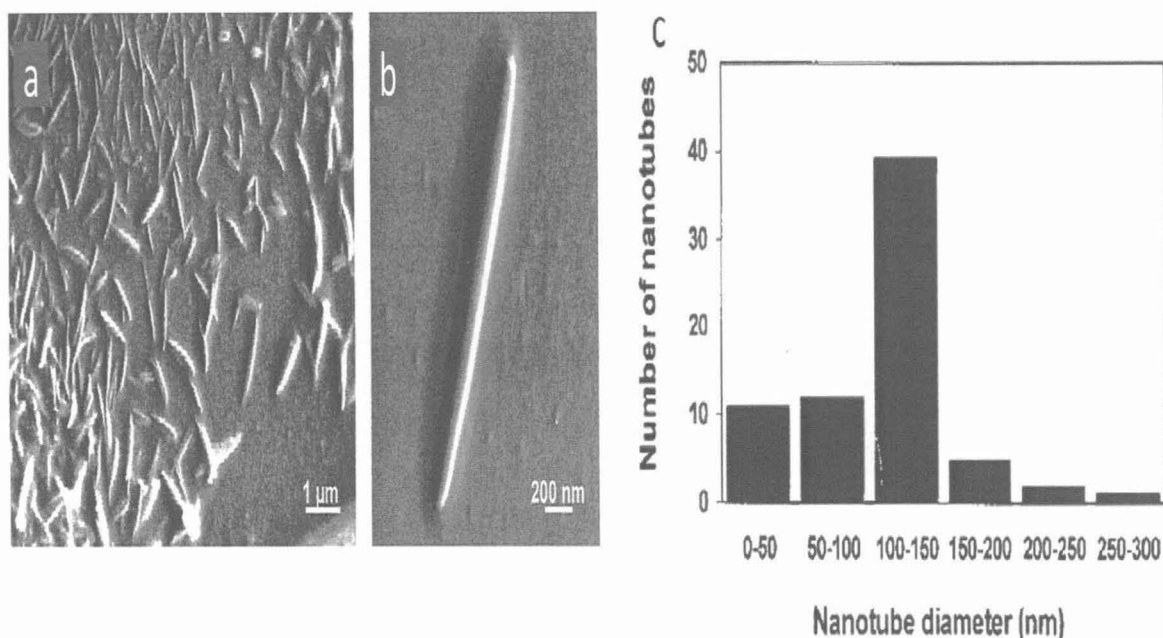
Figure 2-2: Structural analysis of the tubular nanoparticles. (A) Low-magnification SEM images of a field of discrete nanotubes that are present as individual entities. (B) High-magnification SEM image of an individual nanotube. (C) A statistical distribution of nanotube diameters

(*Excerpted from *Science* 25 April 2003:Vol. 300. no. 5619, pp. 625 – 627)

Deeper insight into the mode of assembly of the diphenylalanine monomers occurring in the assembly has been obtained from the crystal structures of the dipeptide obtained by evaporation of an aqueous solution of Phe-Phe at 80°C. The crystal structure of the diphenylalanine dipeptide exhibited the occurence of nearly circular channels formed by the translation of six peptide molecules [125]. The molecular diameter of the channels was 24 Å and the van der Waals' diameter was 10 Å. The monomers were stabilized by extensive π- stacking interaction between the phenyl rings. An extensive network of intermolecular hydrogen bonding between the N- and C-terminus as well as between the amide bond provided additional stability to the structure. Subsequent fibre diffraction studies of the dipeptide in the crystalline and in the nanotubular assembly showed that the molecular arrangement of the monomers was similar in both the cases [111]. This was an interesting

observation as it was previously speculated that the dipeptide molecules arranged themselves with different packing arrangements in the crystals and the self-assembled nanotubes. Further, due to the hollow nature of the nanotubes formed by the diphenylalanine dipeptide, the assembled structures were used as casts for generating metallic nanowires. The organic cast was subsequently proteolytically digested to yield the free nanowires. The studies brought out the ability of short aromatic peptides to self-assemble into distinct nanostructures with potential applications. However, the tunability of the assembling behavior, morphology of the final assembly and the stability of the resultant structures to various conditions are believed to be important determinant for their biomedical applications.

2.3.2 Self assembly of designed dipeptide Phe-ΔPhe into nanotubes.

In this study, the role of conformational constraint in the monomeric dipeptide and its influence on the assembly behavior was investigated as a novel strategy for the generation of peptide based self-assembling systems with greater structural stability as well as resistance to proteolytic degradation. Based on the observation that diphenylalanine dipeptide assembled into nanotubes, we synthesized and characterized the self-assembly of the dipeptide H-Phe-ΔPhe-OH.

2.3.2.1 Microscopic investigation

Optical micrographs of the aggregates were recorded using Differential Interference Contrast microscope, which revealed the presence of distinct tube like assemblies of over a micrometer in length (Figure 2-3a). The TEM analysis with negative staining of the dipeptide showed ordered and tubular assemblies with length in the micrometer range (Figure 2-3b). The width of the independent tubes ranged between 25-30 nm (Figure 2-4). No branching or curving of the tubes was observed in any of the field scans. It was interesting to note the absence of any amorphous aggregates. The process of assembly was kinetically fast, as micrographs taken after a few minutes and after 24 hrs of incubation did not reveal any significant difference in the

morphology of the tubes. The morphology of the tubular structures was also analyzed by Scanning Electron Microscopy (SEM) and Environment Scanning Electron Microscopy (E-SEM) (Figure 2-5), which further suggested that the tubular morphology was not an artifact of sample preparation. The occurrence of relatively uniform and thin size of the tubes formed by Phe-ΔPhe (Figure 2-4) was in contrast to the wider and more dispersed size of tubes formed by the dipeptide, Phe-Phe, the saturated analogue of the dehydro-dipeptide. This suggested the impact of conformational constraint induced by the -ΔPhe- residue leading to the observed difference. It was quite likely that conformational restrictions both in the dipeptide backbone and the side chain of the C-terminal Phe limited the range in size distribution and also led to a more compact assembly. It may therefore be expected that the introduction of conformational constraint could be used as a tool to fine-tune the nature of the existing assemblies particularly where it may be possible to introduce such changes with ease.

2.3.2.2 Stability under different conditions

We next investigated the stability of the nanotubes under acidic (0.1N HCl), neutral and basic (0.1N NaOH) conditions by varying the pH of the medium after tube formation. Interestingly, the morphology of the fundamental tubular unit remained unchanged (27-30 nm,) over the range of pH used though there were changes in the staining features (Figure 2-6) and the average number of tubes in a field. However, at very high concentrations of the acid or alkali (1N and above), we observed disruption of the assembled structure. Thus, it was clear that at physiologically relevant conditions, the tubes would be stable and could be used for potential biomedical applications.
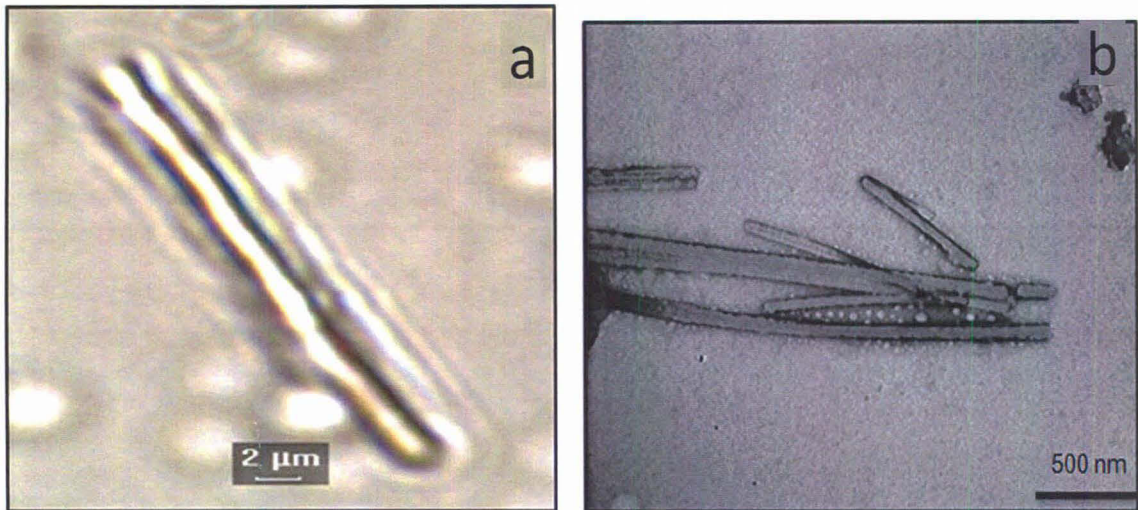
Figure 2-3: Figure showing the (a) differential interference contrast (DIC) and (b) TEM images of self-assembled Phe-ΔPhe showing the occurrence of ordered and tubular assemblies with length in the micrometer range.
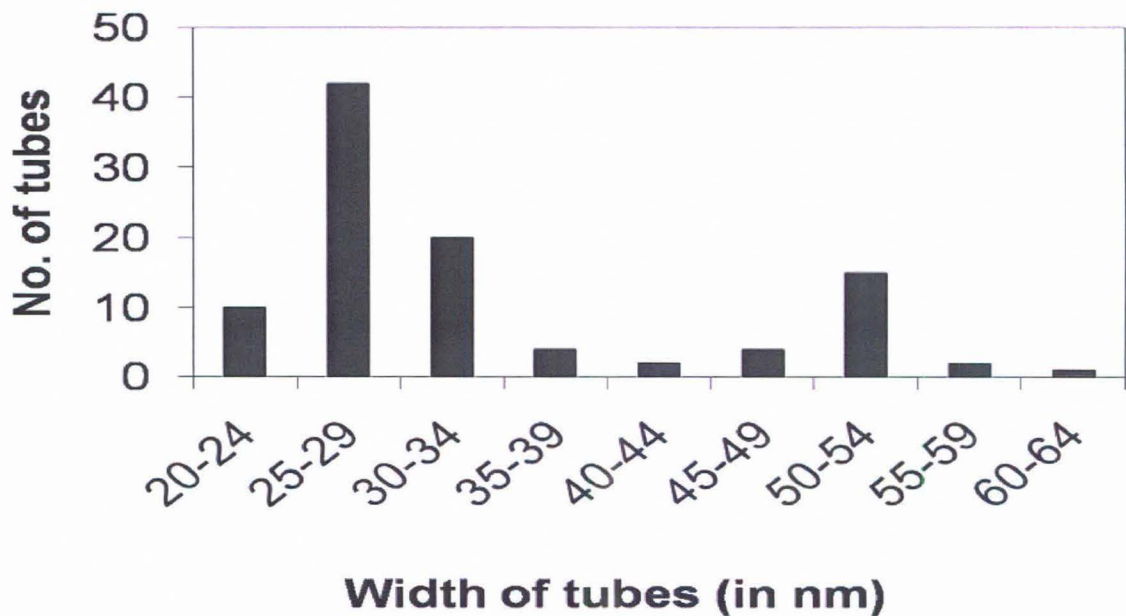

Figure 2-4: The size distribution profile of the nanotubes calculated from the TEM images. The average width of the independent tubes ranged between 25-30 nm. The tube dimensions were smaller to those obtained by the self-assembly of Phe-Phe dipeptide.
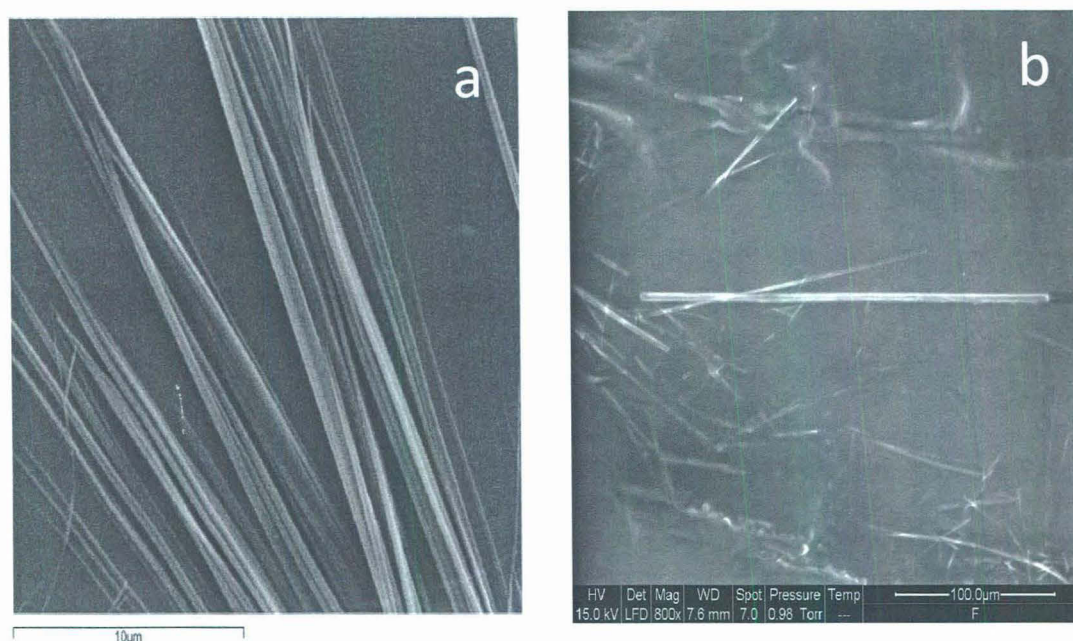
Figure 2-5: (a) Scanning electron microscopy (SEM) and (b) Environment scanning electron microscopy (E-SEM) images of the Phe-ΔPhe nanotubes. The images suggested that the tubular morphology was not an artifact of sample preparation. The tube dimensions were comparable to those obtain under TEM.

Susceptibility to proteolysis has been a major drawback of peptides and peptide-based assemblies especially for *in vivo* delivery applications. However, the introduction of modified or non-protein amino acid could confer a high degree of resistance to enzymatic degradation to the building blocks of the assembling systems. We found that the tubular structures formed by Phe-ΔPhe were intact without any change in morphology when the peptide was left for incubation with proteinase K for more than 36 hours (Figure 2-6). The tubes were also found to be stable to treatment of trypsin, chymotrypsin and cell culture supernatants.

The high stability of the self-assembled tubes over a broad range of pH conditions and to a highly non-specific proteolytic enzyme like Proteinase K could make these tubes interesting candidates for future applications.
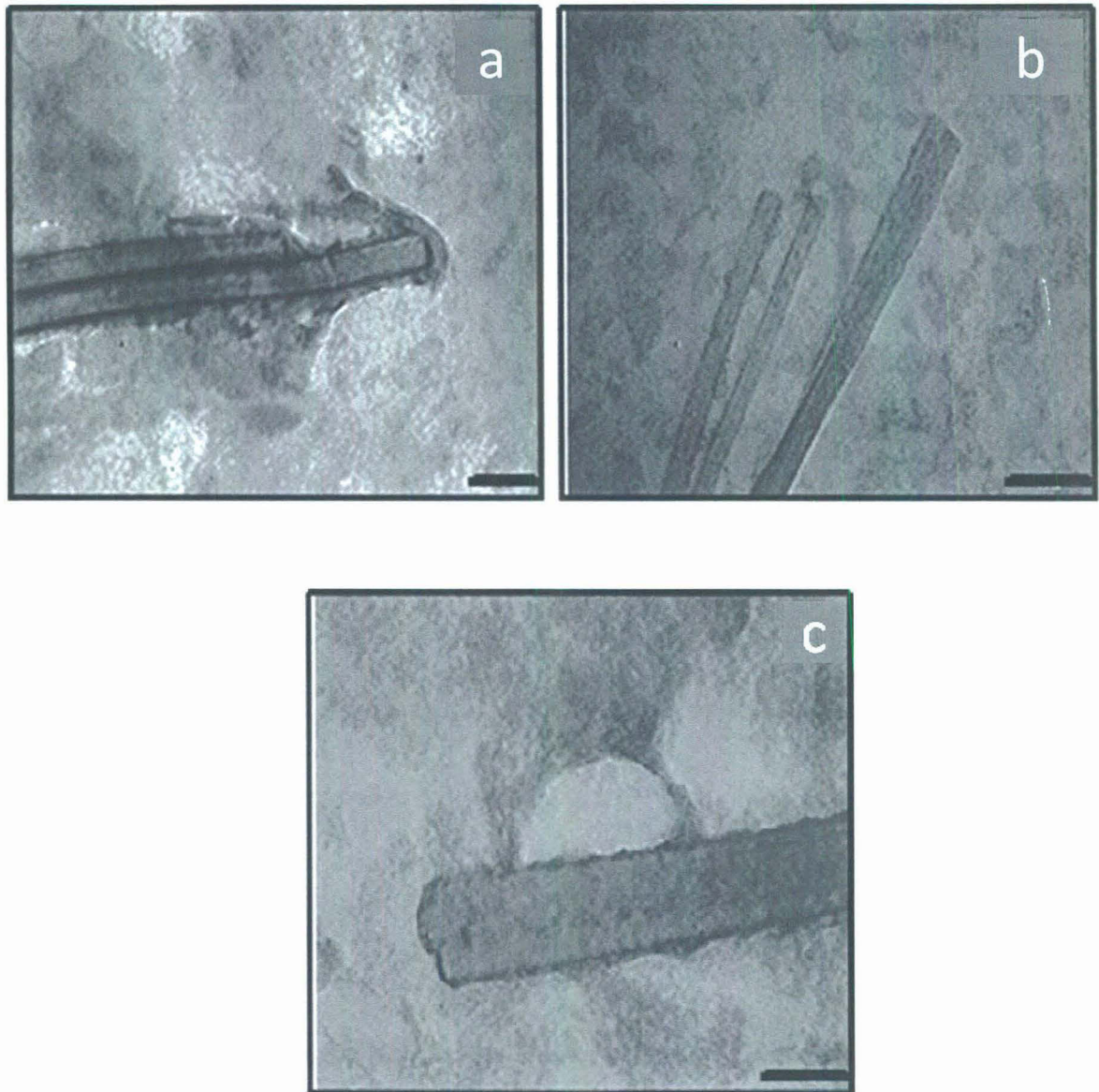
Figure 2-6: TEM images demonstrating the stability of the tubes under different pH conditions (a) acidic (0.1N HCl) (Scale Bar – 200nm), (b) alkaline pH (0.1N NaOH) (Scale Bar – 100nm), proteinase K treatment in 50mM Tris-HCl pH 7.2. (Scale Bar – 100nm).

2.3.2.3 Crystallization studies

Extensive crystallization studies have been conducted on hydrophobic dipeptides in order to investigate the conformational properties of the small peptides[107-135]. Of special interest have been the FF and VA class of dipeptides that crystallized with the occurrence of tubular channels with trapped solvent molecules[122, 125, 132]. Therefore, in order to investigate the molecular structure of the assembly, the dipeptide Phe-ΔPhe was crystallized by controlled slow evaporation of the peptide in acetic acid-water mixture. The crystal structure was solved by our collaborators at Department of Physics, IISc, Bangalore.

In the crystal structure, Phe-ΔPhe existed as a monomer in the crystal asymmetric unit. The tubular structure was formed by four dipeptide molecules (Figure 2-7) resulting in a rectangular channel having Vander Waals dimension of 6.0x4.5Å. As discussed earlier, the saturated analogue, Phe-Phe, had exhibited nearly circular channels formed by the translation of six peptide molecules [125], with a diameter of 24Å. It was interesting to note that by the introduction of a conformational constraint in the molecule, the channel shape and surface area could be modulated to some extent.

According to Gorbitz, as dipeptides contain only one peptide bond and the dihedral angles cannot be defined by classical secondary structural elements, a simplified description of a dipeptide conformation could be made by calculating a torsion angle $\theta = C_1^{\beta}\text{-}C_1^{\alpha}\cdots C_2^{\alpha}\text{-}C_2^{\beta}$ [17]. This angle defined the relative position of the two side chains with respect to the peptide plane. It has been demonstrated that for zwitterionic $_L$-Xaa-$_L$-Xaa dipeptides (Xaa is neither Gly nor Pro), the side chains usually pointed in almost opposite direction with ($|\theta|$) usually being $> 135°$ [122, 125]. According to this torsion angle description, Phe-Phe, occurred in an unusual conformation with θ being 40.2°. The side chains were thus located on the same side of the peptide bond plane and appeared to emanate out from the channel core.

However, for Phe-ΔPhe this torsion angle (|θ|) had a value of 149.70°. This implied that the side chains were present on both side of the peptide bond plane like the other members of the FF class of saturated dipeptides. It might have probably occurred due to the existence of conformational constraint in the molecule induced by the -ΔPhe residue.

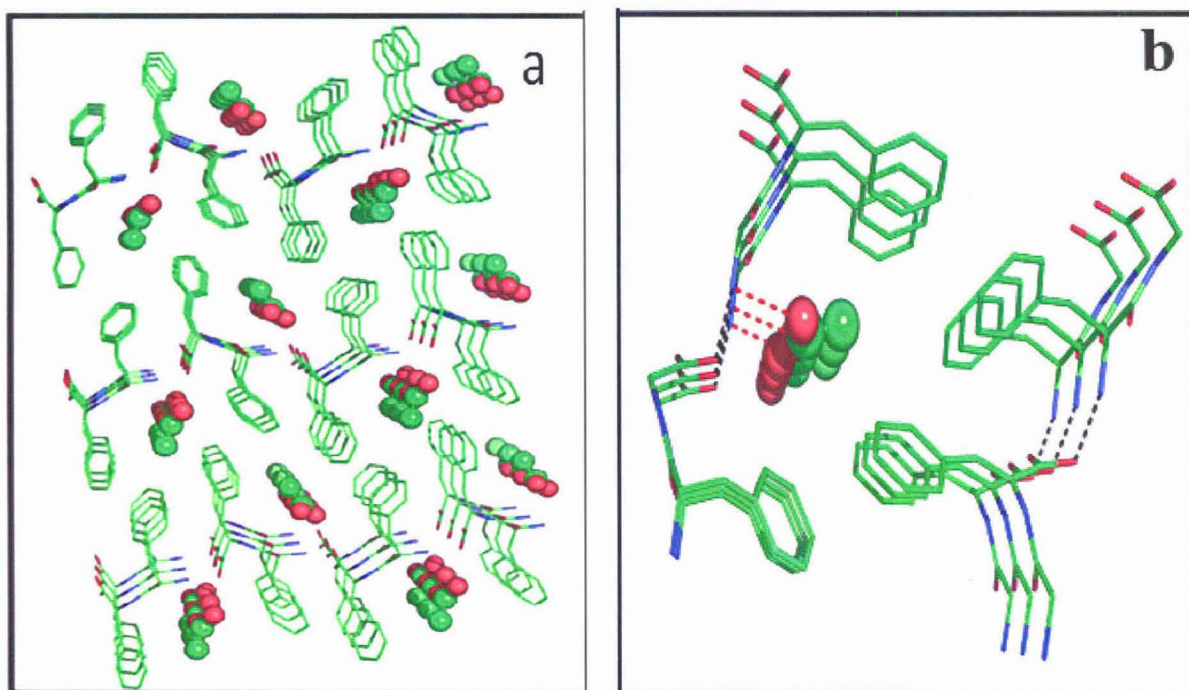**Figure 2-7:** View of the crystal packing (left) reveals a tubular structure formed by the assembly of four dipeptide molecules of Phe-ΔPhe. Enlarged view of the tubular structure (right) formed by the aggregation of four dipeptide molecules of Phe-ΔPhe with the acetic acid molecule being trapped inside the tube. The figure also shows the head-to-tail hydrogen bonding seen in the dipeptide molecule. *(The side chains not involved in the channel core formation has been omitted for clarity.)

The crystal structure of Phe-ΔPhe exhibited molecules of acetic acid trapped in the rectangular channels. The acetic acid molecules were found to be hydrogen bonded to the scaffold suggesting the important role of the solvent molecules in stabilizing the scaffold structure. Similar features had been previously reported in the self-assembly of the dipeptide (R)-Phenylglycine-(R)-Phenylglycine and (R)-(1-Naphthyl) glycyl-(R)-phenylglycine, where the dimensions of the self-assembled structure was shown to be modulated by the nature of the solvate. Interestingly, in these structures, different solvate molecules modulated the overall conformation of the self-assembled structure [245-248]. Though, the crystal structure of the Phe-Phe dipeptide also exhibited the occurrence channels filled with the solvent water molecules, the solvent molecules did not hydrogen bond with the scaffold. The crystal structure of the Phe-ΔPhe dipeptide exhibited a C(8) pattern of head-to-tail hydrogen bonding. Similar pattern of hydrogen bonding have been previously reported in the crystal structure of other hydrophobic saturated dipeptides [122, 125]. The stacked aromatic rings in the dehydro-dipeptide were held by intermolecular C-H···π interactions, giving rise to overall stability to the assembled structure. Stabilization of assemblies by multitude of such weak interactions has been very well known in literature and one of the fundamental requirements in the design of self-assembled nanoparticles.

2.3.2.4 Spectroscopic studies

The molecular structure of the aggregates was also investigated by circular dichroism (CD) and FT-IR spectroscopy. The CD signature of the dipeptide nanotube (Figure 2-8a) was characterized by a strong positive band at 197nm ([θ] ~ 10000; π-π* transition), a second positive band near 220nm ([θ] ~ 8000; n-π* transition) suggestive of a probable turn like structures in solution. The ΔPhe ring contributed the broad negative band with peak near 280nm ([θ ~ 4500) due to charge-transfer transition. The FT-IR spectrum of the tubular assembly was characterized by strong peaks at $1687cm^{-1}$ and $1647cm^{-1}$ (Fig 2-8b). The peak at $1647cm^{-1}$ was assigned to

aperiodic secondary structures involving type I, II, VIa and VIII turns. The peak at 1686cm^{-1} could be assigned as marker band for turn conformation adopted by the molecule [250-253]. As discussed earlier, the conformation of dipeptides cannot be defined in terms of classical secondary structure elements. However, the FTIR and CD spectrum of many homo-aromatic self-assembling dipeptides exhibited spectroscopic features of helices, sheets and turns. Though the exact origin of the spectral features are intriguing, occurrence of such bands do suggest that there might exist similarity between the structural organization of the dipeptides and the classically defined secondary structures [88].

To assess the solvent accessibility of the tubes as a probe for the hollow architecture of the tubes, the technique of H-D exchange was utilized [254, 255]. The ratio of the area under the peak in the amide I peak (1714cm^{-1} to 1626cm^{-1}) to the amide II region (1626cm^{-1} to 1543cm^{-1}) was plotted against time to characterize the exchange kinetics. The results indicated that (Figure 2-9) the ratio decreased with time and saturation was reached within 6 minutes. This suggested that the monomers in the self-assembled structures were highly solvent accessible probably due to the hollow nature of the tube (also suggested by the crystal structure) and thus allowed for the rapid HD exchange. This observation was in contrast to the exchange rates observed in case of β-sheet based fibrillar assemblies that exhibited slower exchange rates. However, it did suggest that the tubes were porous and could thus be used to entrap low molecular weight molecules for potential biomedical applications.

It was thus evident that the incorporation of conformational constraint altered the assembly behavior and the properties of the nanotubes in multiple ways.
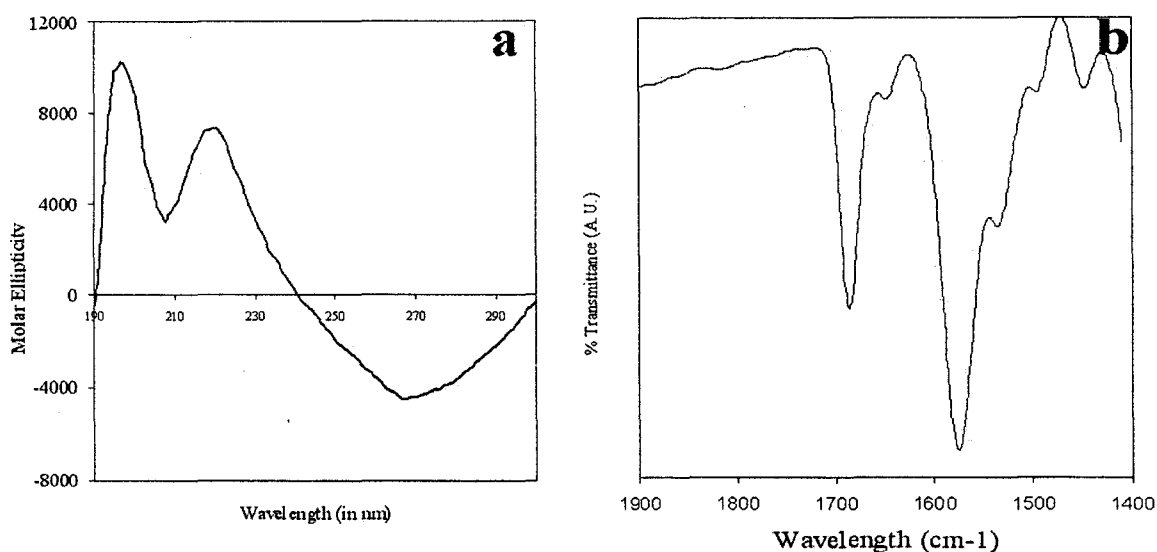
Figure 2-8: (a) Circular dichroism and (b) fourier transform infra red spectrum of the Phe-ΔPhe nanotubes assemblies. Though, the conformation of dipeptides cannot be defined in terms of classical secondary structure elements, the FTIR and CD spectrum of the self-assembling Phe-ΔPhe dipeptide exhibited spectroscopic features of turns.
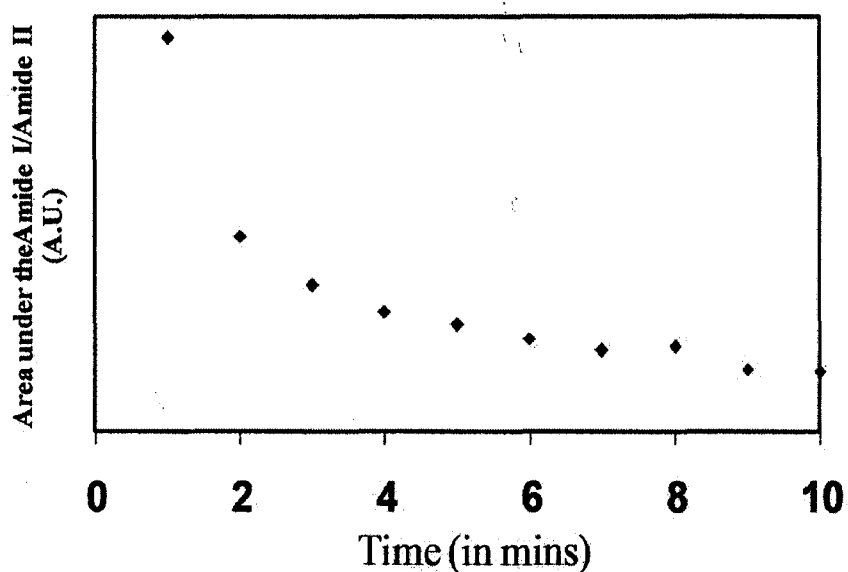

Figure 2-9: Figure showing the ratio of decrease in Amide I peak area with reference to Amide II peak area as an index of hydrogen deuterium exchange.

2.3.3 Role of N-terminal side chain on the self-assembly of nanotubes

In order to probe the role of the side chain of the N-terminal amino acid in the H-Xaa-ΔPhe-OH motif, the self-assembly of the peptides with Xaa from the different groups of the amino acids was investigated.

Electron micrographs of aged aqueous solutions of Gly-ΔPhe and Ala-ΔPhe showed no self-assembly even at very high concentrations of the peptide (~10mg/ml). The peptide Leu-ΔPhe assembled into tightly packed crystalline tubular structures with with tube diameter in the range of 100-150nm. Val-ΔPhe, however, assembled into thin flaky elongated structures (Figure 2-10). Similar two dimensional assemblies have been formed by another dipeptide derivative [88]. The peptide Ile-ΔPhe assembled into long (over many microns) tubular structures with very large (500 nm) diameter (Figure 2-10) that were heavily stained with uranyl acetate probably suggesting a hollow architecture. With Xaa as Glu or Lys, the dipeptides assembled into distinct vesicular structures in aqueous medium. The self-assembly behavior of this class of structures has been discussed in detail in Chapter 4. Dipeptide containing hydroxyl groups like Ser at Xaa position did not form assemblies under the conditions tested. Also amide group containing dipeptide like Gln-ΔPhe did not assemble into nanostructures under conditions tested.

The observations indicate that a minimum level of bulk was necessary to initiate the self-assembly behavior in the dipeptides scaffold with Xaa belonging to the hydrophobic group of amino acids. Moreover, the nature of the functional group at the N-terminus influenced the propensity as well as the nature of the self-assembly in the H-Xaa-ΔPhe-OH dipeptide motif. These results could be utilized for the rational design of dipeptide based nanostructures.
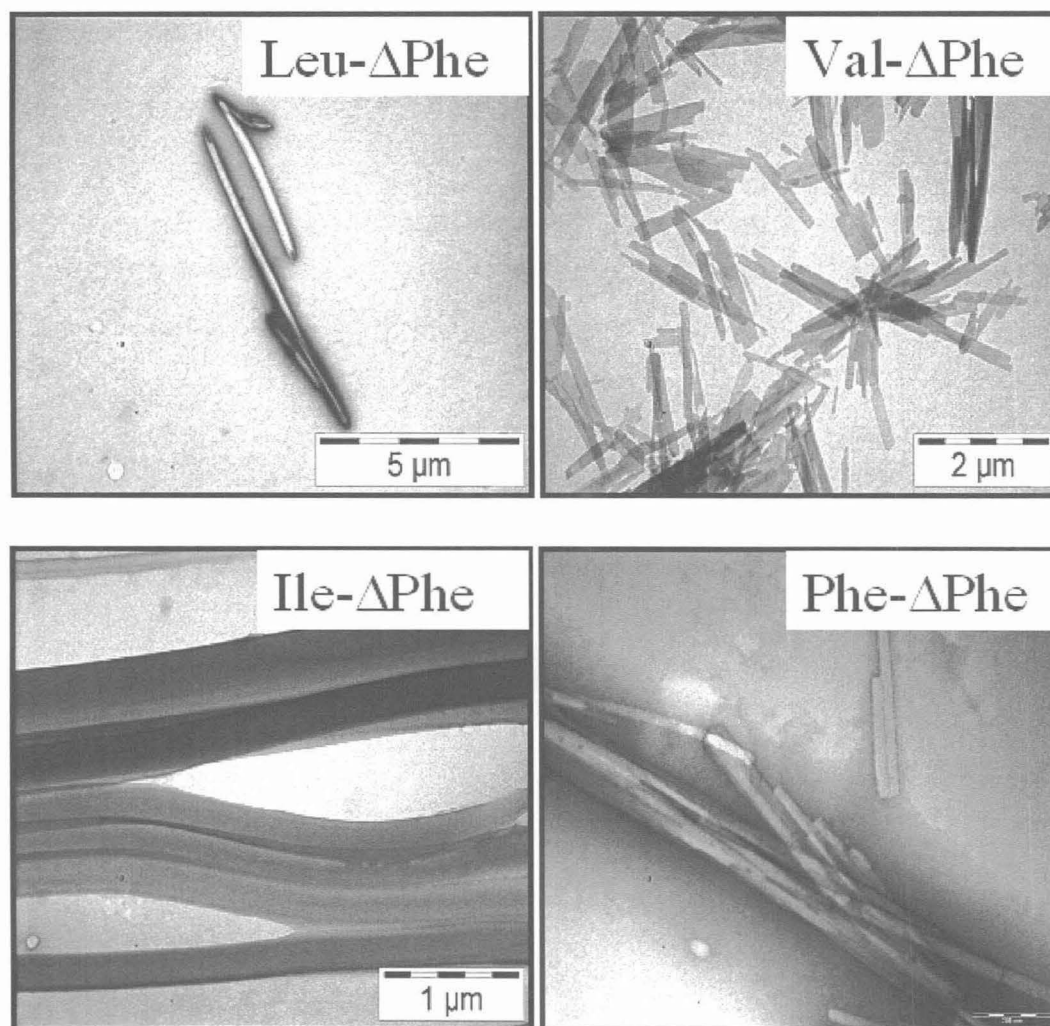
Figure 2-10: Transmission electron micrographs (TEM) of ΔPhe containing free dipeptides. Leu-ΔPhe assembled into tightly packed crystalline tubular structures whereas Val-ΔPhe resulted in thin flaky elongated self-assembled structures. The peptide Ile-ΔPhe assembled into long and wide (~200nm) tubular structures.

2.3.4 Role of aromaticity in the self-assembly of nanotubes

Having established that conformational constraint could be used as a potential strategy to modulate features of self-assembled structures, we investigated the role of peptide Ile-ΔPhe assembled into long (over many microns) tubular structures with large (500 nm) diameter. This suggested that a minimum level of bulk was necessary to initiate the self-assembly behavior in the dipeptides scaffold H-Xaa-ΔPhe-OH with Xaa belonging to the hydrophobic group of amino acids.

aromaticity in the self-assembly of dipeptides into nanotubes. The pi-stacking interactions have been previously proposed to stabilize tubular architectures [74-78, 122, 125]. To probe the necessity of pi-stacking interactions for structures to assemble into tubular architectures, we designed, synthesized and studied for their self-assembling behavior of H-Phe-Phe-OH (Phe-Phe), H-Cha-Phe-OH (Cha-Phe), H- Phe-Cha-OH (Phe-Cha) and H-Cha-Cha-OH (Cha-Cha) where, Cha stands for Cyclohexylalanine, a modified amino acid similar to phenylalanine but with an aliphatic ring.

2.3.4.1 Microscopic Investigations

The electron micrograph of the dipeptide Phe-Phe exhibited large tubular structures with a diameter of 200-400nm and length over 1μm (Figure 2-11). The Cha-Phe dipeptide was characterized by thin fibrils along with a large number of vesicular structures (Figure 2-11). The fibrils were roughly 20nm in diameter and exhibited twisting and curving along their length. The vesicles exhibited an average diameter of 50nm with a tendency to fuse with each other. This suggested that the vesicles were probably the structural precursors of the fibrils. Moroever, on longer incubation (~15 days), the field scans did not show any vesicles suggesting that they were the kinetically trapped intermediates in the pathway of the assembly of the dipeptide fibrils. The electron micrographs of Phe-Cha peptide showed a large number of pleomorphic vesicular structures in a large size range of 10-80nm (Figure 2-11) indicating that the position of the aromatic residue in the dipeptide also affected the

morphology of the assembly. The peptide Cha-Cha also assembled into vesicular structures with an average diameter of 20nm and low poly-dispersity (Figure 2-11). The above observations clearly highlighted the crucial role of aromatic stacking interactions in the self-assembly of nanotubes. It was interesting to note that not only the presence of aromatic residues dictated the assembly but also its position in the dipeptide. However, it appeared that it was not always necessary to have aromatic residues to initiate self-assembly. Thus, appropriately chosen aliphatic ring structures could also act as motifs for self-assembly. This observation was in contrast to the predominant belief that aromatic homo-dipeptides were the central motif for the formation of ordered self-assembled structures [88].

2.3.4.2 Spectroscopic Studies

To delineate the role of molecular conformation on the assembly behaviour of the dipeptide we compared their CD and FTIR spectra. The CD spectra of the assemblies was characterized by the π-π* transition band at 197-198nm and an n-π* transition band between 203-215nm (Table 2-1). The position of n-π* transition band blue shifted with decreasing aromaticity. The FTIR spectra of the dipeptide assemblies were characterized by $v_{C=O}$ (backbone; Amide I) band at 1615cm^{-1} (for Phe-Phe), 1667cm^{-1} (for Cha-Phe), 1665cm^{-1} (for Phe-Cha) and 1670cm^{-1} (for Cha-Cha) (Table 2-1). However, we did not observe any correlation between the nature of assembly and its molecular conformation. This was not surprising as self-assembled dipeptides have been shown exhibit FTIR spectra corresponding to all major classes of secondary structure and there have been no correlations between the morphology and molecular conformations of the peptide based nano-assemblies [88].

The above spectroscopic evidences along with the electron micrographs clearly suggested that appropriately placed aromatic moeities were very crucial in the design of dipeptide based nanotubes. Moroever, aromaticity was not the core driving factor for self-assembly in dipeptides and amino acids containing aliphatic ring side-chains could also be used.
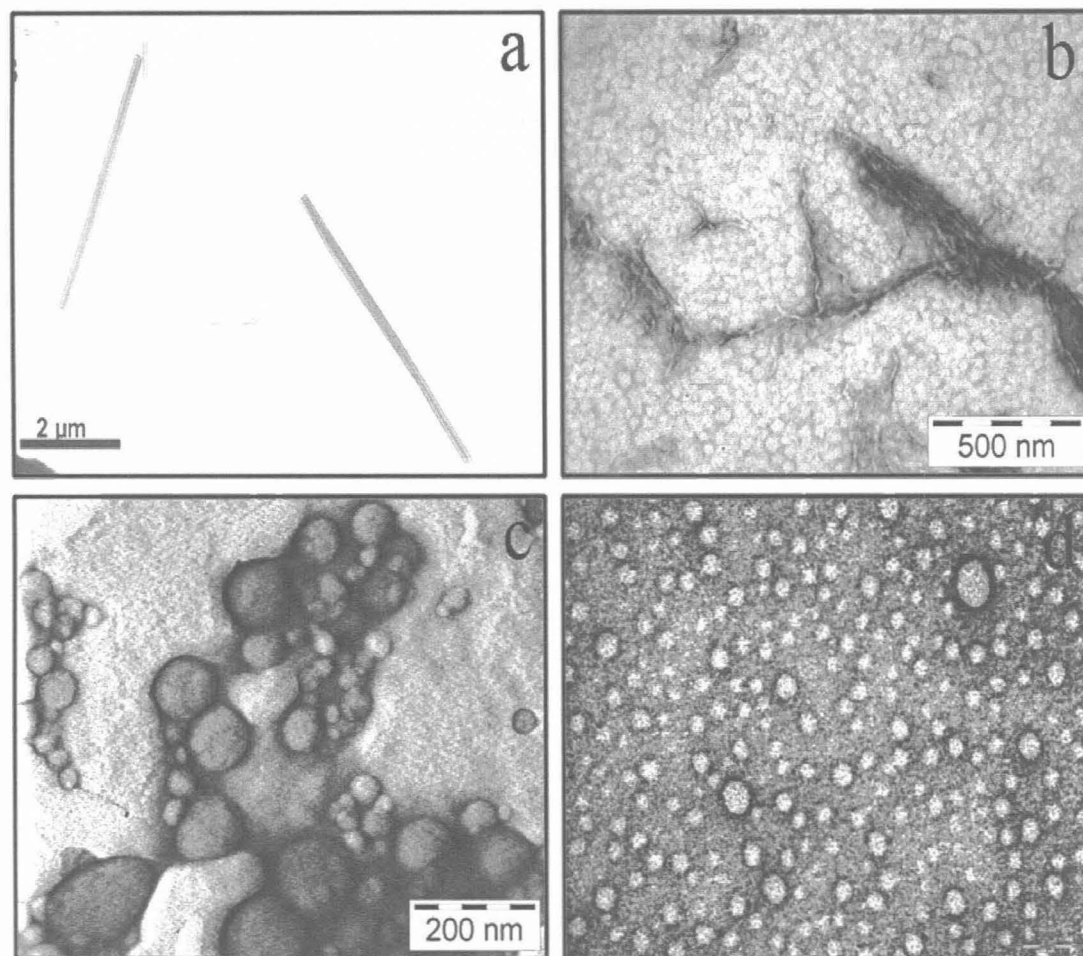
Figure 2-11: TEM images of the nano-structures formed by (a) Phe-Phe, (b) Cha-Phe, (c) Phe-Cha and (d) Cha-Cha. The electron micrograph of the dipeptide Phe-Phe exhibited large tubular structures with a diameter of 200-400nm and length over 1µm (*Excerpted from *Science* 25 April 2003:Vol. 300. no. 5619, pp. 625 – 627). The Cha-Phe dipeptide was characterized by thin fibrils along with a large number of vesicular structures. The fibrils were roughly 20nm in diameter and exhibited twisting and curving along their length. The vesicles exhibited an average diameter of 50nm with a tendency to fuse with each other. The Phe-Cha peptide showed a large number of pleomorphic vesicular structures in a large size range of 10-80nm. The peptide Cha-Cha also assembled into vesicular structures with an average diameter of 20nm and low poly-dispersity.

Table 2-1: FTIR peaks and CD spectra of the nano-structures formed by (a) Phe-Phe, (b) Cha-Phe, (c) Phe-Cha and (d) Cha-Cha.

Peptide	CD		FTIR
	π-π^* Transition (nm)	n-π^* Transition (nm)	Amide I (cm^{-1})
Phe-Phe	197	215	1615
Cha-Phe	197	211	1667
Phe-Cha	197	213	1665
Cha-Cha	198	203	1670

2.5 Conclusion

Although biological scaffolds, including short peptides, offer a myriad of potential applications to nanotechnology, their relative instability may be a major concern in realizing their potential application. The main aim of the present work was to explore the possibility of using non-protein amino acids, capable of providing well-defined conformational characteristics and higher stability, particularly to enzymatic degradation. The introduction of ΔPhe in the dipeptide affected the pattern of peptide assembly resulting in longer and thinner nano-tubes than previously reported peptide based tubular structures. Also, their stability to different pH conditions and proteases could make them potentially useful for various applications. However, the studies also brought out the crucial role of aromatic moieties in the design of dipeptide based self-assembling nanotubes. It was evident that the nature of the side-chain and their position in the dipeptide scaffold also dictated the nature of assembly. Moroever, aromaticity was not the core driving factor for self-assembly in dipeptides; peptide based nanostructures could also be

designed with amino acids containing aliphatic ring side-chains. Thus, it was evident that dipeptides could be rationally designed with chosen kind of functional groups at appropriate position to generate nano-particles with desired properties.

Chapter 3

Self-assembly of α,β-dehydrophenylalanine (ΔPhe) containing amphiphilic dipeptides into nanovesicles.

3.1 Introduction

Self-assembly of soft materials into nanostructures offers exciting applications. "Peptosomes"[257-259], vesicles formed by the self-assembly of peptides, offer superior stability in addition to tailorability of physical, chemical and biological properties along with unmatched bio-compatibility[260]. Encapsulation, controlled release and biological stability of bioactive compounds are some of the potential application areas of vesicular structures[261]. Specific biomedical applications involving actuator functions for temperature, pH, salt triggered release as well as incorporation of adhesion and recognition sites in the assembled structures can be better met with potent designs of 'peptosomes'[261-263]. Recent studies have demonstrated that spontaneous assembly of peptide molecules into vesicles not only form at an appropriate concentration of the amphiphilic molecule, but can also be induced by incorporation of conformational rigidity resulting in restricted conformational entropy[261,264-269]. Medium sized and short peptide sequences have been shown to assemble into vesicles in aqueous medium; however the recent and elegant demonstration of a dipeptide assembling into stable nanovesicular structures that are stable in acidic and alkaline conditions is noteworthy[258].

In the present work, we report the design, synthesis and characterization of two α,β-dehydrophenylalanine residue (ΔPhe) containing amphiphilic dipeptides, H-Glu-ΔPhe-OH and H-Lys-ΔPhe-OH (hereafter denoted as Glu-ΔPhe and Lys-ΔPhe respectively) which self-assembled into anionic and cationic vesicular structures respectively. The design was based on the observations that (i) peptides with a hydrophobic tail and a charged amino-acid at one end self-assembled into vesicles and tubes[260], (ii) aromatic residue containing peptides as small as dipeptides could also self-assemble[258,266] into nanotubes and nanovesicles and (iii) that incorporation of ΔPhe residue, the unsaturated analog of phenylalanine, with a double bond between C^α and C^β atoms provides structural [156-161, 186, 187, 192-226, 230] and proteolytic stability to the self-assembled structures[151, 156, 157]. It was found that the vesicles

formed by the amphiphilic dipeptides exhibited stability to non-specific protease treatment, were able to encapsulate bioactive molecules, were not cytotoxic, and were easily taken up by cells in culture. The novel self-assembled nanostructures could thus have potential applications as vehicles for delivery of biologically relevant molecules.

3.2 Materials and methods

3.2.1 Peptide synthesis: Dipeptides were synthesized as described below:

(a) **H-Glu-ΔPhe-OH**

Boc-Glu(OtBu)-OH (Novabiochem) (1.52g, 5mM) was dissolved in dry tetrahydrofuran (Sigma-Aldrich) and the resulting solution stirred in an ice-salt bath at -15°C. N-methyl morpholine (Sigma) (0.65ml, 5mM) was added to the solution followed by isobutyl chloro-formate (Sigma) (0.7ml, 5mM). After 10min, a pre-cooled aqueous solution of DL-threo-β-phenylserine (Sigma-Aldrich) (1g, 5.5mM) and sodium hydroxide (0.22g, 5.5mM) was added and mixture stirred overnight at room temperature. The reaction mixture was concentrated *in vacuo*, acidified with citric acid to pH 3.0 and extracted with ethyl acetate (Spectrochem) (3×20ml). The ethyl acetate layer was washed with water (2×15ml), with saturated sodium chloride (1×20ml), dried over anhydrous sodium sulfate and evaporated to yield Boc-Glu(OtBu)-DL-threo-β-phenylserine as an oily compound (2.3g, ~100%). The compound, Boc-Glu(OtBu)-DL-threo-β-phenylserine, was then mixed with anhydrous sodium acetate (0.53g, 6.5mM) in freshly distilled acetic anhydride (50ml) and stirred for 36hrs at room temperature. The thick slurry obtained was poured over crushed ice and stirred till the oily suspension gave rise to a yellow colored solid. The precipitate was filtered, washed with 5% NaHCO₃, cold water and dried under vacuum. The resulting azalactone, Boc-Glu(OtBu)-ΔPhe-Azl, was dissolved in methanol,

treated with 1.5 equivalents of 1N NaOH solution and stirred at room temperature for 3-4hrs. The mixture was then partially evaporated to remove methanol, acidified with citric acid to pH 3.0 and extracted with ethyl acetate (3×30ml), the combined ethyl acetate extract was washed with water (2×20ml), dried over anhydrous sodium sulphate and evaporated to yield Boc-Glu(OtBu)-ΔPhe-OH as a white solid. Deprotection at the α-amino group and side chain protection was achieved by treatment with 98% formic acid (30ml) for 3hrs at room temperature. The reaction mixture was evaporated to dryness and the residue was precipitated with anhydrous diethyl ether. The resulting precipitate was filtered, washed several times with dry ether and subsequently lyophilized from 10% acetic acid-water (20ml) to yield the final compound H-Glu-ΔPhe-OH as white powder. Overall yield (0.6g, 48%); R_f = 0.13 (CHCl$_3$-MeOH, 9:1).

The peptide was purified on a preparative reverse phase C$_{18}$ column (Deltapak, C$_{18}$, 15μ, I.D. 300×19mm) using acetonitrile-water linear gradient 5-45% acetonitrile (0.1%TFA)/water (0.1% TFA) at a flow rate of 4ml/min over 25min. The purified peptide was reinjected into an analytical reverse phase C$_{18}$ column (Phenomenex, C18, 5μ, I.D. 250×4.6mm) using a acetonitrile-water linear gradient 5-45% acetonitrile (0.1%TFA)/water (0.1% TFA) at a flow rate of 1ml/min over 25min and was found to be 98% pure with retention time of 13min. The purified peptide was analyzed by mass spectroscopy (Applied Biosystems QStar (Q-TOF)) Observed Mass- 293 Da, Expected Mass- 292.3 Da.

(b) **NH$_2$-Lys-ΔPhe-COOH**

The peptide was synthesized as described above starting with Boc-Lys (Boc)-OH (5mM, 1.73g). Overall yield (0.57g, 39%); R_f = 0.12 (CHCl$_3$-MeOH, 9:1); The peptide was purified as described in the previous section and

analyzed by mass spectroscopy. Retention Time- 13min; Observed Mass-292 Da, Expected Mass-291.38 Da.

3.2.2 Circular Dichroism (CD) Spectrometry: All spectra were recorded on a JASCO-810 polarimeter equipped with a Peltier type thermostat and purged continuously with dry N_2 gas at 10 lit/min (LPM) during data acquisition. Data was collected in a quartz cuvette with path-length of 0.1cm or 1cm between 190nm to 360nm at scan speed of 25nm/min and response time of 16sec. The average of 50 scans was used for analysis of the spectrum. The titration studies were carried out at peptide concentration between 1-10mM. The concentration of the peptide was estimated by UV spectrometry with ε_{205} = 5167 per peptide bond [256]. CD studies were also carried out at different temperatures and in presence of monovalent and divalent cations.

3.2.3 Fourier Transform Infra Red (FTIR) Spectrometry: Spectra were collected on a Perkin Elmer Spectrum BX FTIR spectrometer. The assembled peptide samples were spotted on a CaF_2 window and air-dried at 99% relative humidity. The samples were then rehydrated with D_2O and Hydrogen-Deuterium exchange was monitored every minute for 10min in the spectral range of 1400-1900cm^{-1}. The FTIR spectra were smoothed with smoothing length of 20 units. Two-dimensional correlation spectroscopy [270](2D-COS) maps were generated from the stack of spectra using the freely available software package 2D-Shige. All spectral assignments were done according to published reports [250- 253].

3.2.4 Simulations: The optimized potential energy landscape and the molecular geometry was calculated using PM5 method of MOPAC implemented in Scigress software suite. Briefly, the molecule was built with the structure building module of Scigress using the reported parameters of ΔPhe [136, 215]. The torsional angle between N1-Cα1-C1-N2 was defined as dihedral 1. Similarily, the angle between C1-N2-Cα2-C2 was defined as dihedral 2. The potential energy was calculated by varying dihedral 1 versus dihedral 2 from -180° to +180° in steps of 9° followed by structure

optimization using PM5 method including solvation effects of water simulated by COSMO [271, 272].

3.2.5 Electron Microscopy: For transmission electron microscopy (TEM), the peptide samples were prepared at a concentration of 1-10mg/ml in double distilled water and incubated for 24hrs to make sure that the process of assembly was complete. The sample was adsorbed on a 400 mesh copper grid with carbon coated formvar support and stained with 1% uranyl acetate and viewed under a 120kV mode of a TEM (Tecnai 12 BioTWIN, FEI Netherlands). Photomicrographs were digitally recorded using a Megaview II (SIS, Germany) digital camera. Image analysis was carried using Analysis II (Megaview, SIS, Germany) and ImageJ (http://rsb.info.nih.gov/ij/) software packages.

3.2.6 Proteolytic stability assays: The proteolytic stability of the peptide vesicles was assayed using reverse phase HPLC. The peptide vesicles were incubated with a non-specific protease, Proteinase K, for 24hrs. The samples were then injected into a reverse phase C18 coulmn (Phenomenex, C18, 5µ, I.D. 250×4.6mm) using a acetonitrile-water linear gradient 5-45% acetonitrile (0.1%TFA)/water (0.1% TFA) at a flow rate of 1ml/min over 25min. Decrease in peak area of the native peptide was used as an indicator of proteolytic degradation.

3.2.7 Encapsulation Studies: The relevant bioactive molecules were mixed with preformed vesicles in equal weight ratio and subjected to sonication (Branson 200, 19W) for 2-5min or aspirated through a pipette. The sample was then ultracentrifuged at 120000rpm for 5hrs at 10°C in a Beckman Coulter OptiMax MLA-130 rotor. A small volume was removed from the supernatant and the concentration of the free test molecules was estimated spectrophotometrically. The percentage encapsulation was calculated using the following formula; %Encapsualtion = (Abs of bound molecules/absorbance of total molecules)×100. To visualize protein encapsulation in the nanovesicles, the proteins were tagged to 20nm gold particles (Ted Pella, USA) by adsorption. After overnight incubation of 1mg/ml protein with

50µL of nano-gold, the gold nanoparticles with adsorbed proteins were washed thrice with buffer/water with repeated centrifugation. The conjugates were then mixed with the nanovesicles in a manner similar for encapsulation of small molecules (described above). The samples were then imaged under a Phillips technai 120KV.

3.3 Results and discussion

3.3.1 Self-assembly of the amphiphilic dipeptides:

Self-assembly of the dipeptide nanostructures was initiated by dispersion of 10-20mg of the peptide in a small volume (50µl) of 1,1,1,3,3,3-Hexafluoro-2-propanol (HFIP) and subsequent addition of 1ml of water at near neutral pH. The two peptides formed visibly clear solutions. Also, there was no observable difference in the assembly behavior when the peptides were directly dissolved in water with vigorous stirring and heating.

3.3.2 Electron Microscopy Studies

The morphology of the structures was ascertained using TEM with uranyl acetate staining (Figure 3-1). Glu-ΔPhe assembled into pleomorphic spherical structures (Figure 3-1) in size range of 50-200nm with a mean diameter of 110nm. The grayscale contrast between the vesicle surface and the grid background suggested that a high density of negative charge (anionic) occurred over the surface of Glu-ΔPhe vesicles (Figure 3-1c). The grayscale contrast distribution profile within the imaged spherical structures suggested a flattening effect, most likely due to surface tension of drying during sample preparation. Such an effect is observed in structures that are hollow from within (vesicular) and not rigid spherical structure [23]. The vesicles formed by Lys-ΔPhe appeared mostly spherical (Figure 3-1d) with a mean diameter of 370 nm and a relatively narrow size range (250-450nm). The vesicle surface of Lys-ΔPhe, however, had lighter staining compared to the grid background (Figure 1f) suggesting that the structures had a high density of positive charge (cationic) on their surface. A

flattening effect observed over the imaged spherical structures suggested a vesicular assembly.
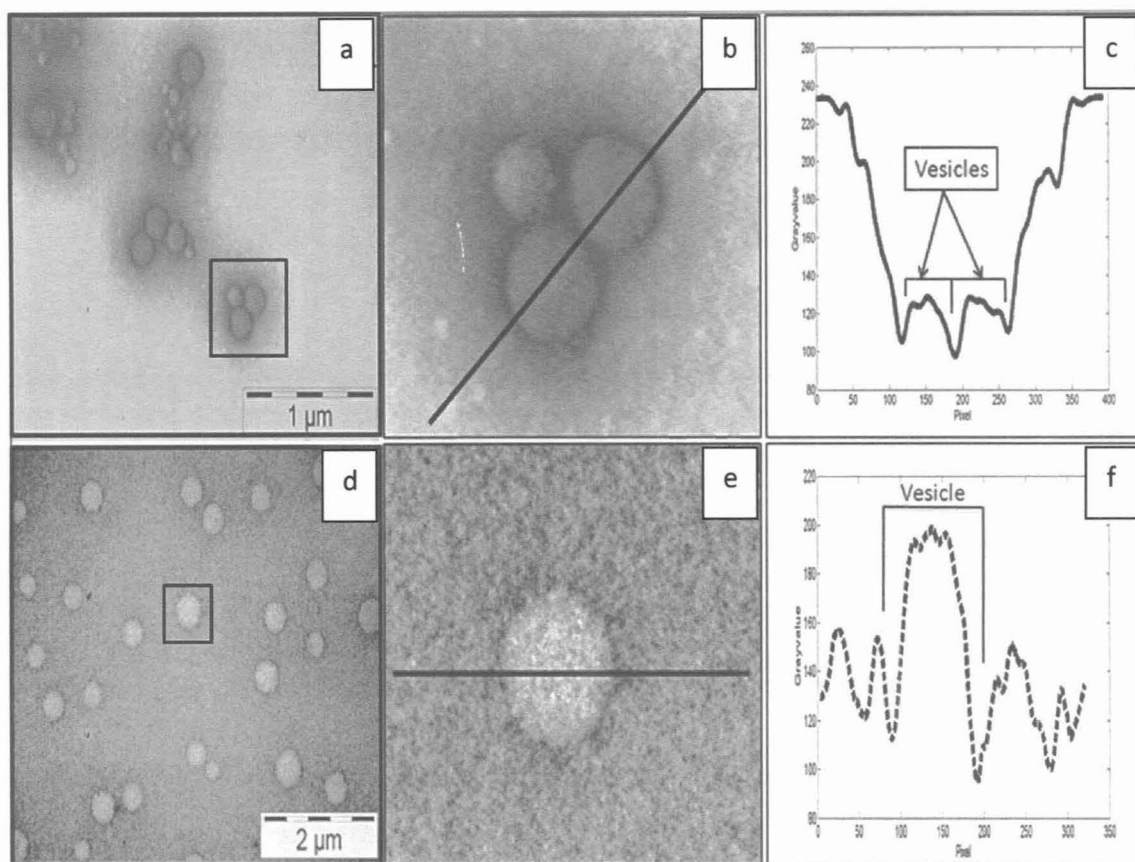
Figure 3-1: Electron micrographs of (a) Glu-ΔPhe and (d) Lys-ΔPhe, (b) and (e) show the enlarged images of the marked areas in (a) and (d) respectively, (c) and (f) show the intensity distribution along the marked lines in (b) and (e) respectively.   Glu-ΔPhe assembled into pleomorphic spherical structures in wide size range of 50-200nm with a mean diameter of 110nm. The vesicles formed by Lys-ΔPhe appeared mostly spherical with a mean diameter of 370 nm and a relatively narrow size range (250-450nm).

3.3.3 Dynamic Light Scattering Studies

To ascertain the stability of the peptide vesicles in solution, dynamic light scattering (DLS) experiments were performed at a peptide concentration of 30mg/ml. It was

observed that the Glu-ΔPhe vesicles had a mean square radius of gyration (z-average) of 200nm whereas Lys-ΔPhe formed larger vesicles with a z-average of 280 nm (Figure 3-2). Glu-ΔPhe vesicles showed a polydispersity index (fractional dispersity) of 0.5 whereas the self-assembled vesicles of Lys-ΔPhe had a lower polydispersity of 0.34. The DLS results correlated well with the electron micrographs which also showed a smaller mean size and a higher size range for Glu-ΔPhe vesicles and a larger average size with a lower size range for the vesicles formed by Lys-ΔPhe peptide. The DLS studies along with the electron micrographs clearly suggested the self-assembly of the two amphiphilic dipeptides into well defined vesicular structures in aqueous medium.

Size Distribution by Intensity
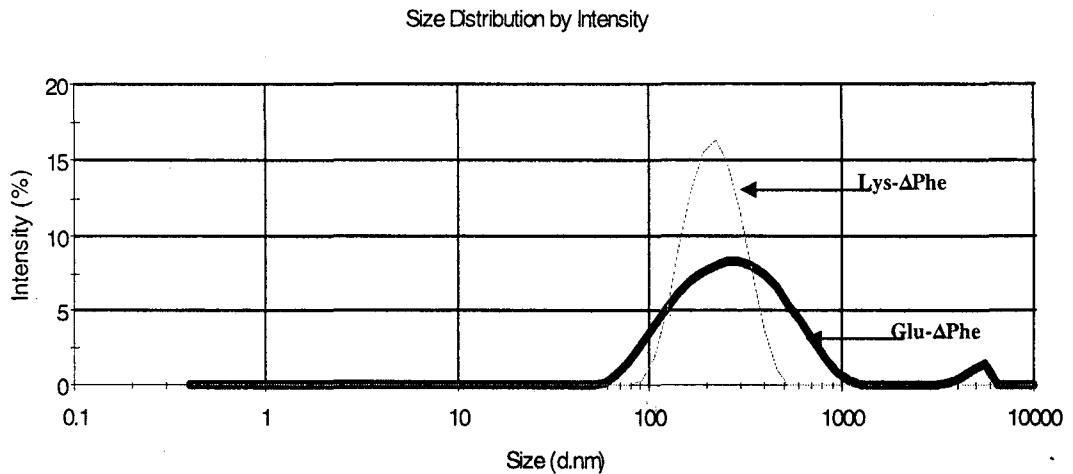
Figure 3-2: Comparison of size distribution profile of Glu-ΔPhe and Lys-ΔPhe (20mg/ml) by DLS. The Glu-ΔPhe vesicles had a mean square radius of gyration (z-average) of 200nm whereas Lys-ΔPhe formed larger vesicles with a z-average of 280 nm. Glu-ΔPhe vesicles showed a polydispersity index (fractional dispersity) of 0.5 whereas the self-assembled vesicles of Lys-ΔPhe had a lower polydispersity of 0.34. The DLS results correlated well with the dimensions obtained through electron microscopy.

3.3.4 Spectroscopic investigation of molecular structure

Crystal structures of several, mostly hydrophobic, small self-assembling peptides[27-32] have provided precise information regarding the molecular arrangement of the self-assembled structures. However, attempts to crystallize Lys-ΔPhe and Glu-ΔPhe were mostly unsuccessful. Glu-ΔPhe did not crystallize under any of the conditions tested. While Lys-ΔPhe did crystallize, the fragile and flaky crystals were not suitable for diffraction studies. CD, 2D-COS FTIR and simulation studies were, therefore, used to characterize the molecular conformation of the peptides in the nanovesicles.

The FTIR spectra of the two peptides (Figure 3-3) in solid state showed characteristic amide carbonyl peaks at 1700cm^{-1} and 1690cm^{-1} for Glu-ΔPhe and Lys-ΔPhe respectively. The 2D-COS FTIR studies were carried out using hydrogen-deuterium exchange and the synchronous correlation maps exhibited auto peaks at 1690cm^{-1} for Glu-ΔPhe and at 1672cm^{-1} for Lys-ΔPhe (Figure 3-4). A lower absorption frequency of the amide I band indicated a stronger hydrogen bonding [250-253, 270] of the peptide backbone in Lys-ΔPhe. The asynchronous map of Glu-ΔPhe exhibited a positive cross peak at (1600cm^{-1}, 1690cm^{-1}) and a negative cross peak at (1695cm^{-1}, 1740cm^{-1}) (Figure 2B) whereas Lys-ΔPhe showed negative cross peak at (1672cm^{-1}, 1683cm^{-1}) and a positive cross peak at (1647cm^{-1}, 1672cm^{-1}) (Figure 3-4) [250-253, 270]. The differences in the FTIR spectra correspond to subtle differences in the molecular conformation acquired by the amphiphilic dipeptides. Though the exact origin of the FTIR bands could not be deciphered, they occurred in the regions corresponding to classically defined secondary structures[250-253, 270]. The auto peaks at 1690cm^{-1} for Glu-ΔPhe and at 1672cm^{-1} for Lys-ΔPhe corresponded to turn-like molecular conformation adopted by the dipeptides. Further, in the 2D-spectrum of Glu-ΔPhe, cross peaks at (1600cm^{-1}, 1690cm^{-1}) and (1695cm^{-1}, 1740cm^{-1}) probably suggested intermolecular interaction between the monomers with 1740cm^{-1} band corresponding to free COOH group.
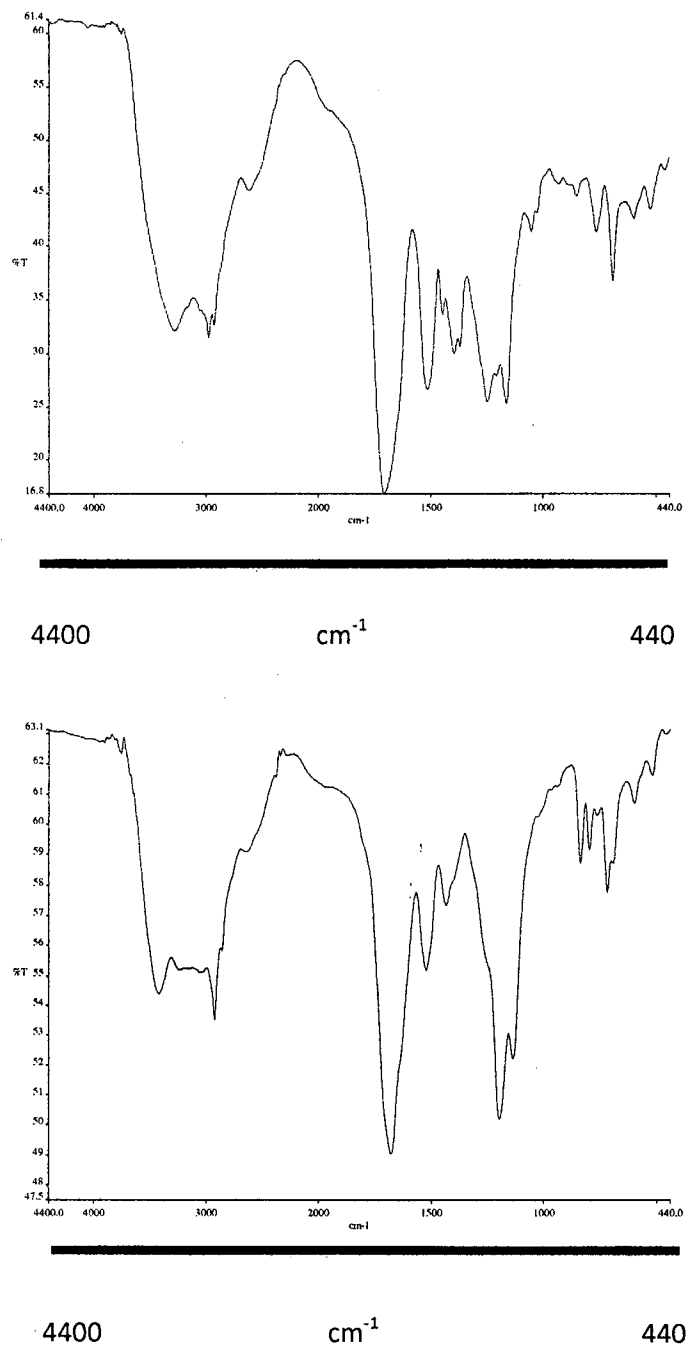
Figure 3-3: Powder FTIR spectra of the peptides (top) Glu-ΔPhe and (bottom) Lys-ΔPhe. The Amide I band carbonyl peaks at 1700 cm-1 and 1690 cm-1 for Glu-ΔPhe and Lys-ΔPhe, respectively. In solution the peak positions shifted to lower frequency suggesting hydrogen bonding with the solvent.
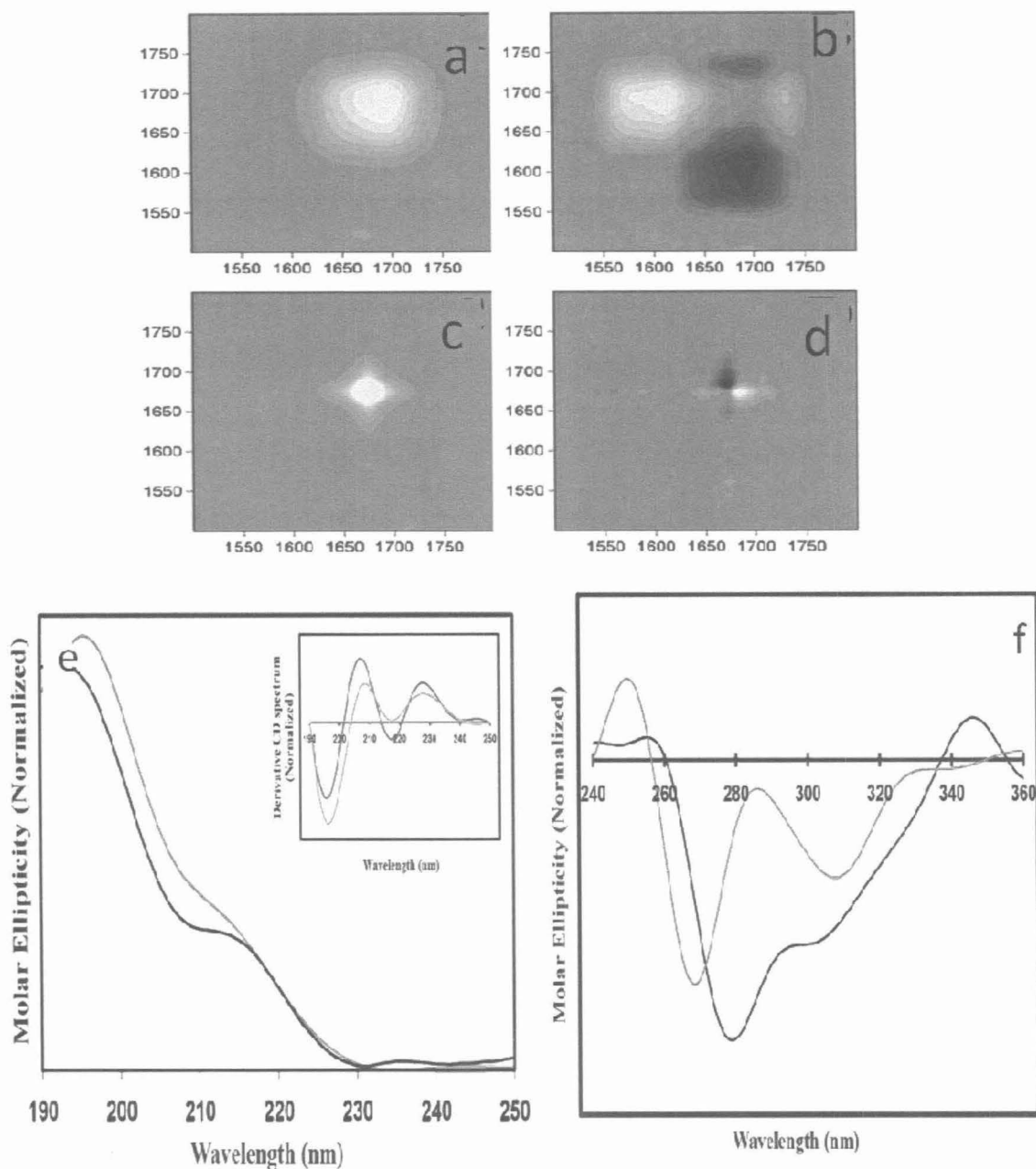
Figure 3-4: Spectroscopic characterization of the molecular structure of nanovesicle forming amphiphilic dipeptides. (a) and (c) 2D-FTIR synchronous map of Glu-ΔPhe and Lys-ΔPhe respectively, (b) and (d)   2D-FTIR asynchronous map of Glu-ΔPhe and Lys-ΔPhe respectively, (e) Far-UV (inset shows 2nd derivative spectrum) and (f) near-UV CD spectrum of the dipeptide nanovesicles formed by Glu-ΔPhe (dark) and Lys-ΔPhe (light) dipeptides.

The 1600cm^{-1} band could not be assigned. The cross peaks occurring in the 2D spectrum of Lys-ΔPhe appeared in the Amide I region and their origin was thus ambiguous [250-253, 270].

The CD spectrum of nanovesicles formed by Glu-ΔPhe and Lys-ΔPhe exhibited positive bands at 217nm (n-π* transition) and at 197nm (π-π* transition) in the far-UV region (Figure 3-4) suggesting a similar backbone conformation for both the amphiphilic dipeptides. However, the deconvoluted near-UV CD spectrum (Figure 3-4) of Glu-ΔPhe is characterized by a band at 280nm (ΔPhe absorption) and a band at 300nm that is assigned to ΔPhe ring stacking interactions [34]. In the near-UV CD spectrum of Lys-ΔPhe, the ΔPhe absorption band position is blue shifted to 267nm and the ring stacking band is red shifted to 305nm pointing out differences in the molecular conformations acquired by the peptides in the vesicular assembly. The observed differences in the molecular conformation of the two dipeptides was not entirely unexpected considering that even small changes at the N-terminus of the dipeptides have been reported to result in different packing arrangements [107-135, 245-248].

In view of the lack of crystal structure data and the ambiguous indications to the conformation of the amphiphilic dipeptides, ab-initio simulation studies were conducted to obtain the probable molecular structures of the investigated dipeptides. The structures were drawn with the biopolymer module of Scigress explorer based on the available information of structural parameters of ΔPhe. The probable molecular structure was then calculated using *in-silico* semi-emperical quantum methods implemented in MOPAC [271, 272]. The calculated potential energy for the lowest energy conformer of Glu-ΔPhe was −364.9 Kcal/mol whereas it was −83.38 Kcal/mol for Lys-ΔPhe. Interestingly, we did not observe any intra-molecular interactions in the resulting structures indicating that inter-molecular interactions stabilized the self-assembled structures. The superposition of the lowest energy structures of the two dipeptides (Figure 3-5) revealed that there was little difference

in the backbone conformation and the ΔPhe ring orientation between the two dipeptides. However, the position of the side chain with respected to the backbone varied greatly between the two dipeptides. Also, the overall topology of the two molecules was different and so was the charge distribution over their vander-wals surface (by virtue of the functional groups present).
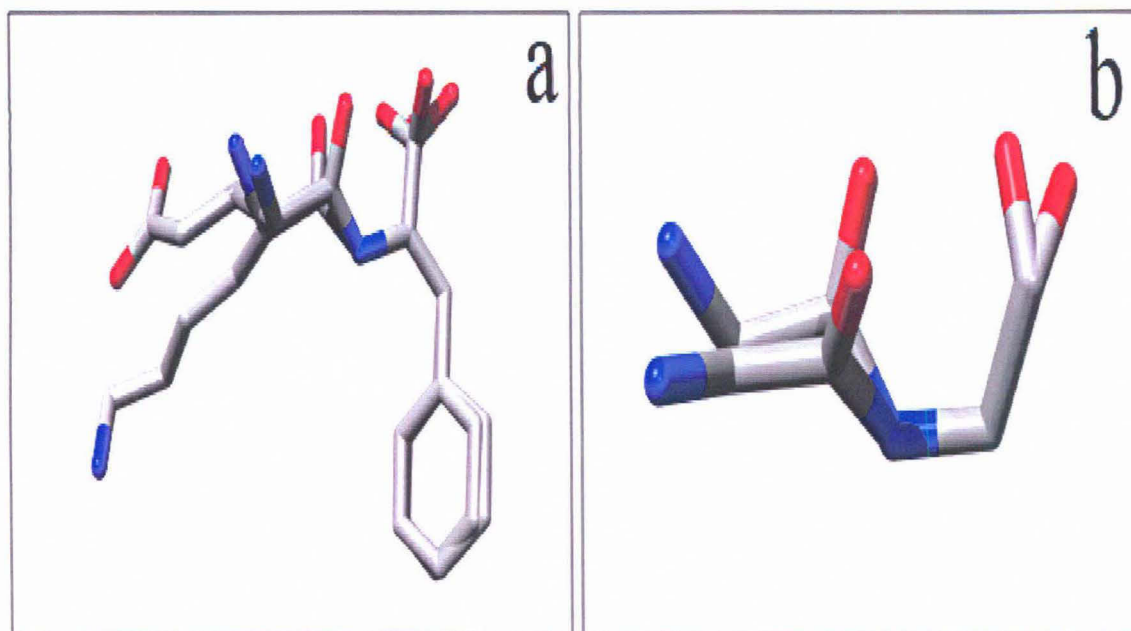

Figure 3-5: The simulated lowest energy structure of the two dipeptides superimposed over each other; (a) whole molecule and (b) backbone only. The probable molecular structure was calculated using *in-silico* semi-emperical quantum methods implemented in MOPAC. The calculated potential energy for the lowest energy conformer of Glu-ΔPhe was –364.9 Kcal/mol whereas it was –83.38 Kcal/mol for Lys-ΔPhe. The superposition of the lowest energy structures of the two dipeptides suggested that there was little difference in the backbone conformation and the ΔPhe ring orientation between the two dipeptides. However, the position of the side chain with respected to the backbone varied greatly between the two dipeptides. No intra-molecular hydrogen bonds were observed.

The above experimental observations and simulation studies tend to suggest that the morphology of the assembled structure depended greatly on the overall molecular structure of the constituent monomer. However, the backbone conformation appeared not to vary greatly in the two amphiphilic dipeptides suggesting that the differences in the morphology of the assembly was probably driven by the altered packing arrangement of the monomers, the side-chain conformation and the charge distribution over the molecule. However, extensive structural characterization would be necessary to discern the molecular mechanism and pattern of assembly.

3.3.5 Stability of nano-assemblies

Surfactant molecules often show self-assembly at critical micellar concentration that is highly dependent on the solvent and temperature conditions. Among the various ways of determining self-aasembly, a change in the molar ellipticity of peptides has often been used as a signature of self-association. We also monitored the change in molar ellipticity of the peptide at 197nm and 217nm as a function of the peptide concentration. The molar ellipticity of the two peptides decreased with the increase in peptide concentration (Figure 3-6) indicative of a concentration dependent assembly.

Resistance to proteolytic degradation is a desirable property in nanoparticles that could have potential biomedical applications. Of many strategies, the introduction of non protein amino acids in peptide sequences provides enhanced stability to proteolytic degradation [152, 157, 159]. Therefore, the proteolytic stability of the nanovesicles formed by the peptide Glu-ΔPhe and Lys-ΔPhe was also investigated. Preformed vesicles were incubated with a highly non-specific proteolytic enzyme, Proteinase K, for 24 hrs at room temperature. The reaction mixtures were subjected to RP-HPLC. We observed that there were no changes in the peak position or the peak area of the peptides. As expected, the results clearly indicated the proteolytic stability of the ΔPhe containing peptide nanovesicles.
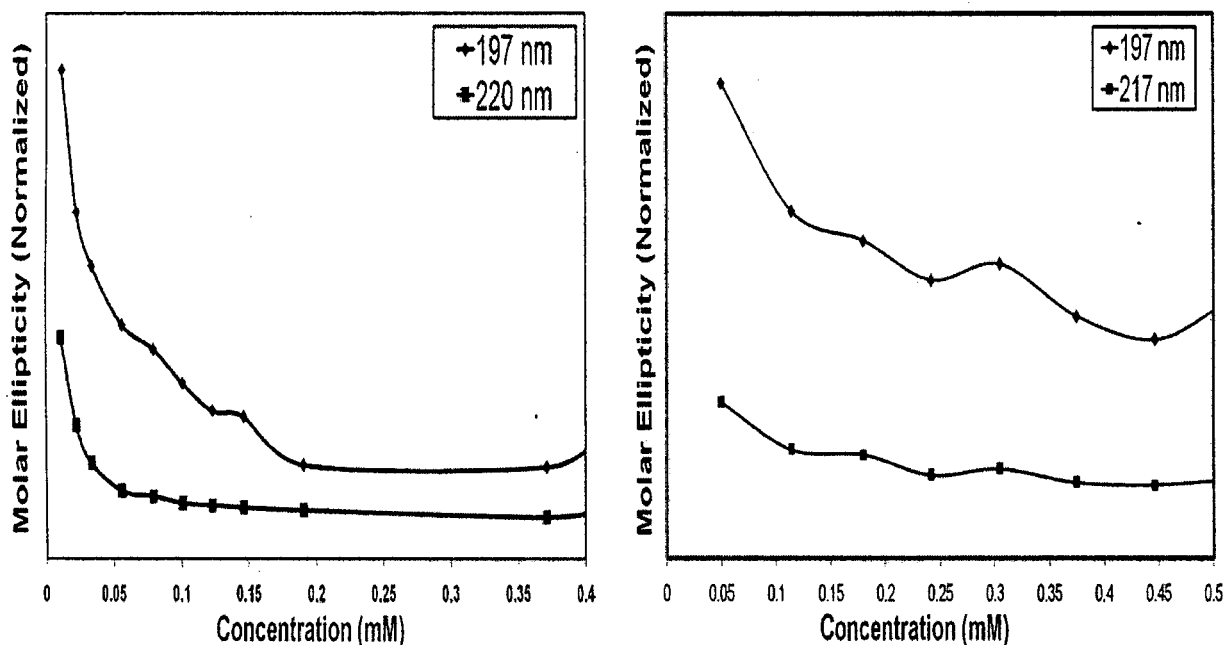
Figure 3-6: The concentration dependent assembly behavior of the peptides, Glu-ΔPhe (right) and Lys-ΔPhe (left), probed by monitoring the decrease in molar ellipticity at 197nm(Π-Π* transition) and 217nm (n-Π* transition).

The presence of monovalent and divalent ions have often be shown to alter the self-assembly behavior either by stabilizing or destabilizing the self-assembled form [61, 273, 274]. The near-UV CD spectrum suggested that addition of physiologically relevant concentrations of monovalent (Na^+) and divalent (Mg^{2+}) to preformed vesicles did not result in any observable destabilization of the assembled structures. The results suggested that the small concentrations of ions were unable to affect the stabilization of the nanostructures resulting from the electrostatic interaction between the monomers.

3.3.6 Encapsulation Studies:

Biomolecule based nanostructures have been considered as excellent carrier systems for delivery of various bioactive molecules into living systems due to their unmatched biocompatibility and their tailorability for targeted delivery [257-266]. Several peptide based self-assembled structures have been described but the ability

of small peptide based vesicles to encapsulate bioactive molecules has remained relatively unexplored. Centrifugation and subsequent quantification of the bioactive molecules spectrophotometrically or by activity assays are the commonly employed techniques to study drug encapsulation in liposomal systems [260]. In order to investigate if the amphiphilic dipeptide based nanovesicles would entrap biomolecules of different sizes, the relevant bioactive molecules were mixed with pre-formed vesicles in an equal weight ratio and then ultra-centrifuged to separate the entrapped molecules from the free molecules. Concentrations of the free molecules were subsequently quantified in the supernatant by UV-Visible spectroscopy and the results were expressed às % encapsulation (Table 3-1). Small commercially available drug molecules were first tested for encapsulation. The results indicated that riboflavin (cLogP = −1.9) was effectively encapsulated in both the vesicles (45% w/w in anionic and 40% w/w in cationic vesicles). On the other hand, Vitamin B_{12} (cLogP = 5) was encapsulated preferentially in the anionic vesicles (28% w/w in anionic and 8% w/w in cationic vesicles). However, other drug molecules like amodiaquin (antimalarial) (cLogP = 3.7), ampicillin (antibiotic) (cLogP = 0.4) and mitoxantron (anticancer) (cLogP = −3.1) were not encapsulated in either of the vesicle.

Many porphyrin molecules and their derivatives are being used as drugs of photodynamic therapy (PDT). Hemin (651 Da) (Fluka) was used as a model compound for investigating the entrapment of porphyrin molecules within the self-assembled vesicles. Ultracentrifugation and electron micrographs (Figure 3-8) showed that hemin was entrapped almost equally in both the vesicles (56% w/w in cationic and 60% w/w in anionic). However, from the limited examples no correlation could be established between the biophysical characters (viz: size, charge or hydrophobicity) of the biomolecules and their entrapment in the peptide vesicles.

Table 3-1: Percentage encapsulation of different proteins in the self-assembled vesicles.

drug	encapsulation, % (w/w)		drug	encapsulation, % (w/w)	
	Lys-ΔPhe	Glu-ΔPhe		Lys-ΔPhe	Glu-ΔPhe
vitamin B_{12}	8	28	Pf MSP-3N	14	12
hemin	56	60	Pf HRP-II	5	24
insulin	61	5	BSA	11	15
synthetic antimicrobial peptide	73	41	lysozyme	40	80
riboflavin	40	45	anti-mouse IgG	20	80
Pf MSP-1_{19}	20	20			

Development of bioactive peptides and proteins as potential drugs has met with limited success mainly due to their short *in vivo* half-life [275 and references therein]. Encapsulation of peptides in delivery vehicles is one way to overcome, atleast partially, this hurdle. We therefore investigated if bioactive peptide and proteins could be encapsulated in the self-assembled vesicles (Figure 3-8). The peptides and proteins under investigation were tagged with FITC prior to mixing them with the preformed vesicles and ultracentrifugation. The degree of encapsulation was estimated by quantifying the concentration of the free molecules by measurement of fluorescence intensity. We found that insulin (5.8kDa) was preferentially entrapped in the cationic vesicles (Lys-ΔPhe; 61% w/w) but not in the anionic vesicles (Glu-ΔPhe; 5% w/w). On the other hand, a synthetic decapeptide (1.5kDa) with strong anti-bacterial activity synthesized in our laboratory was encapsulated appreciably in both vesicles (73% w/w and 41% w/w in cationic and anionic vesicles respectively).
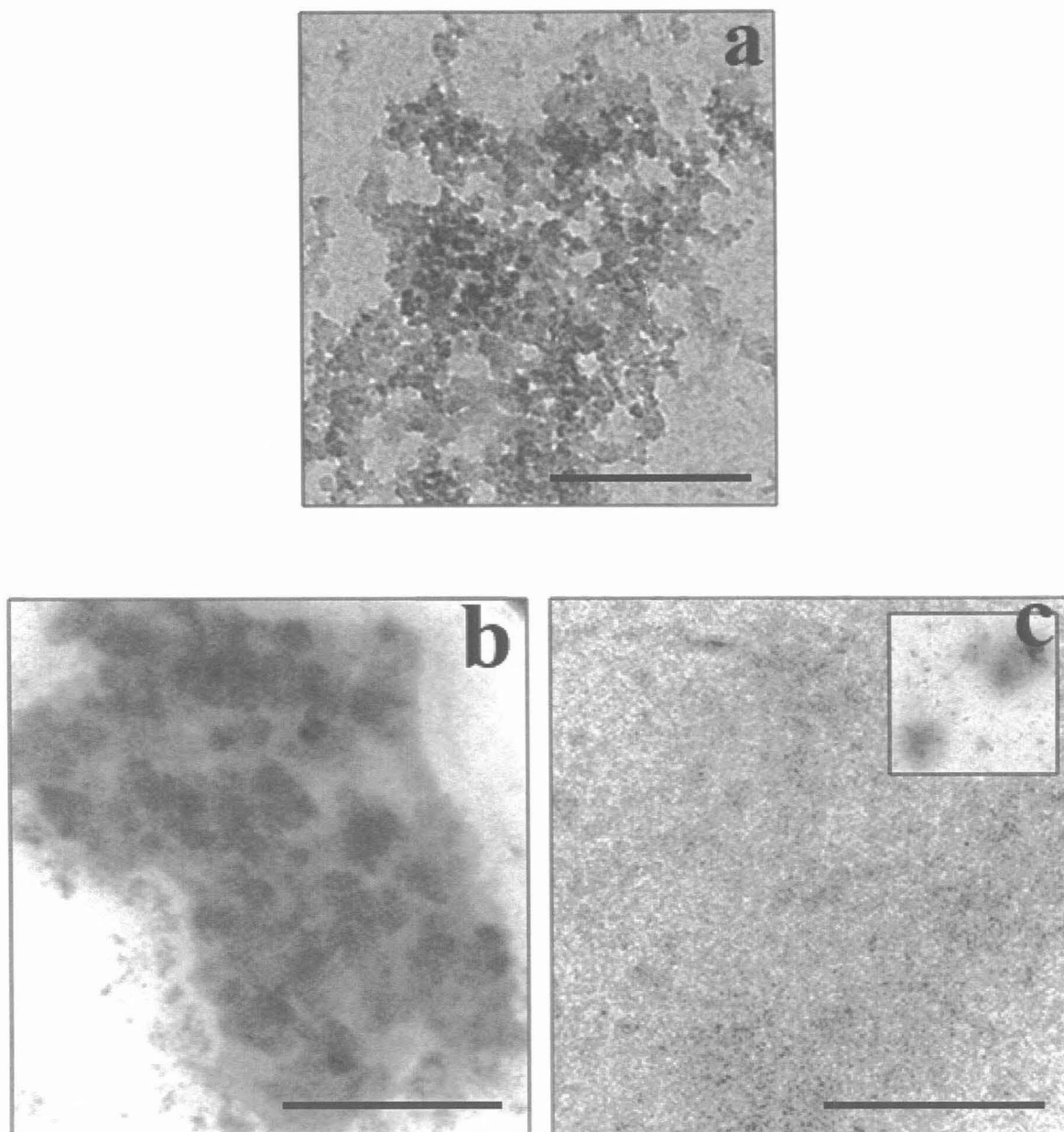
Figure 3-7: The encapsulation of (a) Hemin in the self-assembled vesicles of (b) Glu-ΔPhe and (c) Lys-ΔPhe. Hemin was used as a model porphyrin molecule to test whether porphyrin derivative that are used for photodynamic therapy could be entrapped within the self-assembled vesicles.
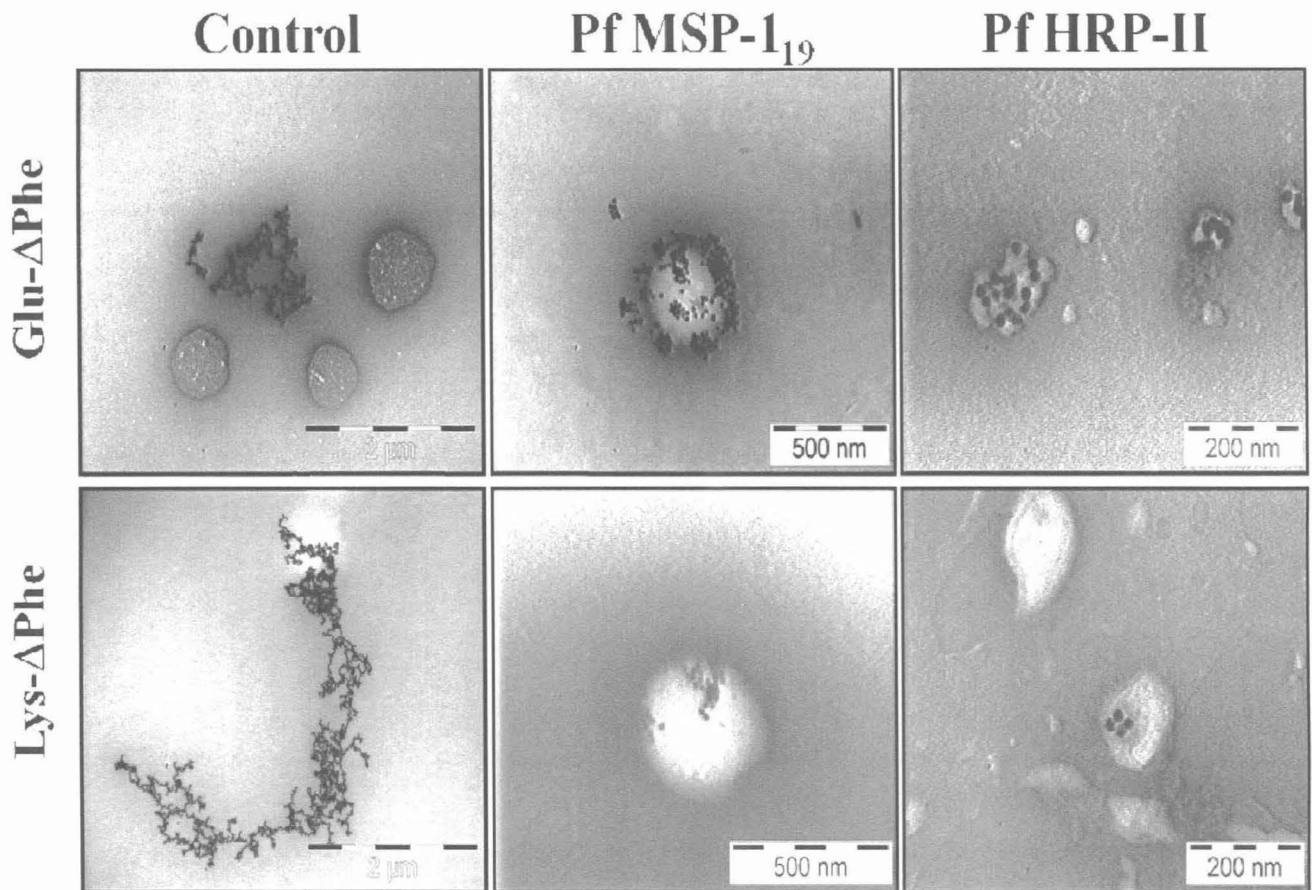
Figure 3-8: Figure showing the encapsulation of two *P.falciparum* proteins into self-assembled nanovesicles. The target proteins were conjugated to 20nm gold particles, mixed with preformed vesicles and then spotted on a TEM grid, stained with uranyl acetate and imaged .The protein Pf HRP- II appeared to be encapsulated within both the vesicles, whereas Pf MSP-1_{19} appeared to localize preferentially on the surface of both the kinds of vesicles. As control, non-conjugated gold nano-particles showed no entrapment by the vesicles.

The ability of the vesicles to entrap proteins of various sizes was also investigated. To do this well characterized protein molecules of different sizes were used, including recombinant malaria vaccine candidates developed in our laboratory, namely merozoite surface protein-1$_{19}$ (Pf MSP-1$_{19}$, 11.2kDa)[276], merozoite surface protein-3N (Pf MSP-3N, 25kDa)[unpublished work] and *P. falciparum* histidine rich protein-2 (Pf HRP-2, 32.9kDa)[277], in addition to chicken egg lysozyme (16.2kDa), bovine serum albumin (BSA, 66.4kDa) and anti-mouse goat IgG (~150kDa). Ultracentrifugation followed by quantification of proteins by fluorescence spectroscopy showed that all proteins interacted with the nanovesicles to varying degrees (Table 3-1).

There were differences in the interactions of protein molecules with the two vesicles. For example, lysozyme and IgG both showed higher affinity for Glu-ΔPhe vesicles than Lys-ΔPhe vesicles. However, ultracentrifugation experiments were not able to reveal whether the vesicle structures were stable upon interaction with the proteins. To investigate if the proteins were indeed encapsulated in the vesicles, the target proteins were conjugated to 20nm gold particles, mixed with preformed vesicles and then spotted on a TEM grid, stained with uranyl acetate and imaged. We first showed that non-conjugated gold nano-particles were not entrapped by the vesicles (Figure 3-9). The protein Pf HRP- II was encapsulated within both the vesicles (Figure 3-9), whereas Pf MSP-1$_{19}$ appeared to localize preferentially on the surface of both the kinds of vesicles (Figure 3-9). However, TEM studies seemed to suggest that other proteins like BSA, lysozyme, Pf MSP-3N and IgG destabilized the structural integrity of the self-assembled nano-vesicles (Figure 3-10). Results of the above studies suggested that while protein molecules interacted with the peptide vesicles, in most cases the structural integrity of the vesicles was compromised. It also appeared that encapsulation of bioactive molecules in the peptide vesicles cannot be predicted and would need to be determined case by case.
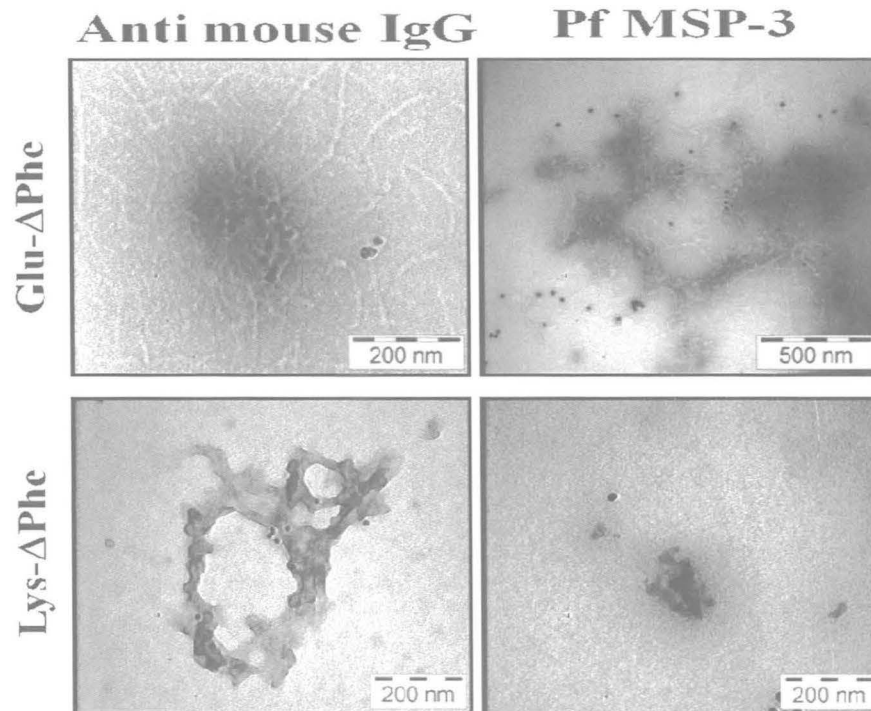
Figure 3-9: Figure showing the encapsulation of few proteins that disrupt the vesicular architecture.

3.3.9 Cellular uptake and cytotoxicity of nanovesicles:

Cellular uptake of nanovesicles into cells has been of primary importance for their development as delivery vehicles. In order to investigate if nanovesicles could be taken up by metabolically active cells, HeLa cells were incubated for 4-24 hrs with the nanovesicles loaded with the fluorescent dye PKH2[278]. Fluorescence microscopy of the cells revealed that the nanovesicles could be internalized by the cells in culture (Figure 3-10). The control cells where an equal amount of dye was added directly to the growing culture did not show any fluorescence. Nanoparticles have often been associated with severe cytotoxic effect[279]. Vero cells were incubated with the peptide vesicles, followed by washing and staining with imido black dye. The relative concentration of the adherent cells was assayed spectrophotometrically. There was

no observable difference in morphology and count of the treated cells compared to cells in the control set (Figure 3-11). The results suggested that described peptide vesicles could have potential applications as delivery systems.
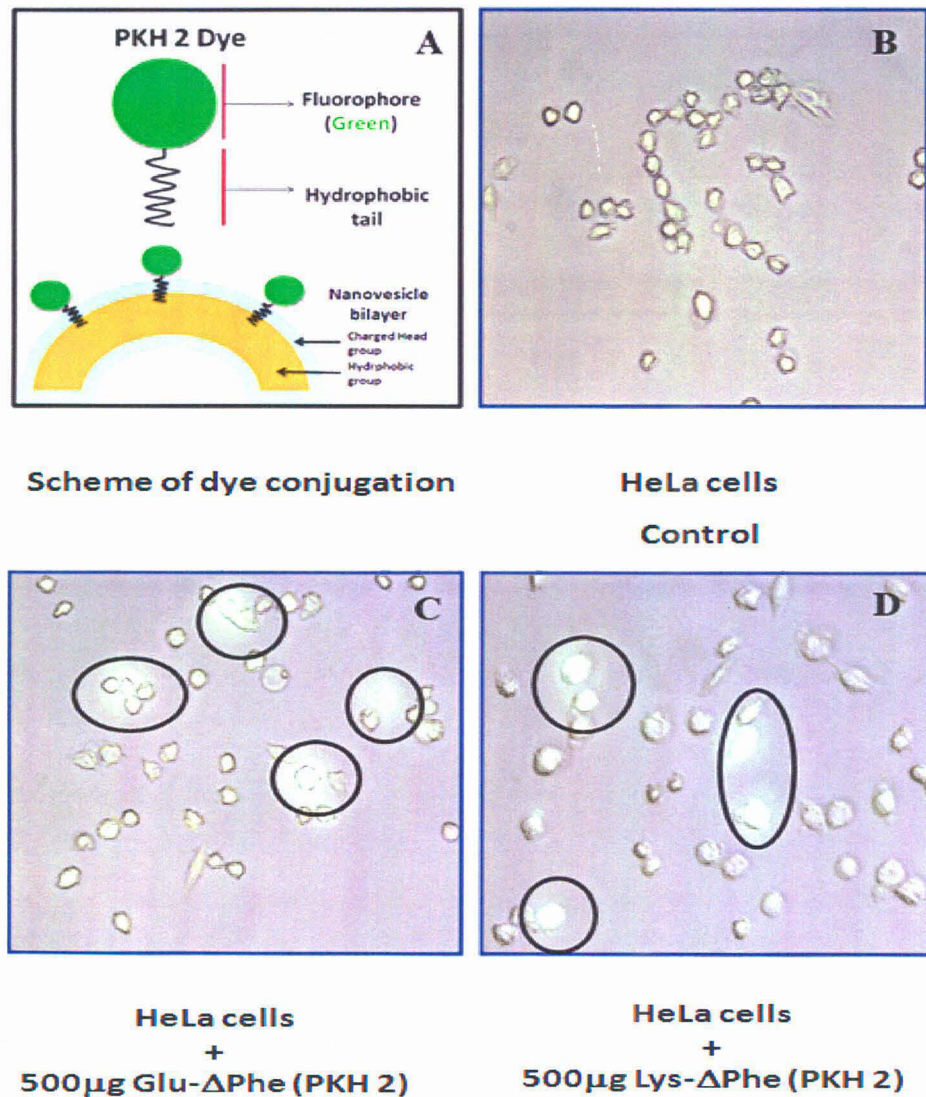
Figure 3-10: Fluorescence and Optical images exhibiting the uptake of fluorescent probe labeled peptide vesicles into HeLa cells after 6hrs. The circled areas show the heavy uptake of the fluorescently labled nanoparticles by the metabolically active cells.
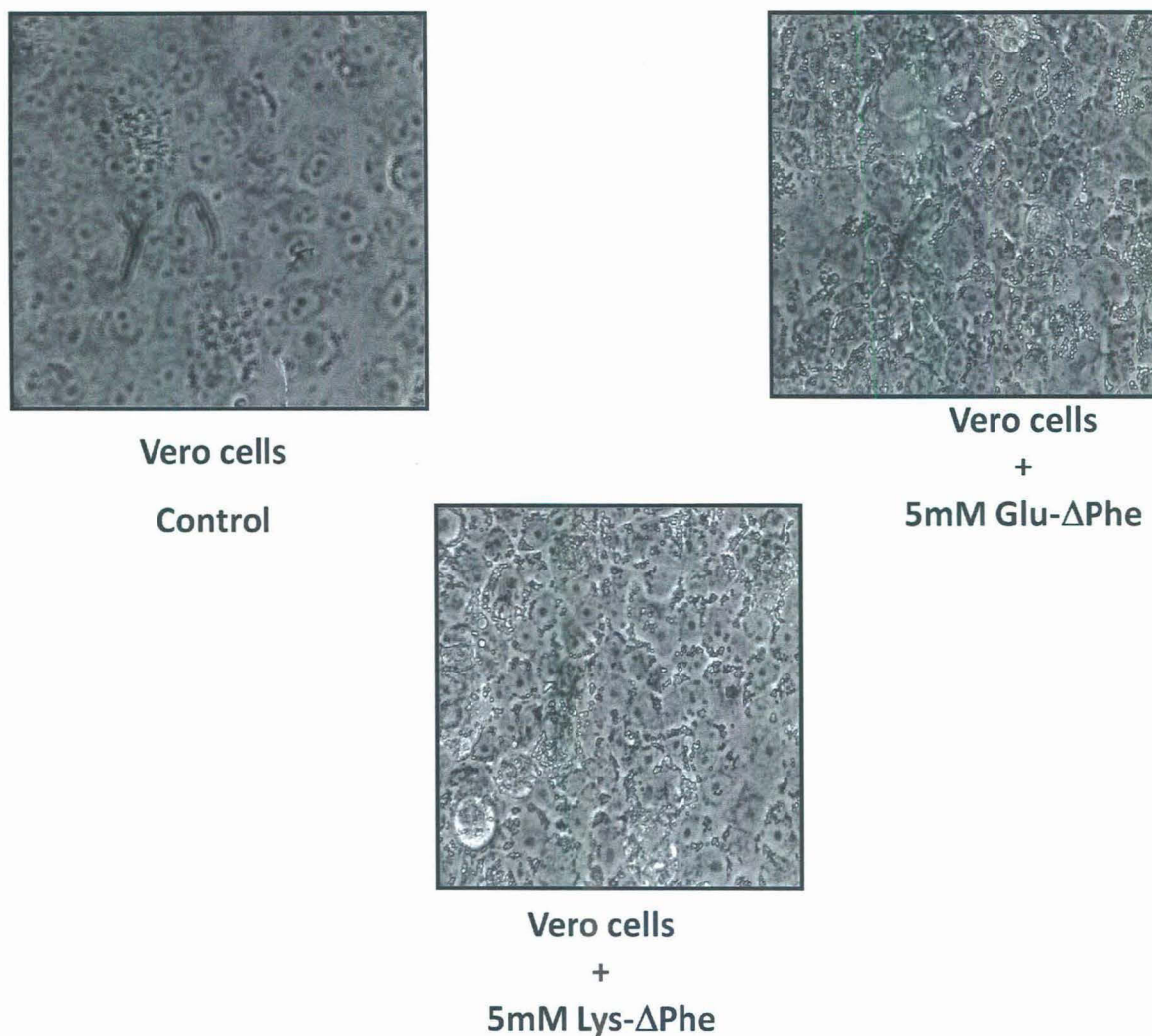
Vero cells

Control

Vero cells

+

5mM Glu-ΔPhe

Vero cells

+

5mM Lys-ΔPhe

Figure 3-11: Optical micrographs of Vero cells (left) treated with Glu-ΔPhe (middle) and Lys-ΔPhe (right). The images suggested no apparent cytopathic effect of the vesicle forming peptides. The morphology as well as the number of cells in a field scan appeared to be comparable to the control.

3.3.10 Ionization dependent shape change of the vesicles

The effect of pH (and thus the role of ionization of specific functional groups) on the morphology of the assembly of the two amphiphilic dipeptides was subsequently investigated. The calculated titration [280-282] curve for the dipeptide Glu-ΔPhe

suggested deprotonation of C-terminus carboxyl group at pH=3.8, side-chain carboxyl group at pH=4.2 and N-terminus at pH=8.1. However, for the dipeptide Lys-ΔPhe, the deprotonation of C-terminus was expected to occur at pH=3.6, side-chain at pH=10.4 and terminal amine group at pH=7.3. The assembly behavior of the anionic dipeptide Glu-ΔPhe was studied at pH=1, 4, 7 and 11 and at pH=1, 7, 9 and 11 for the cationic dipeptide, Lys-ΔPhe, to test if the self-assembled structures could have potential use in triggered drug release applications. The ionization dependent effects on self-assembly was probed by CD, TEM and simulation studies (Figure 3-12, 3-13, 3-14). The near-UV CD spectrum of the assemblies formed by Glu-ΔPhe exhibited a positive band at 285nm at pH=1. The position and intensity of the peak decreased only slightly (15%) at pH=4 suggesting only minor changes in the packing of the aromatic moiety in the assembly. This feature was markedly different from the spectrum at pH=7 suggesting a major reorganization in the packing arrangement of the monomers in the assembly that would reflect on the morphology of the nanovesicles. Interestingly, the electron micrographs of the peptide at pH=1 showed clusters of small vesicular structures with a mean diameter of 20nm. The vesicles did not appear as discrete particles and exhibited a propensity to fuse with each other unlike the vesicles formed at neutral pH. At pH=4, the smaller vesicles appeared to fuse with each other resulting in highly pleomorphic larger structures with a size range of 50-100nm. However, at pH=11 the near-UV CD spectrum was characterized by a negative band at 275 nm with a decrease in intensity compared to the spectrum at pH=7. At alkaline pH, the peptide resulted in clusters of fibrillar assemblies of non-homogenous diameter ranging between 10-30nm. The fibrils had length over microns and exhibit characteristic twisting, curving and branching. Thus, it appeared that the ionization status of the N-terminus amine group and the side-chain carboxyl group had a major influence on the assembly pattern of the anionic dipeptide. However, the ionization state of the C-terminal carboxyl group affected only the size of the assemblies.
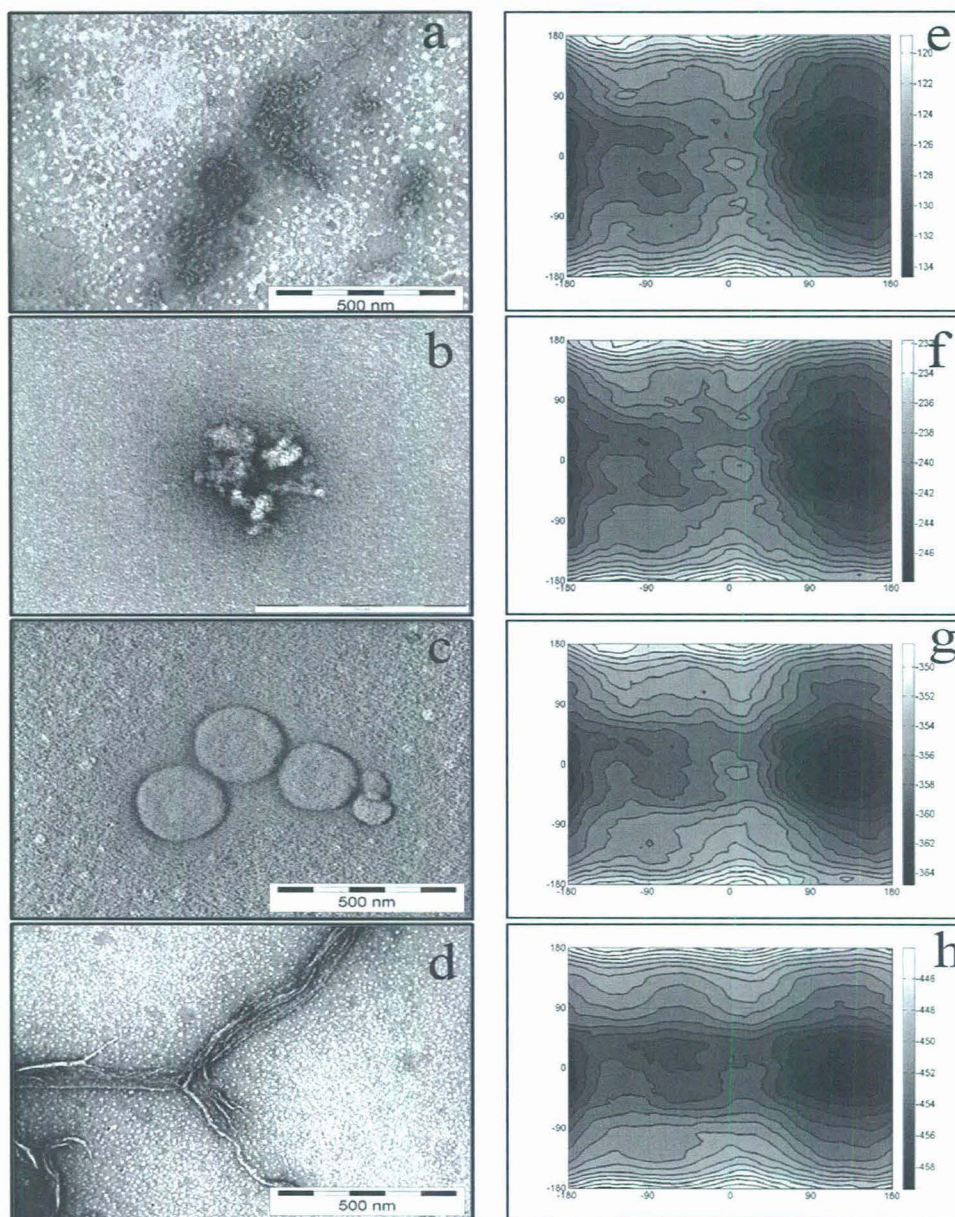
Figure 3-12: Figure showing the morphology of the self-assembly and the backbone conformation landscape of Glu-ΔPhe. (a)(e) pH=1, (b)(f) pH=4, (c)(g) pH=7, (d)(h) pH=11. It was evident that there was no apparent change in the backbone conformation at different ionization states of the molecule.

*The x-axis and y-axis of the conformational map represents Dihedral angle 1 (degree) and Dihedral angle 2 (degree). The z-axis represents Potential energy (Kcal/mol)
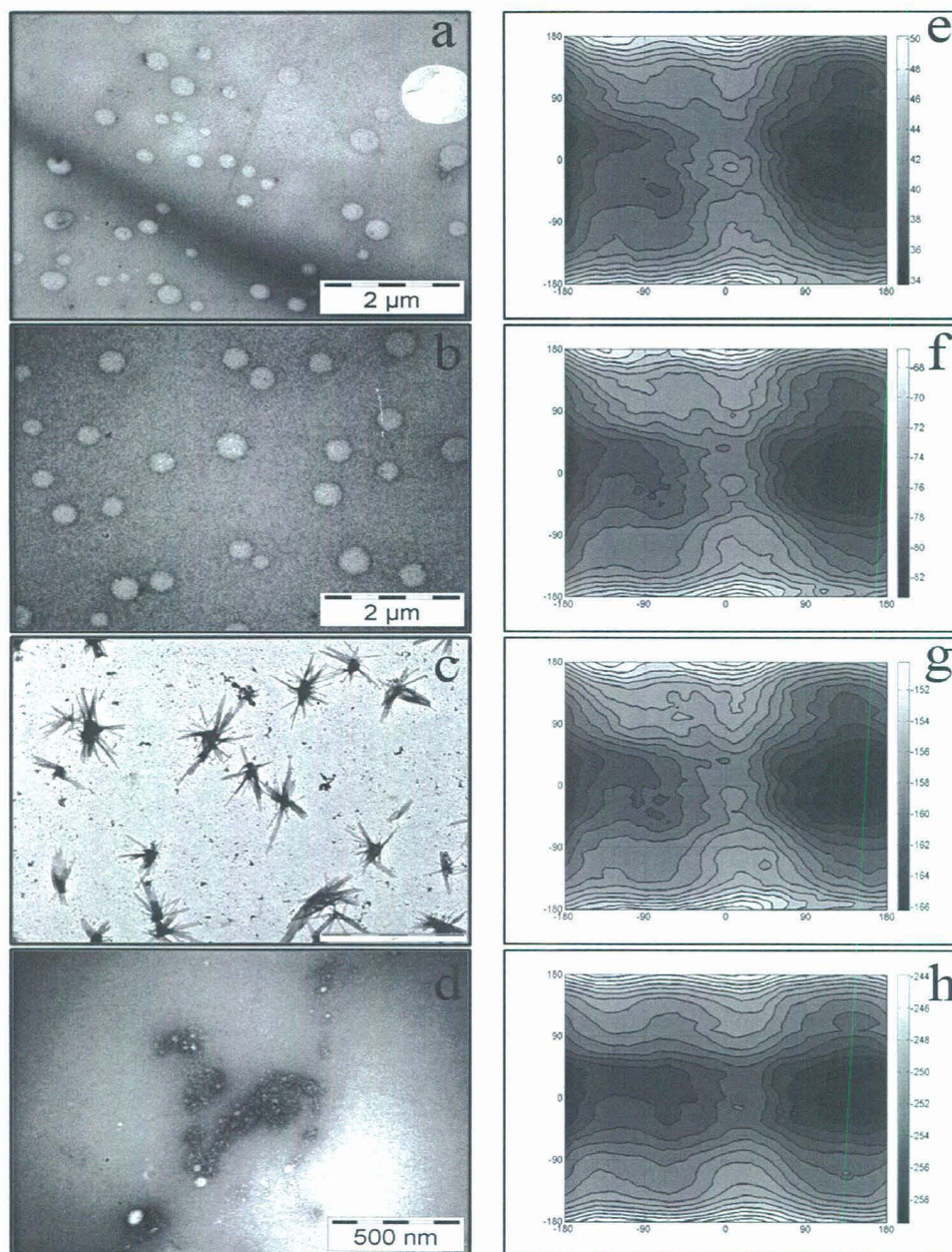
Figure 3-13: The morphology of the self-assembly and the backbone conformation landscape of Lys-ΔPhe. (a)(e) pH=1, (b)(f) pH=7, (c)(g) pH=9, (d)(h) pH=11. It was evident that there was no apparent change in the backbone conformation at different ionization states of the molecule.

*The x-axis and y-axis of the conformational map represents Dihedral angle 1 (degree) and Dihedral angle 2 (degree). The z-axis represents Potential energy (Kcal/mol)
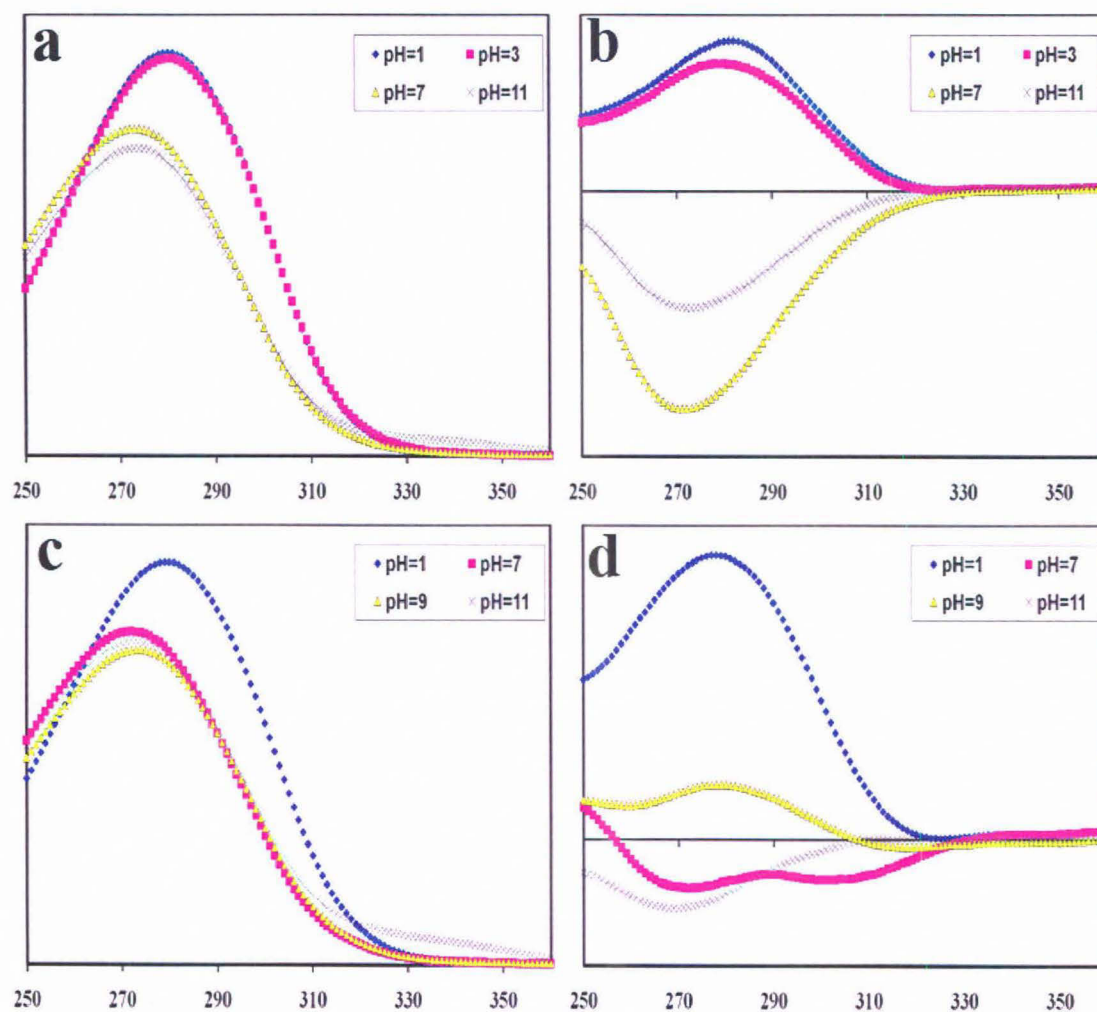
Figure 3-14 : Absorption spectrum of the nano-assemblies of (a) Glu-ΔPhe and (c) Lys-ΔPhe; Near-UVCD spectrum of the nan-assemblies of (a) Glu-ΔPhe and (c) Lys-ΔPhe. The results were indicative of major reorganization of the stacking interactions under different ionization states of the two amphiphilic dipeptides.

(* The concentration of the peptide in each case is constant)

In a similar fashion, the assemblies formed by Lys-ΔPhe also exhibited changes in the near-UV CD spectrum at different pH (Figure 3-14) clearly suggesting that the ionization status of the molecule affects the nature of the assembly. At pH=1, the spectrum was characterized by a positive band at 280nm. At this pH, the electron micrographs suggested that the peptide assembled into vesicular structures with a size range of 50-300nm and an average diameter of 200nm. As described earlier, the peptide assembled as vesicles with a mean diameter of 400nm and exhibited a CD spectrum with peaks at 275nm and 310nm at neutral pH. At higher pH (=9) a very low intensity positive band with peak at 280nm was observed in the near-UV CD spectrum and electron micrographs showed star shaped fractaline assemblies associated with apparently amorphous structures suggesting the important involvement of the N-terminus in stabilizing the vesicular assemblies probably through intermolecular electrostatic interactions. Interestingly, at still higher pH (=11) where even the side-chain amine group was deprotonated, the CD spectrum showed a weak negative band at 270nm and clusters of 2-8nm sized assemblies. This suggested the crucial role of the ionization status of amine groups in dictating the transformation of the assembly from one form to another. As in the assemblies of Glu-ΔPhe, the ionization of the C-terminus of the dipeptide Lys-ΔPhe affected only the size of the vesicles.

3.3.11 Simulation studies to probe the role of ionization status on molecular structure

In order to understand the molecular basis of the observed pH dependent shape-shifting in the dipeptide vesicles, we performed simulated the probable conformation of the peptides in water using semi-emperical quantum calculations (MOPAC) [271,272]. Interestingly, we observed that there were no significant variations in the potential energy surfaces of the peptides at the different ionization states (at different pH) (Figure 3-12, 3-13). Also, the superposition of the backbone atoms of

the simulated lowest energy structures of the dipeptides at the different ionization

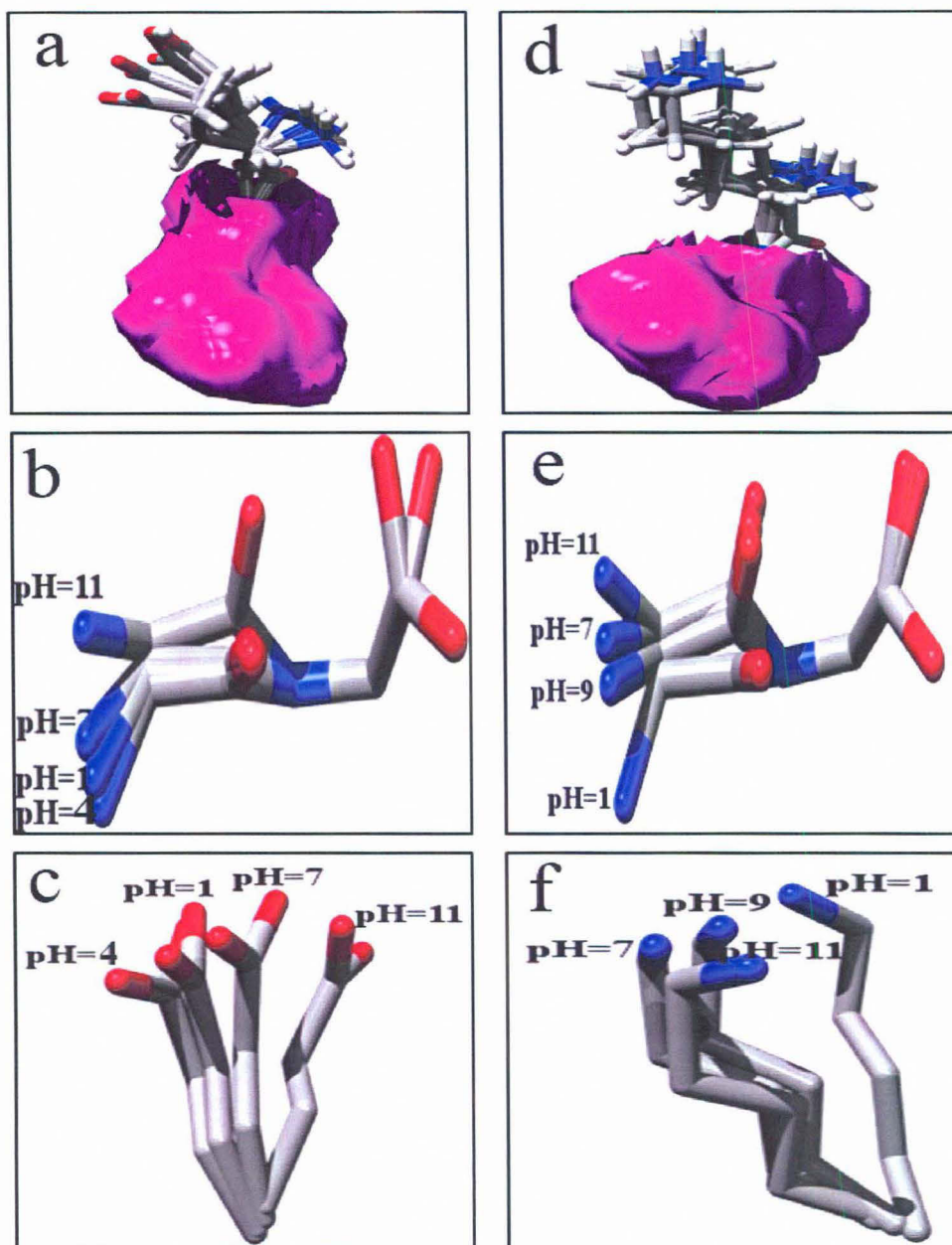states showed insignificant differences between them (Figure 3-15, Table 3-2).

Figure 3-15: Figure showing the superimposition of the lowest energy structures of (a-c) Glu-ΔPhe, and (d-f) Lys-ΔPhe. (a,d) Superposition of all atoms (the surface of the ΔPhe ringhas been colored); (b,e) Superposition of only backbone atoms; (c,f) superposition of only side chain atom. (* H-atoms have not been shown for clarity)

This suggested that the backbone conformation of the dipeptides was not affected by the ionization status of the molecule and hence had no important role in the pH mediated shape changes of the nanostructures. However, it was interesting to observe that the positions of the side-chain groups with respect to the backbone varied significantly (Figure 3-15) at different pH for both the dipeptides with relatively high RMSD values (Table 3-2). Such differences in the molecular structure would in the overall topology of the molecule. Thus, the differences in molecular topology coupled to the changes in the charge based inter-molecular interactions appeared to be the guiding forces for the observed shape changes of the assemblies formed by the two dipeptides.

The results were interesting from the molecular structure point of view. It has been widely believed that back-bone interactions dominate the structural preference in a sequence and side-chains orientations influence only local packing of the structure. However, studies suggested that in a peptide fragment derived from yeast Sup35 protein, both back-bone and side-chain contributed to the enthalpic barrier [283, 284]. Though the back-bone hydrogen bonds favored an anti-parallel arrangement, the interactions between the side-chains favored a parallel aggregate by -6.5 kcal/mol. Other studies provide evidence for the influence of a small number of site-specific hydrophobic interactions (of the side-chains) on the packing of the peptide molecules in the assemblies [285]. Interestingly, molecular studies on the dipeptide Ile-Ile demonstrated that the ionization status of the molecule influenced the hydrogen-bonding capabilities, conformational properties and molecular packing arrangement of the peptide in the crystal [117]. However, the simulation studies on Glu-ΔPhe and Lys-ΔPhe pointed towards a relatively stable back-bone conformation in the different ionization states of the molecule. This could be attributed to the conformation restriction at the side-chain and the back-bone introduced by the C-terminal ΔPhe residue. This also suggested the crucial role of the side-chain interaction and thus, indirectly the important role of the ionization state of the molecule in dictating the structure of the assembly.

Table 3-2 : Tabulated results of RMSD for the lowest energy structure of the peptide under different ionization states.

(a) Glu-ΔPhe

Backbone Atoms

pH	1	4	7	11
1	0	0.013	0.004	0.038
4	0.013	0	0.016	0.026
7	0.004	0.016	0	0.004
11	0.038	0.026	0.004	0

Side-chain Atoms

pH	1	4	7	11
1	0	0.285	0.338	0.287
4	0.285	0	0.613	0.53
7	0.338	0.613	0	0.342
11	0.029	0.53	0.342	0

(b) Lys-ΔPhe

Backbone Atoms

pH	1	7	9	11
1	0	0.009	0.038	0.039
7	0.009	0	0.03	0.035
9	0.038	0.03	0	0.002
11	0.039	0.035	0.002	0

Side-chain Atoms

pH	1	7	9	11
1	0	2.67	0.773	2.81
7	2.67	0	0.247	3.777
9	0.773	0.247	0	1.087
11	2.81	3.777	1.087	0

3.3.12 Entrapment and pH mediated release of drugs from the nano-vesicles

Having established the crucial role of the ionization status of the molecule, at the different pH, on the nature of the self-assembly, the release of encapsulated drugs from the vesicles under pH trigger was investigated. For this the model anti-cancer compound doxorubicin was entrapped in the vesicles at neutral pH. The choice of doxorubicin was driven by the unique fluorescence shielding property of the compound upon entrapment [286]. The results indicated that doxorubicin was entrapped into nanostructures formed by the amphiphilic dipeptides maximally at pH=7 (Figure 3-16). However upon changing the pH, the drug was released from the vesicles to varying degrees (Figure 3-17). We made no systematic investigation to

probe the exact factors governing entrapment and release of the drug from the nanostructures. However, molecular interactions between the drug and the peptide molecules, as well as the size and shape of the nanostructures were expected to be the prevailing factors for the entrapment and release. Subsequent experiments are being conducted in the lab to discern the molecular basis of the phenomenon.
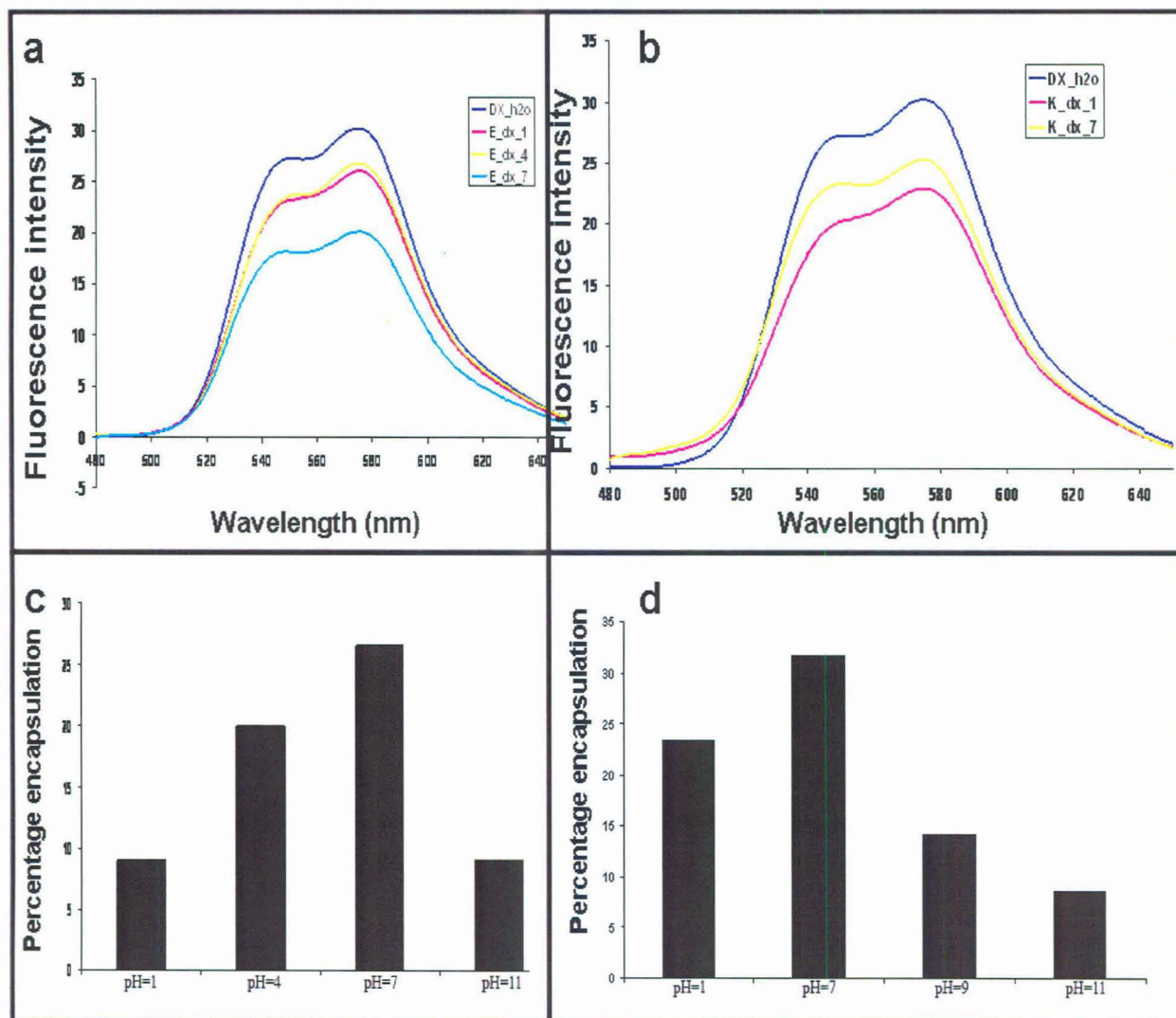

Figure 3-16: (a) and (b) Fluorescence spectrum of entrapped doxorubicin in the self-assemblies of Glu-ΔPhe and Lys-ΔPhe, respectively. (c) and (d) Percentage of doxorubicin entrapment calculated from fluorescence shielding in (a) and (b). Maximum entrapment of doxorubicin in the nano-vesicles occured at pH=7.
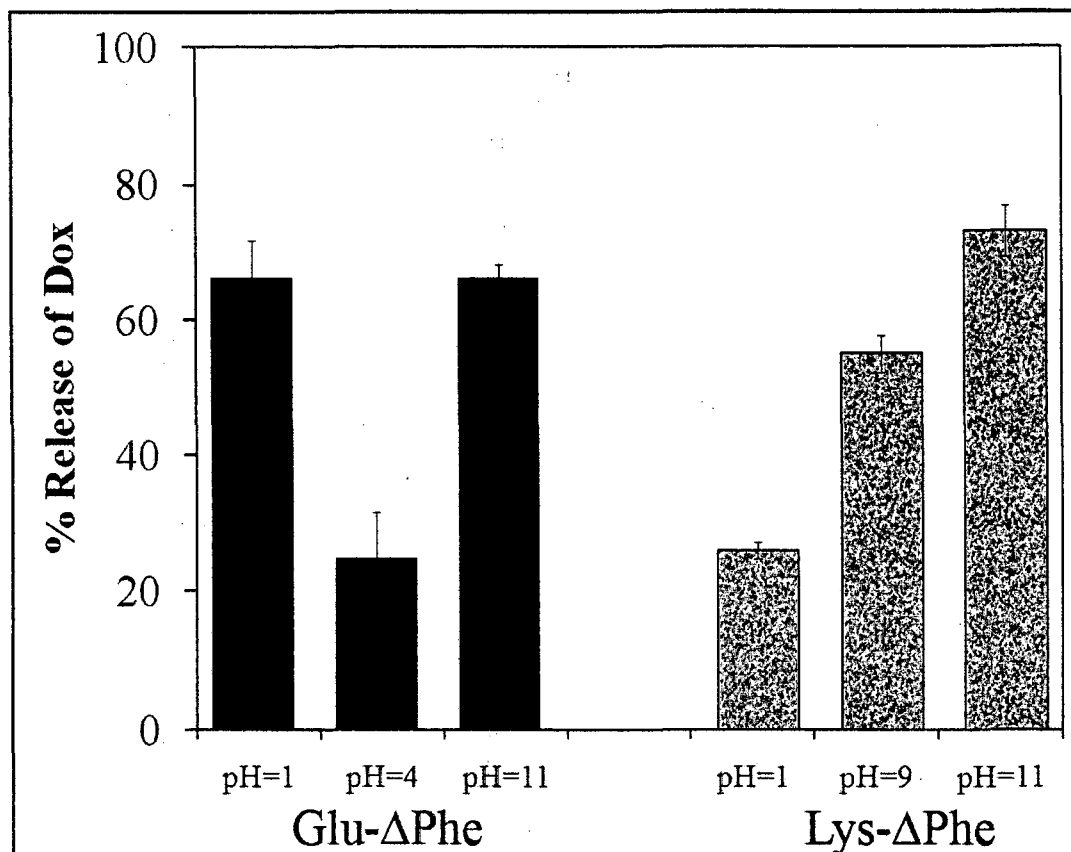
Figure 3-17: Figure showing the percentage release of doxorubicin at different pH from nanovesicles of (a) Glu-ΔPhe and (b) Lys-ΔPhe. The results suggested that entrapped drugs could be released from the vesicles under pH stimulus.

3.4 Conclusion

The bottom-up approach to nano-fabrication of higher order structures is being widely acknowledged as a potent method for developing novel bio-inspired materials. Small peptides offer a myriad of potential applications to nanotechnology but their relative instability to proteolysis is a major concern in realizing their potential application in biomedical sciences. The main aim of the present work was to explore the possibility of using non-protein amino acids, capable of providing well-

defined conformational characteristics and higher stability, particularly to enzymatic degradation, in design of supra-molecular assemblies. The studies showed the ability of very small amphiphilic peptides to spontaneously self-assemble into vesicular structures that are resistant to proteolytic degradation. In addition the peptide vesicles could entrap small drug molecules and a few polypeptides and release them under suitable pH stimulus. They were not toxic to cultured cells and were easily taken up by HeLa cells. The designed peptides were small and simple examples of amphiphilic structures that can be good model systems for the basic understanding of self-assembly. The described peptide structures were easy to synthesize, cost effective and offer novel scaffolds for future design of nano-structures with potential application.

Chapter 4

Self-assembling aromatic dipeptide Phe-
ΔPhe as an amyloid mimick.

4.1 Introduction

Alzheimer disease is a progressive, neurodegenerative disorder characterized by amyloid deposition in senile plaques in the cerebral parenchyma and vasculature [286, 287]. These plaques are composed primarily of fibers of the amyloid β-protein fragment Aβ(1-40)or Aβ (1-42). Aβ is derived by proteolytic processing of the 110-to 130-kDa amyloid precursor protein (APP) within the acidic intracellular compartments such as the early endosomes or distal Golgi complex [288, 289]. Aβ is a normal constituent of human plasma and cerebrospinal fluid [290, 291] and is secreted by a variety of cultured cells, including primary neuronal and non-neuronal cells [292, 293]. In vivo, senile plaques containing dense cores of fibrillar Aβ are intimately associated with areas of neuronal loss, dystrophic neurites, and gliosis [286]. A number of studies have provided information on the structure of fibrils and on factors affecting fibril formation. Electron microscopy (EM) of amyloid plaques has revealed straight or slightly curved fibers 6-10nm in diameter and of indeterminate length [294, 295]. X-ray diffraction studies have demonstrated that these fibers assembled in a cross β-pleated sheet structure [296, 297]. Circular dichroism (CD) and Fourier-transform IR spectroscopic analyses of these fibers have confirmed their β-sheet secondary structures [298-300]. Synthetic full length Aβ peptides form fibers ultrastructurally indistinguishable from those isolated from the brain [296, 297]. However, numerous studies have also demonstrated that short 5-8 residue fragments of Aβ could also assemble *in vitro* into fibers albeit the dimensions of those varied slightly from the natural occurring fibers.

Biochemical and mutational studies on the central hepta-peptide region of Aβ i.e. H-KLVFFAE-OH (Aβ$_{16-22}$) have indicated that this region was critical for fibrillization [320, 322-332]. Moreover, theoretical studies on Ac-KLVFFAE-OH have simulated atomic level intercations involved in Aβ- dimer formation therby providing a detailed picture of forces that drive the interaction between the fragments [332]. The studies suggested that at physiologically relevant temperature (310 K) an anti-parallel dimer was

favored. The backbone contact of the central region of the sequence i.e. Phe[19]-Phe[20] between two molecules of the peptide drove the dimer formation. The results were highly consistent with the proposition that the diphenylalanine motif formed the core region responsible for Aβ fibrillization [76]. Further, the residue level contact map for backbone-backbone and side chain- side chain interactions in the anti-parallel strand orientation revealed a strong hydrophobic interaction between the side-chains of Phe residues with the aromatic stacking interactions providing a favorable energetic contribution as well as directionality [75 and references therein].

Similar to the predominant role of the aromatic interaction in the fibrillization of Aβ, studies also have brought out the crucial role of the aromatic phenylalanine residue in promoting fibrillization of the human islet amyloid polypeptide (hIAPP) [309, 321]. hIAPP (or amylin) is a 37-residue polypeptide hormone that is produced by pancreatic β cells and play a central role in glucose homeostatis. The peptide has been shown to form amyloid fibrils *in vitro* and to exert a cytotoxic effect to pancreatic β cells in culture. A six residue peptide fragment of hIAPP i.e. NFGAIL, has been demonstrated to form amyloid fibrils that are similar to those formed by full length peptide [309] thus qualifying the hexa-peptide fragment as the basic amyloidogenic unit. However, the penta peptide fragment FGAIL, also assembled into fibrils with morphology different from those formed by the full length peptide. Mutation studies with substitution of phenylalanine with other amino acids ameliorated fibril formation highlighting the crucial role of Phe in fibrillization of the peptide [309].

The ability of synthetic peptides to form amyloid fibrils in vitro have been utilized to examine how a variety of parameters, including temperature, pH, solvent composition, peptide concentration, and peptide sequence influence the final fibril state and also assay for inhibition potency of anti-fibrillization agents [301-304, 312, 315, 316]. However, the most limiting factor for search of anti-amyloid compounds has been the extremely difficult synthesis of model amyloid peptides and also the

exorbitant price of commercially available Aβ peptide. Thus, small peptide based fibrillizing systems exhibiting essential properties of Aβ could be very useful for development of cost-effective high throughput assays for discovering novel anti-amyloids.

In the present work, the self-assembly of the peptide H-Phe-ΔPhe-OH (Phe-ΔPhe) into amyloid like fibrils has been probed. The peptide, Phe-ΔPhe, fibrillized at very low concentrations (~0.1mg/ml) into structure closely resembling native amyloid fibrils. Though, the CD and FTIR spectroscopy did not exhibit a β-sheeted secondary structure, fibre-XRD and the dimensions of the fibrils resembled closely to that of amyloids. The dynamics and kinetics of fibril assembly was also very similar to the native Aβ with the kinetics of fibril growth strongly dependent on peptide concentration. The rate of fibril growth was also highly stochastic. The fibrils exhibited congo-red binding with associated birefringes and also resulted in fluorescence enhancement of Thioflavin T. These features made the Phe-ΔPhe dipeptide fibres as potential mimic of model amyloids.

4.2 Materials and methods

4.2.1 Synthesis of dipeptides: The synthesis of the dipeptides were carried out as follows-

a) H-Phe-ΔPhe-OH

Boc-Phe-OH (Novabiochem) (1.52g, 5mM) was dissolved in dry tetrahydrofuran (Sigma-Aldrich) and the resulting solution stirred in an ice-salt bath at -15°C. N-methyl morpholine (Sigma) (0.65ml, 5mM) was added to the solution followed by isobutyl chloro-formate (Sigma) (0.7ml, 5mM). After 10min, a pre-cooled aqueous solution of DL-threo-β-phenylserine (Sigma-Aldrich) (1g, 5.5mM) and sodium hydroxide (0.22g, 5.5mM) was added and mixture stirred overnight at room temperature. The reaction mixture was concentrated *in vacuo*, acidified with citric acid to pH 3.0 and extracted with

ethyl acetate (Spectrochem) (3×20ml). The ethyl acetate layer was washed with water (2×15ml), with saturated sodium chloride (1×20ml), dried over anhydrous sodium sulfate and evaporated to yield Boc-Phe-DL-threo-β-phenylserine as an oily compound (2.3g, ~100%). The compound, Boc-Phe-DL-threo-β-phenylserine, was then mixed with anhydrous sodium acetate (0.53g, 6.5mM) in freshly distilled acetic anhydride (50ml) and stirred for 36hrs at room temperature. The thick slurry obtained was poured over crushed ice and stirred till the oily suspension gave rise to a yellow colored solid. The precipitate was filtered, washed with 5% NaHCO$_3$, cold water and dried under vacuum. The resulting azalactone, Boc-Phe-ΔPhe-Azl, was dissolved in methanol, treated with 1.5 equivalents of 1N NaOH solution and stirred at room temperature for 3-4hrs. The mixture was then partially evaporated to remove methanol, acidified with citric acid to pH 3.0 and extracted with ethyl acetate (3×30ml), the combined ethyl acetate extract was washed with water (2×20ml), dried over anhydrous sodium sulphate and evaporated to yield Boc-Phe-ΔPhe-OH as a white solid. Deprotection at the α-amino group and side chain protection was achieved by treatment with 98% formic acid (30ml) for 3hrs at room temperature. The reaction mixture was evaporated to dryness and the residue was precipitated with anhydrous diethyl ether. The resulting precipitate was filtered, washed several times with dry ether and subsequently lyophilized from 10% acetic acid-water (20ml) to yield the final compound H-Phe-ΔPhe-OH as white powder. Overall yield (0.6g, 48%); R$_f$ = 0.15 (CHCl$_3$-MeOH, 9:1).

The peptide was purified on a preparative reverse phase C$_{18}$ column (Deltapak, C$_{18}$, 15μ, I.D. 300×19mm) using acetonitrile-water linear gradient 5-45% acetonitrile (0.1%TFA)/water (0.1% TFA) at a flow rate of 4ml/min over 25min. The purified peptide was reinjected into an analytical reverse phase C$_{18}$ column (Phenomenex, C18, 5μ, I.D. 250×4.6mm) using a acetonitrile-water

linear gradient 5-45% acetonitrile (0.1%TFA)/water (0.1% TFA) at a flow rate of 1ml/min over 25min and was found to be 98% pure with retention time of 15min. The purified peptide was analyzed by mass spectroscopy (Applied Biosystems QStar (Q-TOF)) Observed Mass- 310.8 Da, Expected Mass- 311 Da.

b) NH$_2$-Lys-ΔPhe-COOH

The peptide was synthesized as described above starting with Boc-Lys (Boc)-OH (5mM, 1.73g). Overall yield (0.57g, 39%); R$_f$ = 0.1(CHCl$_3$-MeOH, 9:1); The peptide was purified as described above and analyzed by mass spectroscopy. Retention Time- 13min; Observed Mass- 292 Da, Expected Mass-291.38 Da.

c) NH$_2$-Glu-ΔPhe-COOH

The peptide was synthesized as described above starting with Boc-Glu (Otbu)-OH (5mM, 1.5g). Overall yield (0.8g, 59%); R$_f$ = 0.1(CHCl$_3$-MeOH, 9:1); The peptide was purified as described above and analyzed by mass spectroscopy. Retention Time- 13min; Observed Mass- 292.6 Da, Expected Mass-293 Da.

d) NH$_2$-Ser-ΔPhe-COOH

The peptide was synthesized as described above starting with Boc-Ser(tbu)-OH (5mM, 1.3g). Overall yield (0.57g, 39%); R$_f$ = 0.1(CHCl$_3$-MeOH, 9:1); The peptide was purified as described above and analyzed by mass spectroscopy. Retention Time- 9min; Observed Mass- 235.76 Da, Expected Mass-236 Da.

b) NH$_2$-Gly-ΔPhe-COOH

The peptide was synthesized as described above starting with Boc-Gly-OH(5mM, 0.8g). Overall yield (0.57g, 39%); R$_f$ = 0.1(CHCl$_3$-MeOH, 9:1); The peptide was purified as described above and analyzed by mass spectroscopy. Retention Time- 9min; Observed Mass- 219.2 Da, Expected Mass-220 Da.

4.2.2 Assembly of fibrils: The fibrils were assembled in water at neutral pH by dissolving the Phe-ΔPhe peptide powder in 50μL of acetic acid and subsequently diluting it in 2000 μL of water to achieve the desired concentration.

4.2.3 Electron Microscopy: For transmission electron microscopy (TEM), the peptide samples were prepared at a concentration of 1-10mg/ml in double distilled water and incubated for 24hrs to make sure that the process of assembly was complete. The sample was adsorbed on a 400 mesh copper grid with carbon coated formvar support and stained with 1% uranyl acetate and viewed under a 120kV mode of a TEM (Tecnai 12 BioTWIN, FEI Netherlands). Photomicrographs were digitally recorded using a Megaview II (SIS, Germany) digital camera. Image analysis was carried using Analysis II (Megaview, SIS, Germany) and ImageJ (http://rsb.info.nih.gov/ij/) software packages.

4.2.4 Congo red binding: 10uL of an aqueous solution of Congo red (6mg/ml) was added to the fibrils during the process of assembly of Phe-ΔPhe (1mg/ml) and incubated for 30 mins thereafter. A small quantity of the stained sample was spotted on a glass slide, dried to a relative humidity of 99%, and imaged under a microscope under cross polarization mode.

4.2.5 Thioflavin T binding: 10uL of an aqueous solution of thioflavin T (6mg/ml) was added to the fibrils during the process of assembly of Phe-ΔPhe (1mg/ml) and incubated for 30 mins thereafter. The excitation and the emission spectrum of the amyloid bound dye was characterized by a Perkin-Elmer LS50B spectrofluorimeter.

4.2.6 Fibre-XRD: Unoriented fibers of the Phe-ΔPhe dipeptide were collected in a 0.1 mm quartz capillary and diffracted on a Cu Kα rotating anode. The data was collected on a MAR-research image plate (MAR research, Hamburg,Germany) for a 20 min exposure.

4.2.7 Dynamic light scattering: DLS Measurements were performed at 25°C with a 288-channel Photocor-FC correlator and a JDS uniphase He-Ne laser (632 nm). The

scattering angle was 90°. The peptide was made to assemble and the intensity and the autocorrelation function of the scattered light were automatically measured for periods of 5-60 min. By 60 mins, fibril growth was typically finished. Some samples were kept at room temperature and reexamined periodically during the next few days. Experiments with soluble dipeptides (Gly-ΔPhe, Ser-ΔPhe, Lys-ΔPhe and Glu-ΔPhe) were done in a similar fashion, except that Phe-ΔPhe was dissolved in acetic acid already containing the appropriate concentration of the soluble peptide. The size distribution of fibrils in solution was determined by a discrete component analysis using regularization package Dynals. The observed distribution of diffusion coefficients was relatively narrow; therefore, the average hydrodynamic radii (R_h) of the scattering particles are presented in the experiments. The following interpolation, appropriate for a cylinder of length L and diameter d (34), was used to relate the experimentally measured R_h values to the fibril length:

$$R_h = \frac{L}{2} \cdot \left(\sqrt{1 - x^2} \bigg/ \ln \frac{1 + \sqrt{1 - x^2}}{x} \right),$$

$$x = \frac{d}{L} \left[1 + \frac{0.37(L - d)}{L} \right].$$

4.3 Results and Discussion

4.3.1 Structure of dipeptide fibrils:

The Phe-Phe dipeptide motif of Aβ has been shown to self assemble into fibrilar structures at a peptide concentration of 2-5mg/ml in aqueous solution [76, 77]. The fibril of Phe-Phe dipeptide exhibited many properties of amyloid fibrils including congo red staining and thioflavin T binding. The fibrils had a diameter of 100-150nm and possessed length over microns [76]. The fibrils exhibited a CD spectrum with a positive band at 197nm and 210nm (turn-like) and an FTIR peak at 1620cm^{-1} (β-sheet) [76]. However, values of dihedral angles obtained from crystal structure of the

peptide corresponded to the dihedral angles of the second and third residues in a typical type II β-turn turn [124].

The dipeptide Phe-ΔPhe fibrillized in a highly reproducible manner even at very low concentrations (~0.1mg/ml). Importantly, the morphology of the fibers produced under these conditions was highly similar to that observed in Alzheimer plaque amyloid (Fig. 4-1). The fibers were of Phe-ΔPhe dipeptide were unbranched, straight, or slightly curved and had a diameter of 15±2 nm with length over microns. Analysis of peptide secondary structure by CD (Chapter 2) showed that the dipeptide fibrils were not composed of β-sheet unlike in typical amyloids. FTIR spectra also confirmed the absence of β-sheeted structure (Chapter 2). The ψ, φ dihedral angles obtained from the crystal structures of the peptide Phe-ΔPhe were 165°, 36° respectively. Similar values of the dihedral angles are adopted by the second and third residues in classical type 1 β turns, thus suggesting a turn like conformation [124] for Phe-ΔPhe peptide. But the essential feature of Aβ amyloidosis, i.e. aromatic stacking mediated self-assembly was retained in the fibril assembly of Phe-ΔPhe dipeptide. Moreover, introduction of β turn favoring residue at position 22 of Aβ$_{(1-42)}$ have been shown to promote greater aggregation and cytotoxicity [342]. Simulation studies have also pointed towards the presence of turn and bend structures rather that helices or sheets in small fragments of Aβ [343, 333]. Also, it was not unusual for turn assuming dipeptide structures to cause fibril formation [88].

However, particularly interesting was the unoriented fiber diffraction spectrum (Figure 4-1c) with bands at 5.8Å, 7.2Å, 8.95Å, 13.6 Å and 20 Å. The fiber diffraction patterns of many amyloids typically exhibit a meridional reflection at 4.75Å corresponding to the backbone separation of main chains in a β-pleated structure and 10Å reflection corresponding to the spacing between the sheets making up the fiber. However, the positions of the diffraction bands seemed to vary in different

comparison with the crystal structure of Phe-ΔPhe crystallized in acetic-acid water solution, the 5.8 Å band was attributed to the spacing between the backbone atoms and was somewhat larger than that typically found in amyloids. The larger distance might be a result of weakly held dipeptide molecules due to the absence of the stabilizing backbone H-bonds. The pair of reflections at 7.2Å and 8.95Å probably corresponded to the distance between the N-terminal Phe ring of one molecule and C-terminal ΔPhe ring of another molecule in an edge-to-face stacking between the two layers of monomers in the tube. Diffraction bands in this region have been frequently observed in amyloid fibrils, but their exact origin is unknown [336]. The 13.6 Å band correlated well with the distance between two ΔPhe rings of the stacked molecules. The 20Å band, however, could not be assigned. Moroever, the crystal structure of the peptide also showed the occurrence of channels along the crystal with a diameter of roughly 0.6nm (Chapter 3) which correlated well with the size of the channels occurring in amyloid fibrils [336].

4.3.2 Congo red and Thioflavin T binding

Amyloids were historically identified in plaques in neuronal sections by congo red staining. Congo red shows reasonably high degree of binding to amyloids [337-339]. The stained amyloid fibres appear red under normal unpolarized light. However, the high degree of anisotropy in the fibril architecture results in the appearance of strong green-gold birefringes under cross-polarized light. Interestingly, fibrils formed by Phe-ΔPhe stained with congo red and also exhibited birefringes under cross polarized light (Figure 4-2a). The absorbtion spectrum of congo red also exhibited a shoulder at 540nm suggesting its binding to amyloid fibrils.
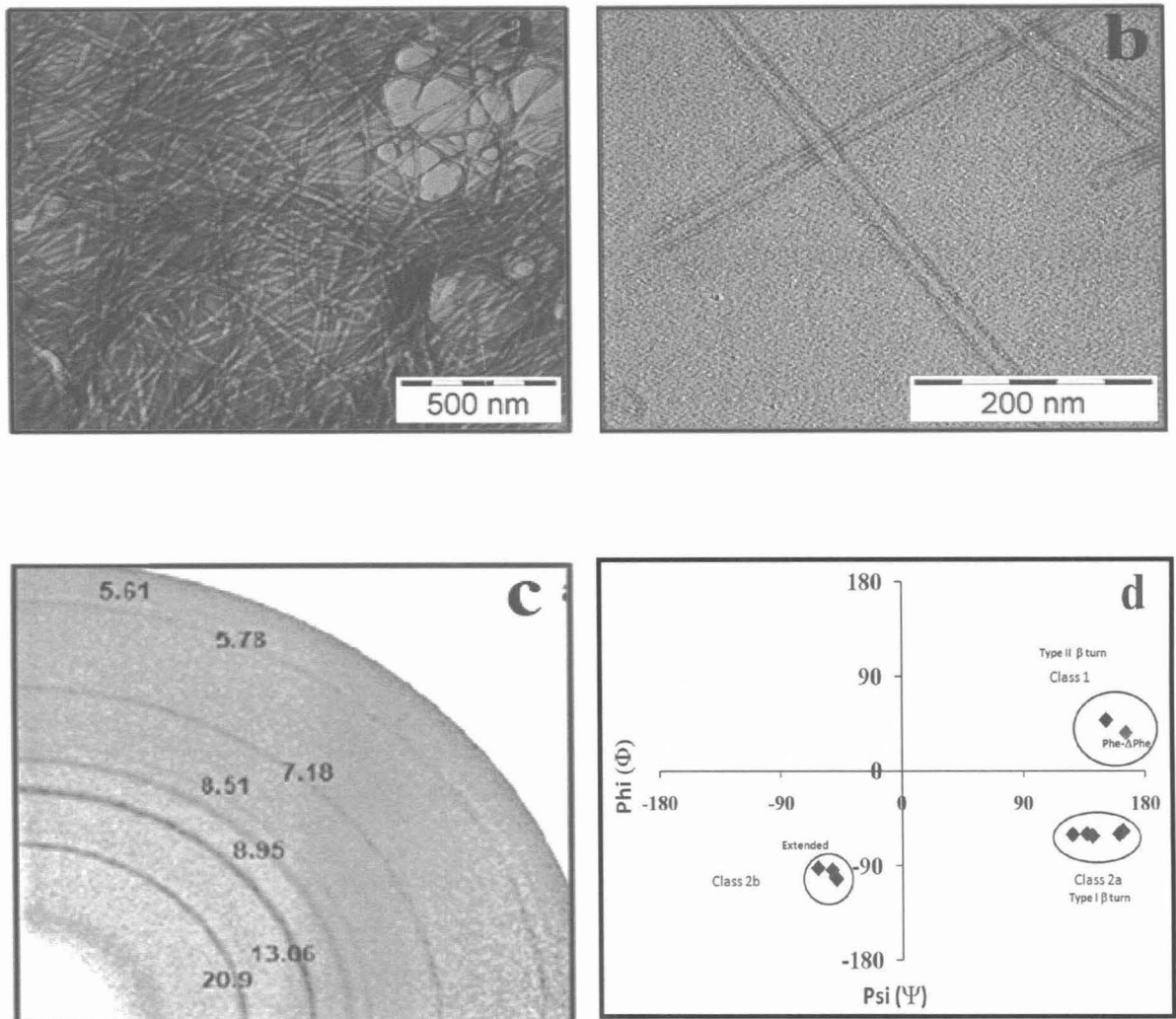
Figure 4-1 : Transmission electron micrographs of the fibrils of Phe-ΔPhe at (a) low and (b) high magnification. The fibers appear unbranched, straight, or slightly curved and had a diameter of 15±2 nm and length over microns. (c) unoriented fiber diffraction of the fibrils with bands at 5.8Å, 7.2Å, 8.95Å, 13.6 Å and 20 Å. (d) torsion angle of Phe-ΔPhe showing similarity with turn structures [124].

Enhancement of fluorescence emission of thioflavin T dye on binding to amyloids is another feature that has been frequently used to monitor properties of amyloid fibrils [339-341]. Thioflavin T is believed to intercalate between the parallel and/or anti-parallel β-sheets in a fibril that provide a non-polar environment and result in increased fluorescence. The fibrils formed by Phe-ΔPhe exhibited over 100 fold increase in fluorescence of thioflavin T with an excitation and emission maximum at 435nm and 470nm. This suggested its ability to intercalate between the aromatic rings that stabilize the fibrillar assembly (Figure 4-2b). These features suggested that the dipeptide fibrils shared similarity in essential structural architecture associated with typical amyloids.

4.3.4 Kinetics of fibril growth

To examine the concentration dependence of Phe-ΔPhe fibrillogenesis, 5 different initial peptide concentrations, C_0, in the range of 0.125mM to 1.25mM were studied. In each case, fibril formation manifested itself as a temporal increase in observed hydrodynamic radius, R_h, and in the intensity of the scattered light, I_s, and an initial nucleus size of roughly 45.8nm. The intensity grew proportionately with R_h, consistent with a fibrillar structure of the assembly [314]. There was an increase in the observed hydrodynamic radius with time. The final asymptotic mean hydrodynamic radius (R_h) of 115±28nm occurred after 1hr. Using the previously reported interpolation, appropriate for a cylinder of length L and diameter d, to relate the experimentally measured R_h value of fibril length, the final length of fibrils obtained were approximately 1000±160nm (Figure 4-3). This value correlated well with fibril dimensions observed in the electron micrographs.
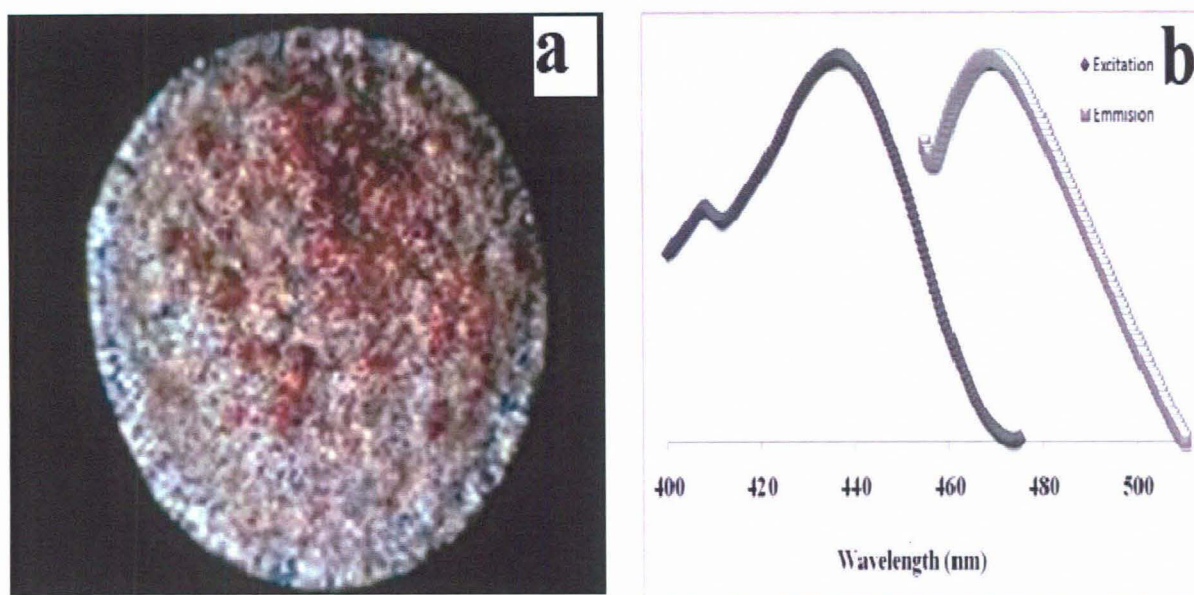
Figure 4-2: (a) Bifrefringes observed in fibrils after Congo-red staining, a typical characteristic of amyloid fibrils. (b) Excitation and emmision spectrum of thioflavin T on binding to fibrils. The fibrils formed by Phe-ΔPhe exhibited over 100 fold increase in fluorescence of thioflavin T with an excitation and emission maximum at 435nm and 470nm. These features suggested that the dipeptide fibrils shared similarity in essential structural architecture associated with typical amyloids.

As described earlier, a structure with an ensemble average Rh ≈ 50 nm was observed immediately after initiation of fibrillogenesis in light scattering experiments suggesting the existence of a nucleated polymerization. Electron micrographs of the filtrate after the filtration of the matured fibrils through a 0.2µ membrane, also, exhibited spherical assemblies with a size average of 40 ± 25nm. The dimensions obtained from the DLS experiments correlated well with the electron micrographs indicating that the observed spherical assemblies might represent the nucleus of the fibrils. It was further observed that addition of peptide stock solution to the filtered nucleus preparation resulted in fibril formation (Figure 4-4a).

Interestingly, a similar size of nucleus was obtained after boiling the fibrils at 100°C for 15mins and then allowing it to cool. At room temperature, the spherical nucleus was observed to transform into mature fibrils with time (Figure 4-4b). These observations clearly suggested the existence of a nucleus in the dynamic pathway in the formation of fibrils. Albeit, the size of the nucleus was not very well defined and thus would have greater probability to promote heterogenous nucleation events during fibril formation.
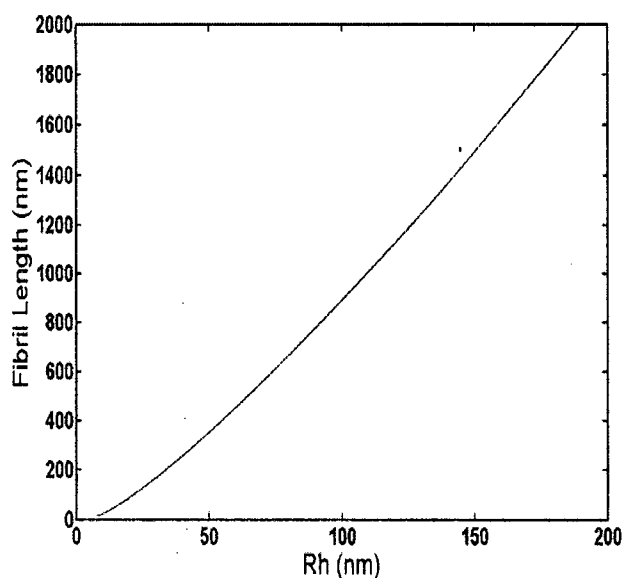
$$R_h = \frac{L}{2} \cdot \left(\sqrt{1 - x^2} \Big/ \ln \frac{1 + \sqrt{1 - x^2}}{x} \right),$$

$$x = \frac{d}{L}\left[1 + \frac{0.37(L - d)}{L}\right].$$

Figure 4-3 : Plot of observed hydrodynamic radius (R_h) versus calculated fibril length using rigid cylinder approximation appropriate for a cylinder of length L and diameter d (=13nm), was used to relate the experimentally measured R_h values to the fibril length.
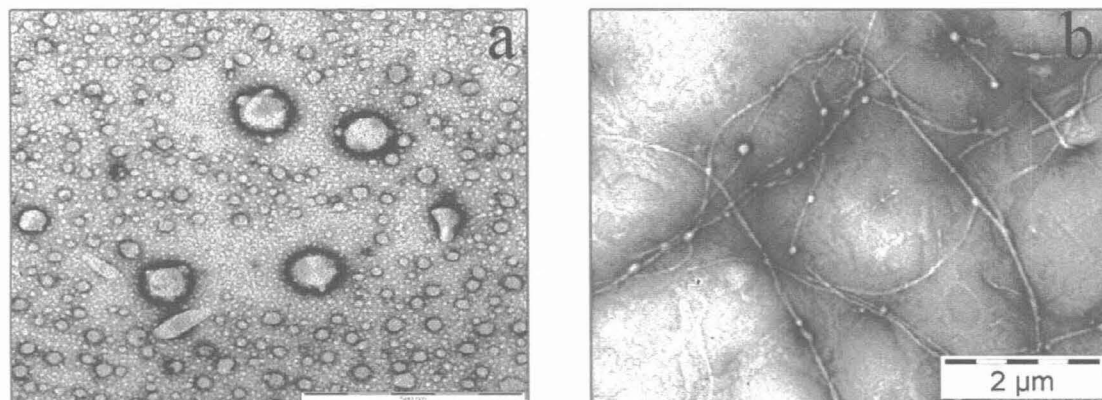
Figure 4-4: Electron micrographs of the spherical nucleus in the dynamic pathway of fibrillogenesis in (a) filtrate after the filtration of the matured fibrils through a 0.2μ membrane and exhibiting spherical assemblies with a size average of 40 ± 25nm and (b) after heating and cooling the spherical nucleus was observed to transform into mature fibrils with time
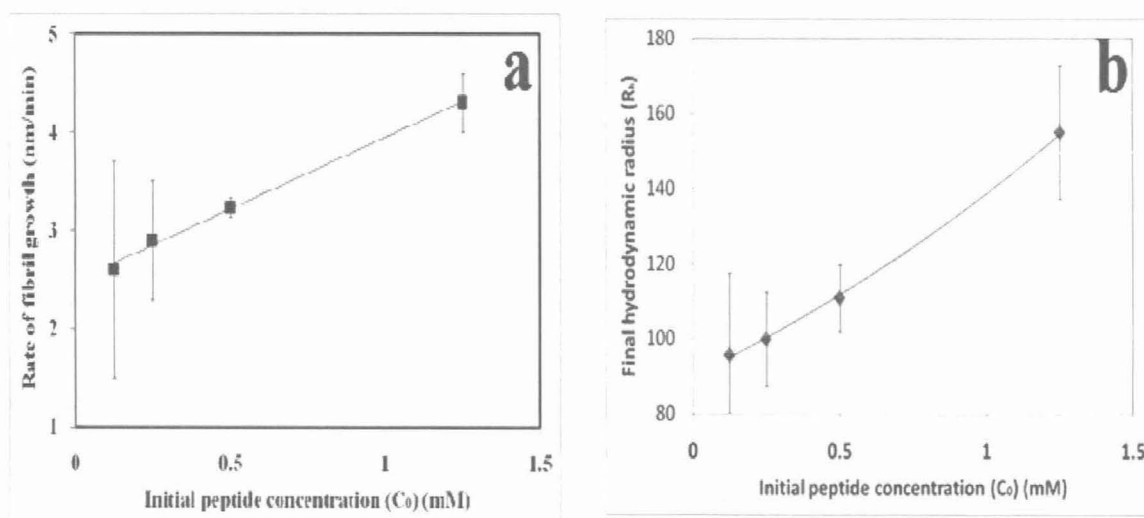
Figure 4-5: Figure shows the dependence of (a) rate of fibril growth and (b) final hydrodynamic radius with initial peptide concentration indicating a heterogenous nucleation pathway mediated fibrillogenesis. The average initial rate of fibril growth rate was 3.3±0.8 nm/min over the entire range of concentration tested. The initial rate of fibril growth (K_e) increased linearly with the initial concentration of the peptide (C_0). The final fibril length (L_f) exhibited an exponential dependence on C_0, however, the average final fibril length (L_f) stood at 1000±160nm under the condition for fibrillization.

The initial rate of fibril growth (K_e) increased linearly with the initial concentration of the peptide (C_0) (Figure 4-5a) with an average of 3.3±0.8 nm/min. It was also seen that the initial concentration (C_0) had no correlation with the time (T) required to achieve the final fibril length. The final fibril length (L_f) exhibited an exponential dependence on C_0, however, the average final fibril length (L_f) stood at 1000±160nm under the condition used for fibrillization of the dipeptides.

Typically for amyloid fibrillogenesis, in the concentration domain $C_0 > c^*$ (where c^* is the cmc of the peptide under the solvent conditions used), a defined nucleus is formed and thus there exists a nucleus-monomer equilibrium. This would maintain an almost constant monomer concentration in the solution that is available for fibril growth. The initial rate of growth is thus constant and independent of the initial concentration with a value approximately equal to $K_e c^*$ (where Ke is the fibril elongation rate). However at time (T), the pool of nucleus is depleted resulting in an exponential decrease of the free monomer concentration (C) and thus the fibril elongation rate. Interestingly, T and also the final fibril length (L_f) are independent of the initial concentration (C_0) in the described model. However, in the concentration domain $C_0 < c^*$, the initial concentration of the monomer is essentially equal to the concentration of the dissolved peptide. Thus, the number of growing fibers (N_f) are equal the number of heterogenous nuclei present in the sample. Due to the binding of monomers to the growing fibril, C decreases exponentially with a rate $K_e N_f$ resulting in a gradual decrease in fibril growth. Direct quantitation of N_f in a sample has not been experimentally feasible, however relative quantitation of fibril elongation rates under similar experimental conditions would be possible.

The kinetic behaviour of fibril growth exhibited by the dipeptide Phe-ΔPhe suggested that fibril growth occurred primarily via heterogenous nucleation pathway. The fibrillization appeared to be governed primarily by the heterogenous size and the number of the nucleus (also observed under TEM) formed by the same peptide.

It was also interesting to observe that there was a high degree of intra-sample variation resulting in a high standard deviation in the values obtained. It was not surprising as previous work [317] has suggested that the nucleation was under influence of a stochastic factor that could manifest itself in profound macroscopic differences in the aggregation kinetics of otherwise indistinguishable amyloid samples. Intra-sample variation in initial growth rate (K_eN_f) and final fibril length (L_f) was higher at lower C_0 probably due to greater predominance of heterogenous nucleations at lower peptide concentrations as well as influence of other factors.

4.3.5 Effect of temperature on fibrillization

We also investigated the effect of temperature in the range of 20 to 37°C on the kinetics of fibrillization of Phe-ΔPhe. Interestingly, the initial rate of fibril growth (K_eN_f) did not show any variation with temperature and exhibited an average value of growth rate at 4nm/min with estimated activation energy (E_A) roughly equal to zero (Figure 4-6a) [314]. This was in marked contrast to the fibril growth kinetics of amyloids wherein the fibril growth rate decreases dramatically with decrease in temperature with an associated activation energy ($\approx 22.8 \pm 1.1$ Kcal/mol for Aβ 1-40 in 0.1N HCl) [314]. The observation clearly suggested that unlike in Aβ and other related amyloids, no discernable activation event (structural transition) occurred in the dipeptide during fibril growth. This was not surprising given the small and rigid molecular conformation of the dipeptide unlike larger peptides (like Aβ) that are believed to undergo structural transition preceeding fibrillization. Moreover, it has been demonstrated that the primary forces that stabilize the assembly were pi-stacking and h-bonding interactions. It also appeared that the final fibril length had no correlation with temperature (Figure 4-6b) further suggesting that there was probably no thermodynamic contribution to fibrillization of Phe-ΔPhe. Dynamic light scattering experiments also suggested that the ensemble average size of the nucleus was smaller (≈ 46.8 nm) at 37°C and larger (≈ 73.6 nm) at 20°C. The observations suggested that temperature probably affected only the size and not the number (N_f)

of the nucleus, and thus the fibril elongation rate (K_eN_f) remained constant. As expected, the number distribution analysis also suggested that the number of nuclei (N_f) were nearly equal in both the cases [314].
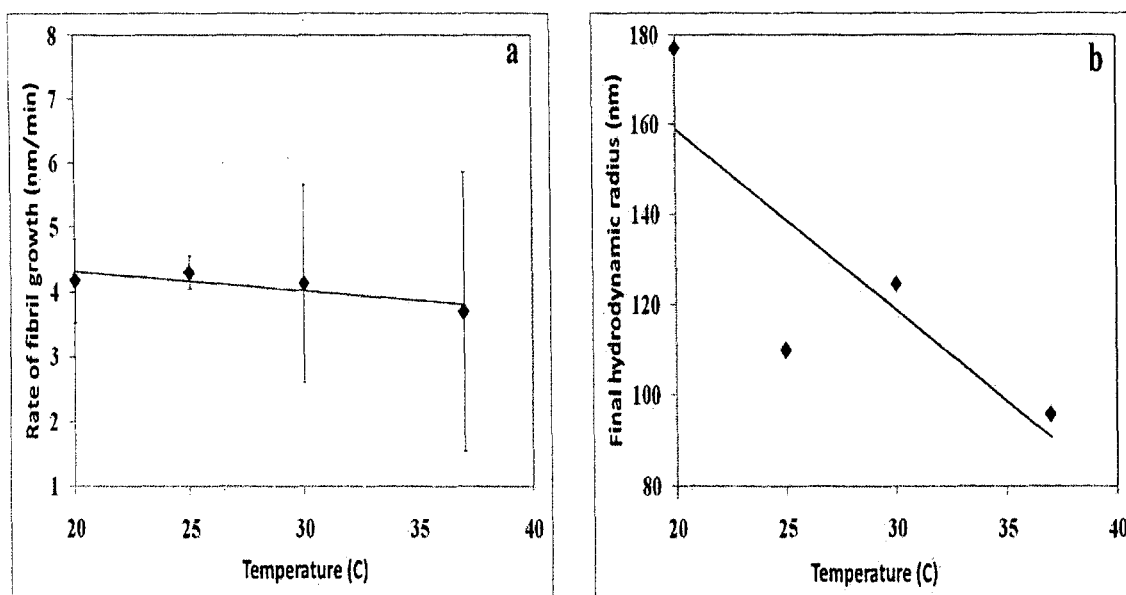

Figure 4-6: Figure shows the dependence of (a) rate of fibril growth and (b) final hydrodynamic radius with temperature. The initial peptide concentration is 0.125mM. The initial rate of fibril growth (K_eN_f) did not show any variation with temperature and exhibited an average value of growth rate at 4nm/min with estimated activation energy (E_A) roughly equal to zero. The final hydrodynamic radius (the final fibril length decreased at higher temperatures.

From the above results it was evident that the dipeptide Phe-ΔPhe exhibited many properties of amyloids including congo-red and thioflavin T binding, hollow tubular morphology stabilized by ring stacking and hydrogen bonding interactions, and exhibited fibril formation by heterogenous nucleation pathway. Moreover, there was no observable thermodymanic contribution to the kinetics of the assembly within

physiologically relevant temperature range. Also, the kinetics of the assembly could be quantified in terms of fibril elongation rates, final fibril length and relative amount of fibrils. These features help make use of this peptide as a mimick of amyloids.

4.3.6 Effect of non-assembling dipeptides on the fibrillization of Phe-ΔPhe

The ultra-structure studies of the amyloid fibrils have suggested that the amyloid fibers are stabilized by numerous hydrogen bonding interactions occurring between the β-sheets in the cross β-pleated sheet structure. Most small molecule and synthetic peptide based amyloid inhibitors are specifically designed to disrupt Aβ fibrils by disruption of native hydrogen bonding. This strategy has been commonly referred to as "β-breaker strategy" and relied on the ability of synthetic peptides that share sequence similarity with the native amyloid fragment yet do not adopt a β-sheeted structure. Such inhibitors interacted with the native fragment and prevented it from adopting the necessary β-sheet secondary structure causing disruption of amyloids [305-308]. The other effective strategy has been the disruption of the nucleus by use of amphiphilic/detergent molecules and hence results in inhibition of fibrillization [312, 314]. However, such molecules exhibited poor biocompatibility and hence could not be used as drugs. As pointed out earlier, the stacking of the diphenylalanine moiety in the amyloid β-protein fragment Aβ(1-40) or Aβ (1-42) fragment has been implicated to be the major driving factor for amyloidogenesis [22, 75, 76, 78, 309]. Therefore, inhibitors that could target the disruption of the aromatic interaction face, and thus affect the nucleation and fibril growth, could prove to be efficient anti-amyloids. Infact, many low molecular weight polyphenols have been shown to disrupt amyloids by the aforesaid mechanism [310, 311, 312].

In the previous chapters it has been demonstrated that the peptides H-Gly-ΔPhe-OH (Gly-ΔPhe), H-Gln-ΔPhe-OH (Gln-ΔPhe), and H-Ser-ΔPhe-OH (Ser-ΔPhe) did not assemble in aqueous medium even at high concentrations (Chapter 2). Also, the ampiphillic dipeptides H-Lys-ΔPhe-OH (Lys-ΔPhe), H-Glu-ΔPhe-OH (Glu-ΔPhe) do not assemble at low peptide concentrations (Chapter 3). The dipeptides were

characterized by a free N- and C-terminus, a rigid and planar aromatic ring of ΔPhe and the side-chain of the N-terminal residue being either charged (anionic as in Glu-ΔPhe; cationic as in Lys-ΔPhe) or neutral (hydroxyl as in Ser-ΔPhe; carbonyl as in Gln-ΔPhe) functional groups thus, sharing structural similarility with amphiphilic molecules. Therefore, the effect of these peptides on the fibrillization of amyloid mimic, Phe-ΔPhe, was investigated in terms of fibril length, rate of fibrillization ($K_e N_f$) and relative degree of fibrillization (I_s).

The dipeptides were used at a concentration at which they did not assemble to ensure that the change in fibril elongation rate ($K_e N_f$) was solely due to the available free monomers in the solution. Interestingly, it was observed that the dipeptide Glu-ΔPhe, Gln-ΔPhe and the control dipeptide (Gly-ΔPhe) did not exhibit any substantial change in $K_e N_f$ of the fibrils (Figure 4-7). The final fibril lengths were comparable to that achieved by the Phe-ΔPhe dipeptide alone. However, there was a decrease in the mean scattering intensity (I_s) in the treated samples suggesting that the inhibitors could probably disrupt only a few growing fibrils resulting in only a minor overall decrease of fibrillization. The cationic dipeptide, however, enhanced the process of fibrillogenesis by increasing the rate of fibril elongation by a factor of 2 and also resulted in the longer fibril lengths (Figure 4-7). Previous reports have also suggested that a lysines containing amyloid inhibitor peptide resulted in enhancement of amyloid fibrillogenesis by enhanced protofibril association [318, 319]. Interestingly, the uncharged polar dipeptide, Ser-ΔPhe, exhibited profound reduction in fibrillogenesis even at equimolar concentration. The fibril elongation rate decreased by an almost 17% of the untreated sample. The final fibril length achieved was about 1100nm (R_h=126nm) compared to 1800nm (R_h=186nm) for untreated fibrils implying an almost 40% reduction in the length of fibrils. The mean scattering intensity decreased by a factor of 5 (Figure 4-7). The above observations clearly suggested that Ser-ΔPhe resulted in substantial inhibition of Phe-ΔPhe fibrillogenesis.
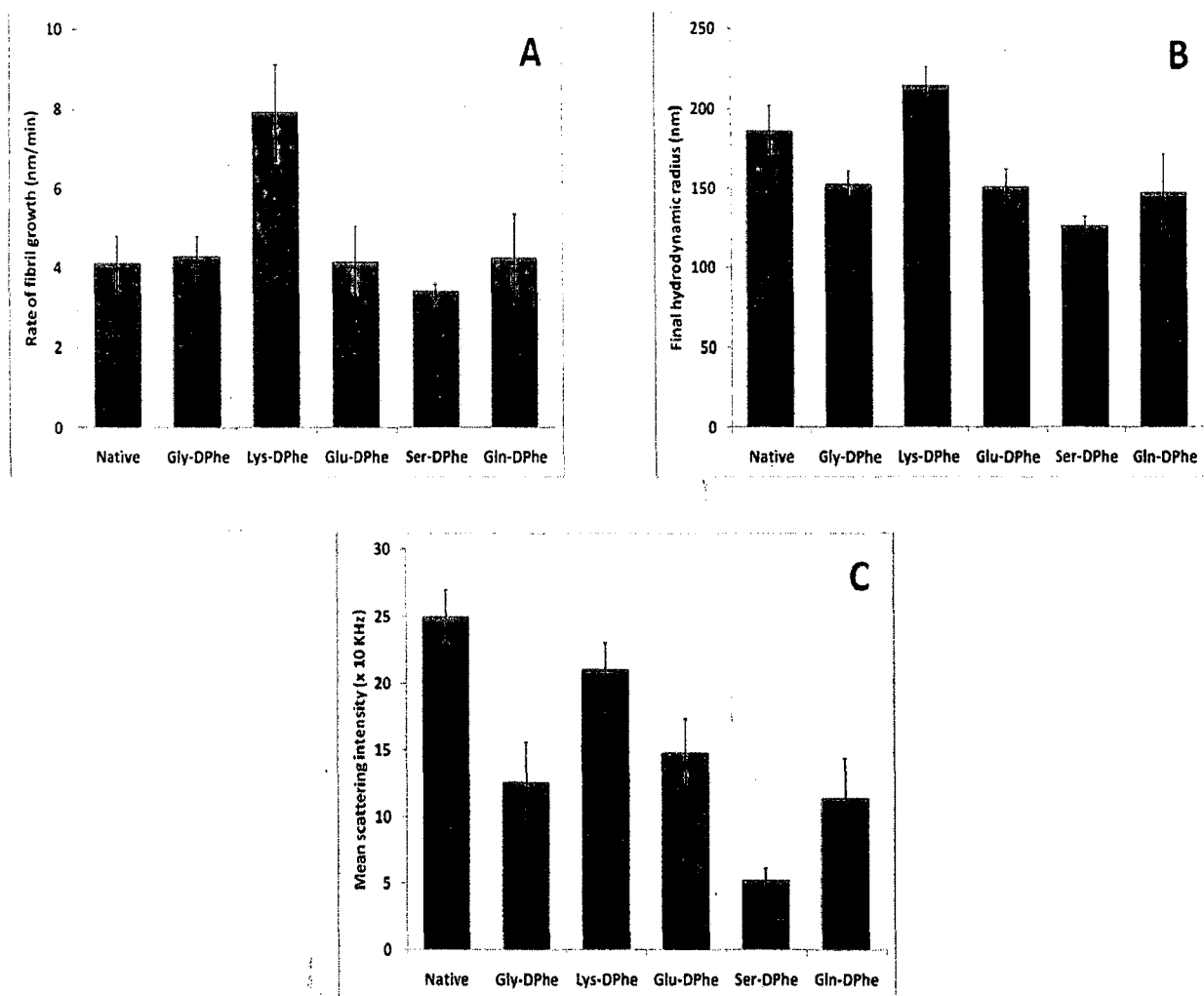
	Native	Gly-ΔPhe	Lys-ΔPhe	Glu-ΔPhe	Ser-ΔPhe	Gln-ΔPhe
Rate of fibril growth (nm/min)	4.1±0.7	4.3±0.5	7.9±1.2	4.15±0.9	3.4±0.2	4.25±1.1
Final hydrodynamic radius (nm)	186±16	152±9	214±12	151±11	126±6	147±24
Mean Scattering Intensity (x10KHz)	25±2	12.6±3	21±2	14.8±2.5	5.2±0.9	11.4±3

Figure 4-7: Figure showing the effect of dipeptides on the (a) rate of fibril growth, (b) final hydrodynamic radius and (c) mean scattering intensity on the fibrillization of Phe-ΔPhe.

4.3.7 Inhibition of model amyloids by Ser-ΔPhe

Prompted by the inhibitory activity of Ser-ΔPhe on Phe-ΔPhe fibrillization, other model amyloidogenic fragments of Aβ and hIAPP were challenged with the dipeptide in order to investigate its potential anti-amyloid activity on fibrillizing system primarily driven by aromatic interactions.

To begin with a fragment of Aβ$_{(16-20)}$ defined by the sequence H-KLVFF-OH was used as a model fibrillizing system [323]. Similar to the studies on a related sequence Ac-KLVFFAE-OH, the chosen peptide could self-assemble to form amyloid like fibrils. The inhibition was investigated in terms of reduction of fibril elongation rates, average hydrodynamic radius after a definite time period and well as reduction in mean scattering intensity. The results suggested that Ser-ΔPhe inhibited the fibril formation of KLVFF in a dose dependent manner. A saturation of inhibitory activity was reached at 1:1 molar ratio between the fibrillizing peptide and Ser-ΔPhe (Figure 4-8). There was reduction in the fibril elongation rate by a factor of 10 in comparison to the native fibrils of KLVFF (Table 4-1). The final hydrodynamic radius of the final fibrils was also very low (Av. = 139 nm) compared with the native fibrils having an average value of 539 nm suggesting a 4-fold reduction in fibril length. The mean scattering intensity also decreased by a factor of 2 (50% inhibition of fibrillization). Interestingly, at equimolar concentrations, the inhibitor dipeptides Gly-ΔPhe, Glu-ΔPhe and Gln-ΔPhe resulted in only 8%, 17% and 12% inhibition respectively. The dipeptide Lys-ΔPhe promoted fibrillization of KLVFF.
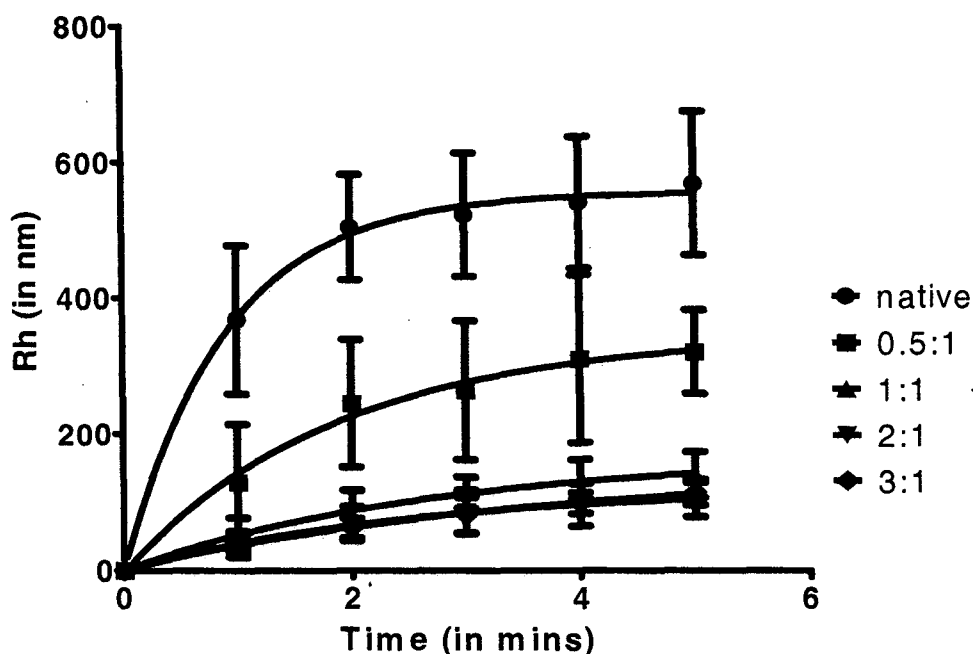
Figure 4-8: The kinetic curves for the temporal increase of hydrodynamic radius during fibrillization of KLVFF. The native represents the fibrillization kinetics of only KLVFF peptide in the absence of the inhibitor molecule. The inhibitor Ser-ΔPhe was mixed with the peptide KLVFF in the molar ratio of 0.5:1, 1:1, 2:1 and 3:1 (Ser-ΔPhe:KLVFF) before initiating the process of fibrillization.

Table 4-1: The inhibition of the rate of fibrillization (slope) upon addition of the inhibitor Ser-ΔPhe.

Statistical values	Native	0.5:1	1:1	2:1	3:1
Rate of fibril growth (Slope)	252.0± 66.97	90.90± 18.30	27.45± 3.640	20.22± 3.047	21.47± 2.116
Nucleus size	38.67± 86.46	22.90± 34.24	18.29± 11.02	13.82± 9.226	12.10± 6.406
1/slope	0.003968	0.011	0.03643	0.04946	0.04658
Goodness of fit (r^2)	0.934	0.925	0.9343	0.9167	0.9626

This clearly suggested that results obtained for the fibrillization inhibition of Phe-ΔPhe also applied to larger peptide models. However, more studies need to be done to firmly establish the reliability of the described assay system. Further, the potential anti-amyloid activity of Ser-ΔPhe needs to be tested against other domains of Aβ polypeptide as well as full length $A\beta_{(1-39)}$, $A\beta_{(1-40)}$, and $A\beta_{(1-42)}$.

The anti-amyloid activity of Ser-ΔPhe was also tested on the fibrillizing peptides H-Ala-Gln-Phe-Leu-Val-OH (ANFLV), H-Ala-Gln-Phe-Leu-Val-His-Ser-Ser-OH (ANFLVHSS), H-Ser-Gln-Gln-Phe-Gly-Ala-Ile-Leu-OH (SNNFGAIL) and H-Gln-Phe-Gly-Ala-Ile-Leu-OH (NFGAIL) derived from the two domains of humain islet amyloid precursor protein (hIAPP). Interestingly, we observed that the dipeptide resulted in decrease in the mean scattering intensity (I_s) of the different domains of hIAPP by 30% or more with respect to the untreated samples (Figure 4-9). The full length $hIAPP_{(1-37)}$ peptide was challenged with equimolar concentration of Ser-ΔPhe and inhibition of fibril formation of the native peptide was observed. Light scattering studies indicated that the fibrillization of the full length native peptide decreased by 60% (st.dev. 7.2%) when treated with equimolar concentration of the inhibitor dipeptide Ser-ΔPhe. The above results demonstrated the potential anti-amyloid activity of the dipeptide Ser-ΔPhe against two different fibrillizing systems. However, the exact mechanism of action has not been probed at the molecular levels.
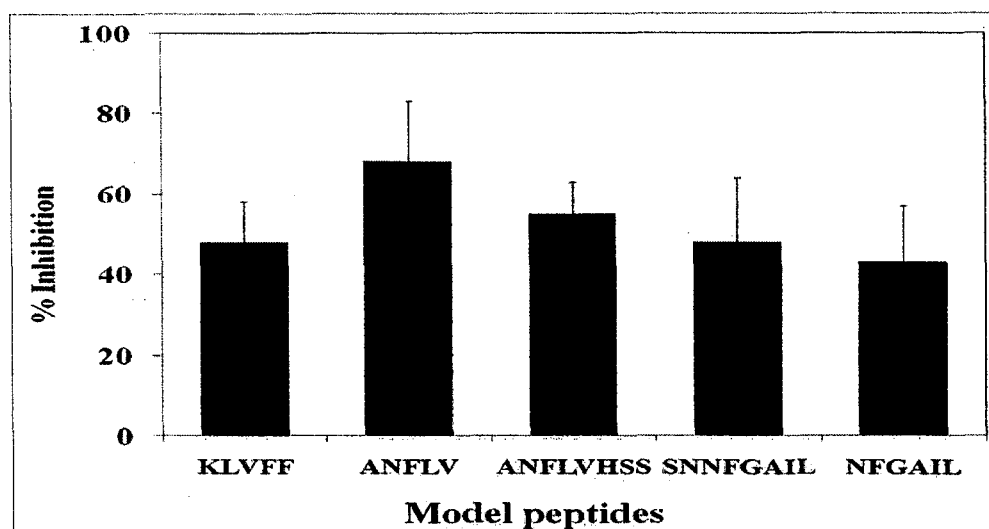
Figure 4-9: Figure showing the effect of dipeptide Ser-ΔPhe on fibrillization of model peptides derived from Aβ$_{(1-40)}$ and hIAPP. The fibrillization of model amyloid systems tested were inhibited by Ser-ΔPhe at equimolar concentration.

(*Percentage inhibition calculated from decrease in mean scattering intensity (I_s) when fibrillization was initiated in presence of equimolar concentration of Ser-ΔPhe)

A survey of known polyphenolic amyloid inhibitors indicated that the dipeptide Ser-ΔPhe shared a few basic structural features of many polyphenols. A polyphenol, apomorphine, has been shown to inhibit α-synuclein and Aβ(1-40) *in vitro*. Screening of several apomorphine derivatives has suggested two important structural features necessary for anti-amyloid activity. Firstly, it was required to have two hydroxyl groups on the D-aromatic ring for its inhibitory effectiveness. Secondly, an additional ring structure that made it more hydrophobic caused increase in its affinity for binding to Aβ [333]. Water soluble tannic acid has also been shown to be an effective fibrillization inhibitor of PrP^{sc} and Aβ. Tannic acid is composed of phenol-carboxylic

and gallic acid groups [334]. Curcumin and rosmarinic acids have also shown effective amyloid inhibition in vitro. It has been proposed that their compact and symmetric structure might bind to free monomers and inhibit the polymerization of fibrils. Curcumin has been shown to inhibit the formation of Aβ oligomers and fibrils, bound plaques, and reduced amyloid *in vivo*. In this study, the structural similarity of curcumin to Congo red was suggested as a possible factor for its inhibition characteristics [335]. Furthermore, the structural similarity of curcumin and chrysamine G, a brain permeable compound, was considered as a possible factor for blood–brain barrier permeability. It was also shown that curcumin had structural similarity to a β-sheet breaker, N,N'- bis(3-hydroxyphenyl)pyridazine-3,6-diamine (named RS-0406). Enzyme-linked immunosorbent assay (ELISA) and TEM studies showed that curcumin effectively blocked the formation of soluble β-amyloid oligomers [335]. Other polyphenols like myricetin, morin, quercetin, gossypetin, exifone, pentahydroxy benzophenone, baicalein, catechin, hypericin and epicatechin gallate have also been demonstrated to have potent anti-amyloid activity [311]. All the above mentioned molecules shared similarity in structure in having one or multiple hydroxyl groups over aromatic rings (Table- 4-2 and Table 4-3). However, Ser-ΔPhe possessed the hydroxyl group over a non-aromatic carbon i.e. $C_\alpha H_3$ group. Thus, it appeared that an amphiphilic dipeptide Ser-ΔPhe having uncharged polar group could exhibit effective anti-amyloid activity. A few variants of the molecule are being presently synthesized in the laboratory to investigate the structural basis of the anti-fibrillizing activity.

4.4 Conclusion

Thus, we observed that the fibrillogenesis of the dipeptide Phe-ΔPhe followed similar profiles of in-vitro amyloid assembly. Moreover, Phe-ΔPhe fibrillogenesis represented the class of fibril formation based on heterogenous nucleation events that represented near *in-vivo* conditions considering the interaction of Aβ peptide with numerous proteins in the cellular mileu. This is unlike most of the larger peptide

models used for investigation of amyloidogenesis. Added to them are the low cost of synthesis, the stability of the peptide and its amenability to crystallization. Moroever, the fibrillogenesis of Phe-ΔPhe can be effectively used to screen for potential low molecular weight inhibitors for amyloids that could translate into effective anti-fibrillization agents for larger amyloid systems. Based on the experiments, Ser-ΔPhe qualified as an effective anti-fibrillizing compound *in vitro*. The results did suggest that Ser-ΔPhe could act as a minimal fragment exerting an effective anti-amyloid activity even at low molar ratio of the inhibitor. More potent inhibitors could be rationally designed based on this design scaffold. Moroever, the low molecular weight, ease of synthesis and purification, proteolytic stability and its cross reactivity with other fibrillizing systems makes the dipeptide inhibitor useful for development of peptide based anti-amyloid agents.
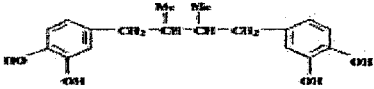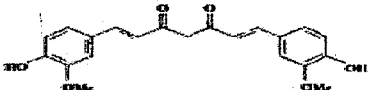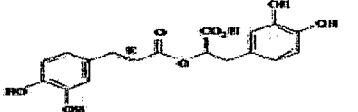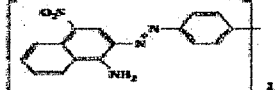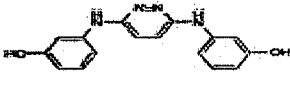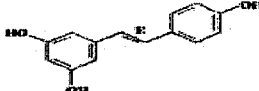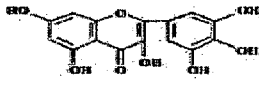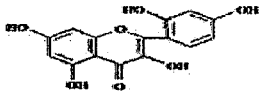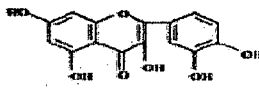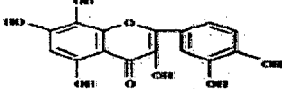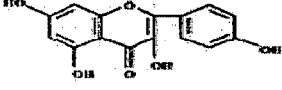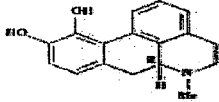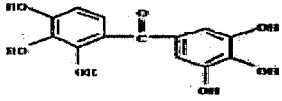
Table 4-2: List of reported polyphenol based amyloid inhibitors.
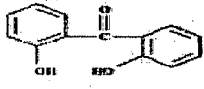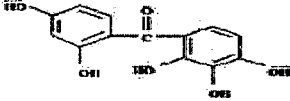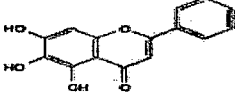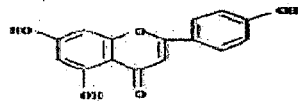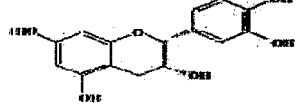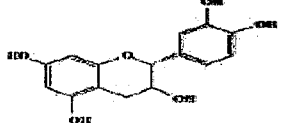
Polyphenol	Studied protein	IC_{50} in vitro, μM		
NDGA	β-Amyloid$_{1-40}$	0.14	, 0.16	
	β-Amyloid$_{1-42}$	0.86	, 0.74	
Curcumin	β-Amyloid$_{1-40}$	0.81		
	β-Amyloid$_{1-42}$	0.63		
Rosmarinic acid	β-Amyloid$_{1-40}$	0.29		
	β-Amyloid$_{1-42}$	1.1		
Resveratrol	β-Amyloid$_{25-35,1-40,1-42}$	n.d. in vitro		
Dobutamine	α-Synuclein	n.d. in vitro		
Myricetin	β-Amyloid$_{1-40}$	0.29	0.9	0.2
	β-Amyloid$_{1-42}$	0.40	0.34	
Morin	β-Amyloid$_{1-40}$	0.24		
	β-Amyloid$_{1-42}$	0.67		
Quercetin	β-Amyloid$_{1-40}$	0.24		
	β-Amyloid$_{1-42}$	0.72		
Exifone	β-Amyloid$_{1-40}$	0.7		
	Tau$_{612}$	3.3		
Kaempferol	β-Amyloid$_{1-40}$	1.7		
	β-Amyloid$_{1-42}$	3.2		
2,3,4,2',4'-Pentahydroxybenzophenone	β-Amyloid$_{1-40}$	2.8		
	Tau$_{612}$	2.4		
Gossypetin	β-Amyloid$_{1-40}$	1.3		
	Tau$_{612}$	2.0		
Purpurogallin	β-Amyloid$_{1-40}$	0.5		
	Tau$_{612}$	5.6		
THBP (2,3,4-Trihydroxybenzophenone)	β-Amyloid$_{1-40}$	3.1		
	Tau$_{612}$	12.2		
Baicalein	α-Synuclein	4.0		
Catechin	β-Amyloid$_{1-40}$	2.9		
	β-Amyloid$_{1-42}$	5.3		
Epicatechin	β-Amyloid$_{1-40}$	2.8		
	β-Amyloid$_{1-42}$	5.6		
	Tau$_{612}$	>200		
Phenolsulfonphthaleine	IAPP	1.0		
	Insulin	1.5		
	β-Amyloid$_{1-40}$	17		
Epicatechin gallate	β-Amyloid$_{1-40}$	3.0		
	Tau$_{612}$	1.8		
Epigallocatechin gallate	β-Amyloid$_{1-40}$	0.18		
	Insulin	17.0		
	Calcitonin	4.9		
	Prion PrP^{sc}	n.d. in vitro		
Hypericin	β-Amyloid$_{1-40}$	0.9		
	Tau$_{612}$	26.8		
Tannic acid	Prion PrP^{sc}	0.1		
	β-Amyloid$_{1-40}$	0.012		
	β-Amyloid$_{1-42}$	0.022		
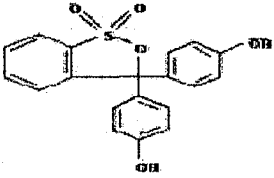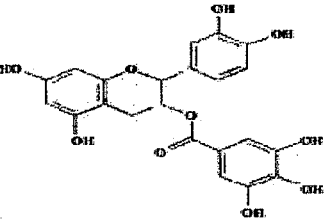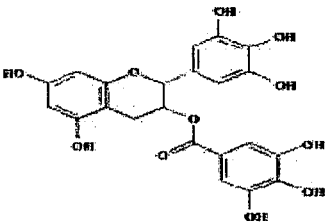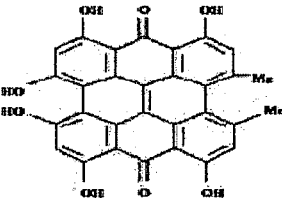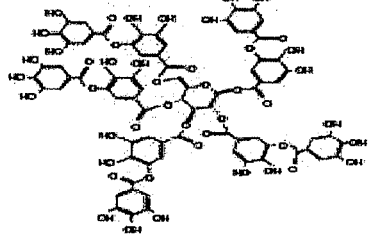
n.d., not determined.

(*Excerpted from Chem Biol Drug Des 2006; 67: 27–37)

Table 4-3: The chemical structure of the reported polyphenol based amyloid inhibitors listed in table 4-2.

Polyphenol (ref)	2D structure
NDGA[a] (50, 51)	
Curcumin[a] (51, 52)	
Dobutamine[b] (44)	
Rosmarinic acid[b] (51)	
Congo red[a] (19, 20, 32)	
RS-0406[b] 3,3'-bis(3-hydroxyphenyl)pyridazine-3,6-diamine (53)	
Resveratrol[a] (39, 46, 47, 68, 73, 74)	
Myricetin[a] (50, 54)	
Morin[a] (50)	
Quercetin[a] (50)	

Gossypetin[b] (54)	
Kaempferol[a] (50)	
Apomorphine[a] (45)	
Exifone[b] (55)	
2,2'-Dihydroxybenzophenon[b] (54)	
2,3,4,2',4'-Pentahydroxyben-zophenone[b] (54)	
Baicalein[a] (57)	
Apigenin[b] (54)	
Catechin[b] (50, 54, 71)	
Epicatechin[a] (50, 54, 71)	

Phenolsulphonphthalein[a] (56)	
Epicatechin gallate[b] (49, Levi, M. et al., unpublished data)	
Epigallocatechin gallate[b] (49, 61, 62, 64, 65)	
Hypericin[a] (54)	
Tannic acid[b] (48, 49)	

(*Excerpted from Chem Biol Drug Des 2006; 67: 27–37)

Conclusion

Molecular self-assembly as a phenomenon has been observed ubiquitously in chemistry, materials science, and biology as well. In recent years, self-assembly has emerged as a discrete field of study and as a synthetic strategy. The formation of molecular crystals, colloids, lipid bilayers, phase-separated polymers, and self-assembled monolayers are all considered to be examples of molecular self-assembly, as are the folding of polypeptide chains into proteins and the folding of nucleic acids into their functional forms. Even the association of a ligand with a receptor is also termed as self-assembly; the semantic boundaries between self-assembly, molecular recognition, complexation, and other processes that form more ordered from less ordered assemblies of molecules expand or contract at the whim of those using them. Interest in self-assembly as a route to aggregation of components larger than molecules has grown because new types of aggregates can be generated with potential for application in microelectronics, photonics, near-field optics, and the emerging field of nanoscience that have become increasingly important technologically. There are many opportunities for fabrication of useful structures of nano- and macroscale components using self-assembly of molecular components. The focus on self-assembly of biomolecular components into distinct geometrical shapes has grown recently due to the simple reason that such structures could have interesting in-vivo application. Of special interest have been peptide based nano-structures due to the relative ease of design, synthesis and bio-compatibility. However, the costs of synthesis and immune reactions to large peptides have limited their potential application. The results in the thesis bring out the potential use of dipeptides containing conformation constraining residues in design of stable nanostructures.

In summary,

Dipeptides can self-assemble into nano-structures in aqueous medium and the nature of the constituent amino-acids dictates the morphology and properties of the assembly. Also, conformation constraining residues can be effectively used to

generate stable self-assembled nano-structures that may have potential bio-medical applications as drug encapsulation and delivery agents.

Fibrillizing dipeptides can be developed as a mimick of amyloid with quantifiable properties of fibrillogenesis. Also, soluble dipeptides with N-terminal hydroxyl group side-chain containing amino acids and C-terminal ΔPhe could show inhibition of fibrillization in model amyloids.

Future Directions

Insights into the self-assembly behavior of dipeptides, gained from the work in the thesis, can be successfully extended to the design of new generation stimuli responsive biocompatible nanoparticles for drug delivery and triggered release applications.

Publications

Panda JJ, **Mishra A**, Basu A, Chauhan VS. Stimuli responsive self-assembled hydrogel of a low molecular weight free dipeptide with potential for tunable drug delivery. Biomacromolecules (2008), 9(8), 2244.

Gupta M, Acharya R, **Mishra A**, Ramakumar S, Ahmed F, Chauhan VS. Dehydrophenylalanine (DeltaPhe) as a beta breaker: extended structure terminated by a DeltaPhe-induced turn in the pentapeptide Boc-Phe1-Ala2-Ile3-DeltaPhe4-Ala5-OMe. Chembiochem (2008), 9(9), 1375.

Mishra A, Panda JJ, Basu A, Chauhan VS. Nanovesicles based on self-assembly of conformationally constrained aromatic residue containing amphiphilic dipeptides. Langmuir (2008), 24(9), 4571.

Gupta M, Bagaria A, **Mishra A**, Mathur P, Basu A, Ramakumar S, Chauhan VS, Self-Assembly of a Dipeptide Containing Conformationally Restricted Dehydrophenylalanine Residue to Form Ordered Nanotubes. Adv Mater (2007), 19, 858.

Bibliography

1) Philip D, Stoddart JF, Angew. Chem. Int. Ed. (1996), 35, 1155.

2) Ball P, The Self-Made Tapestry: Pattern Formation in Nature (Oxford Univ. Press, Oxford, 1999).

3) Singh R, Maru VM, Moharir PS, J. Nonlinear Sci. (1998), 8, 235.

4) Desiraju GR, Crystal Engineering: The Design of Organic Solids (Elsevier, New York, 1989).

5) Isaacs L, Chin DN, Bowden N, Xia Y, Whitesides GM, in Supramolecular Technology, D. N. Reinhoudt, Ed. (Wiley, New York, 1999).

6) Jakubith S, Rotermund H, Engel W, Oertzen AV, Ertl G, Phys. Rev. Lett. (1990), 65, 3013.

7) Hess B, Naturwissenschaften (2000), 87, 199.

8) Aizenberg J, Black AJ, Whitesides GM, Nature (1999), 398, 495.

9) Blaaderen AV, Ruel R, Wiltzius P, Nature (1997), 385, 321.

10) Burns MM, Fournier JM, Golovchenko JA, Science (1991), 252, 1049.

11) Bowden N, Choi I, Grzybowski BA, Whitesides GM, J. Am. Chem. Soc. (19990, 121, 5373.

12) Grzybowski BA, Bowden N, Arias F, Yang H, Whitesides GM, J. Phys. Chem. B (2001), 105, 404.

13) Iijima S, Nature (1991), 354, 56.

14) Ajayan PM, Ebbeson TW, Rep. Prog. Phys. (1997), 60, 1025.

15) Chopra NG, Luyken RJ, Cherrey K, Crespi VH, Cohen MI, Louie SG, Zettl A, Science (1995), 269, 966.

16) Meier WM, Olson DH, Atlas of Zeolite Structure Types, Butterworths, London, 1988.

17) Dessau RM, Schlenker JL, Higgins JB, Zeolites (1990), 10, 522.

18) Whitesides GM, Grzybowski B, Science (2002), 295, 2418.

19) Harper JD, Lansbury PT, Annu.Rev.Biochem. (1997), 66, 385.

20) Sipe JD, Cohen AS, J.Struct.Biol. (2000), 130,88.

21) Gazit E, Drugs Future (2004), 29, 1.

22) Whitesides GM, Boncheva M, Proc Natl Acad Sci USA (2002), 99, 4769.

23) Ghadiri MR, Tirrell DA, Curr Opin Chem Biol (2000), 4, 661.

24) Zhang S: Molecular self-assembly. In Encyclopedia of Materials: Science & Technology. Oxford, UK: Elsevier Science (2001), 5822.

25) Petka WA, Harden JL, McGrath KP, Wirtz D, Tirrell DA, Science (1998), 281, 389.

26) Nowak AP, Breedveld V, Pakstis L, Ozbas B, Pine DJ, Pochan D, Deming TJ, Nature (2002), 417, 424.

27) Gao X, Matsui H, Adv. Mater. (2005), 17, 2037.

28) Zhang S, Marini DM, Hwang W, Santoso S, Curr. Opin. Chem. Biol. (2002), 6, 865.

29) Hartgerink JD, Clark TD, Ghadiri MR, Chem. Eur. J. (1998), 4(8), 1367.

30) Aggeli A, Nyrkova IA, Bell M, Harding R, Carrick L, McLeish TCB, Semenov AN, Boden N, Proc Natl Acad Sci USA (2001), 98:11857-11862.

31) Marini DM, Hwang W, Lauffenburger DA, Zhang S, Kamm RD. Nano Letters (2002), 2, 295.

32) Marsh EN, DeGrado WF, Proc Natl Acad Sci USA (2002), 99, 5150.

33) Moffet DA, Case MA, House JC, Vogel K, Williams RD, Spiro TG, McLendon GL, Hecht MH, J Am Chem Soc (2001), 123, 2109.

34) Whaley SR, English DS, Hu EL, Barbara PF, Belcher AM, Nature (2000), 405, 665.

35) Lee SW, Mao C, Flynn CE, Belcher AM, Science (2002), 296, 892.

36) Holmes TC, Delacalle S, Su X, Rich A, Zhang S, Proc Natl Acad Sci USA (2000), 97, 6728.

37) Vauthey S, Santoso S, Gong H, Watson N, Zhang S, Proc Natl Acad Sci USA (2002), 99, 5355.

38) Santoso S, Hwang W, Hartman H, Zhang S. Nano Letters (2002), 2, 687.

39) Caplan MR, Moore PN, Zhang S, Kamm RD, Lauffenburger DA, Biomacromolecules (2000), 1, 627.

40)   Hartgerink JD, Beniash E, Stupp SI .Science 2001, 294:1684-1687.

41)   Hartgerink JD, Beniash E, Stupp SI. Proc Natl Acad Sci USA 2002, 99:5133-5138

42)   Kisiday J, Jin M, Kurz B, Hung H, Semino C, Zhang S, Grodzinsky AJ. Proc Natl
       Acad Sci USA 2002, 99:9996-10001.

43)   Ryadnov, MG, Woolfson, DN, Nat. Mater. (2003), 2, 329-331.

44)   Matsui, H, Gologan, B, J.Phys.Chem. B (2000), 104, 3383-3386

45)   Shimizu, T, Kogiso, M, Masuda, M, J. Am. Chem.Soc., (1997), 119, 6209-6211

46)   Douberly GJ, Pan S, Walters D, Matsui H, J.Am.Chem.Soc., (2001), 105,

47)   Banerjee, IA, Yu, L, Matsui, H, J.Am.Chem.Soc. (2003), 125, 9542

48)   Djalali, R, Chen, Y-F, Matsui, H, J.Am.Chem.Soc. (2002), 124, 13660

49)   Matsui, H, MacCuspie, RI, Nano lett. (2001), 1, 671.

50)   Nuraje, N, Banerjee, IA, MacCuspie, RI, Yu, L, Matsui, H, J.Am.Chem.Soc.
       (2004), 126, 8088

51)   Yu, L, Banerjee, IA, Matsui, H, J.Am.Chem.Soc. (2003), 125, 14837.

52)   Djalali, R, Chen, Y-F, Matsui, H, J.Am.Chem.Soc. (2003), 125, 5873.

53)   Banerjee, IA, Yu, L, Matsui, H, Proc. Natl. Acad. Sci. (2003), 100, 14678.

54)   Yu, L, Banerjee, IA, Shima, M, Rajan, K, Matsui, H, Adv. Mater. (2004), 16, 709.

55)   Hwang W, Marini DM, Kamm RD, Zhang S. J. Phys. Chem. B (2002), 106.

56)   Nyrkova IA, Semenov AN, Aggeli A, Boden N, Eur. Phys. J. B (2000), 17, 481.

57)   Nyrkova IA, Semenov AN, Aggeli A, Bell M, Boden N, McLeish TCB, Eur. Phys. J.
       B (2000), 17, 499.

58)   Selinger JV, Spector MS, Schnur JM, J. Phys. Chem. B (2001), 105, 7157.

59)   Wang WX, Hecht MH, Proc. Natl. Acad. Sci. USA, (2002), 99, 2760.

60)   Ryadnov MG, Woolfson DN, Angew.Chem.Int.Ed. (2003), 42, 3021.

61)   Tsurkan MV, Ogawa MY, Chem. Commun. (2004), 2.

62)   C. H. Hassall, in Proceedings of the Third American Peptide Symposium (Ed.: J.
       Meinhoffer), Ann Arbor Science, Ann Arbor, MI (1972), 153.

63)   Karle IL, Handa BK, Hassall CH , Acta. Crystallogr. 1975, B31, 555.

64)   Ghadiri MR, Granja JR, Milligan RA, McRee DE, Khazanovich N, Nature (1993),
       366, 324.

65)   Seebach D,Matthews JL, Meden A, Wessels T, Baerlocher C, McCusker LB,
       Helv. Chim. Acta (1997), 80, 173.

66)   Clark TD, Buehler LK, Ghadiri MR, J. Am. Chem. Soc. (1998), 120, 651.

67)   Clark TD, Ghadiri MR, J. Am. Chem. Soc. (1995), 117, 12364.

68)   Clark TD, Buriak JM, Kobayashi K, Isler MP, McRee DR, Ghadiri MR, J. Am.
       Chem. Soc. (1998), 120.

69)   Ghadiri MR, Granja JR, Buehler LK, Nature (1994), 369, 301.

70)   Granja JR, Ghadiri MR, J. Am. Chem. Soc. (1994), 116, 10785.

71)   Hartgerink JD, Ghadiri MR, Chem. Eur. J. (1998), 4, 8, 1367.

72)   Percec V, Dulcey AE, Balagurusamy VSK, Miyura Y, Smidrkal J, Peterca M,
       Nummelin S, Edlund U, Hudson SD, Heiney PA, Hu DA, Magnov SN, Vinogradov
       SA, Nature (2004), 430,764.

73)   Zhou M, Bentley D, Ghosh J, J.Am.Chem.Soc. (2004),126,734.

74)   Gazit E, Angew. Chem. Int. Ed. Engl.(2002), 41, 257.

75)   Gazit E, FASEB J. (2002), 16, 77.

76)   Reches M, Gazit E. Science (2003), 300, 625.

77)   Gazit E, Unfolding, and Misfolding. In: Encyclopedia of Polymer Science and
       Technology. (2003), John Wiley & Sons Ltd.

78)   Reches M, Gazit E. Nano Lett. (2004), 4, 581.

79)   Gilead S, Gazit E, Supramol. Chem. (2005), 17, 87.

80)   Gazit E, Peptides for Nanotechnological Applications. In: Shoseyov, O., and
       Levy, I. (eds.) NanoBioTechnology: BioInspired Device and Materials of the
       Future. Humana Press, Totowa NJ, USA. (pp. 385-395).

81)   Yemini M, Reches M, Rishpon J, Gazit E, Nano Lett. (2005), 5, 183.

82)   Carny O, Gazit E, FASEB J. (2005), 19, 1051.

83)   Reches M, Gazit E, Israel J. Chem. (2005), 45, 363.

84)   Yemini M, Reches M, Gazit E, Rishpon J, Anal. Chem. (2005), 77, 5155.

85) Kol N, Abramovich L, Barlam D, Shneck RZ, Gazit E, Rousso I, Nano Lett. (2005), 5, 1343.

86) Gazit E, FEBS J. (2005), 272, 5971.

87) Adler-Abramovich L, Reches M, Sedman VL, Allen S, Tendler SJB, Gazit E, Langmuir (2006), 22,1313.

88) Reches M, Gazit E, Phys. Biol. (2006), 3, S10.

89) Mahler A, Reches M, Rechter M, Cohen S, Gazit E, Adv. Mater. (2006), 18, 1365.

90) Gazit E, Nanomedicine (2006), 1, 135.

91) Sedman VL, Adler-Abramovich L, Allen S, Gazit E, Tendler SJB, J. Am. Chem. Soc.(2006), 128, 6903.

92) Carny O, Shalev D, Gazit E, Nano Lett. (2006), 6, 1594.

93) Reches M, Gazit E, Nature Nanotech. (2006), 1, 195.

94) Reches M. and Gazit E. Peptide Nanomaterials: Self-Assembling Peptides as Building Blocks for Novel Materials. In: Nanomaterials Chemistry: Novel aspects and New Directions edited by Rao, C.N.R., Mueller, A., and Cheetham, A.K. Wiley-VCH, Weinheim Germany (pp 171-183).

95) Gazit E, FEBS J. (2007), 274, 317.

96) Ghosh S, Reches M, Gazit E, Verma S, Angew. Chem. Int. Ed. Engl. (2007), 46, 2002.

97) Reches M, Gazit E, J. Nanosci. Nanotechnol. (2007), 7, 2239.

98) Colmbo G, Soto P, Gazit E, Trends Biotechnol. (2007), 25, 211.

99) Gazit E, Prion (2007), 1, 32.

100) Gazit E, Chem. Soc. Rev. (2007), 36, 1263.

101) Adler-Abramovich L, Perry R, Sagi A, Gazit E, Shabat D, ChemBioChem (2007), 8, 859.

102) Hendler N, Sidelman N, Reches M, Gazit E, Rosenberg Y, Richter S, Adv. Mater. (2007), 11, 1485.

103)   Hill RJA, Sedman VL, Allen S, Williams P, Paoli M, Adler-Abramovich L, Gazit E, Eaves L, Tendler SJB, Adv. Mater. (2007), 19, 4474.

104)   Sopher NB, Abrams ZR, Reches M, Gazit E, Hanein Y, J. Micromech. Microeng. (2007), 11, 2360.

105)   Cherny I, Gazit E, Angew. Chem. Int. Ed. Engl. (2008), 47, 4062.

106)   Adler-Abramovich L, Gazit E, J. Pep. Sci. (2008), 14, 217.

107)   Görbitz CH, Hartviksen LM, Acta Crystallogr C. (2008), 64(3), 171.

108)   Görbitz CH, Rise F, J Pept Sci. (2008), 14(2), 210.

109)   Görbitz CH, Chemistry. (2007). 13(4), 1022.

110)   Görbitz CH, Acta Crystallogr C. (2006), 62(6), 328.

111)   Görbitz CH, Chem Commun. (2006), 14(22), 2332.

112)   Görbitz CH, Bruvoll M, Dizdarevic S, Fimland N, Hafizovic J, Kalfjøs HT, Krivokapic A, Vestli K, Acta Crystallogr C. (2006), 62(1), 22.

113)   Görbitz CH, Nilsen M, Szeto K, Tangen LW, Chem Commun. (2005), 14(34), 4288.

114)   Johansen A, Midtkandal R, Roggen H, Görbitz CH, Acta Crystallogr C. (2005), 61(4), 198.

115)   Görbitz CH, Acta Crystallogr C. (2004), 60(11), 810.

116)   Helle IH, Løkken CV, Görbitz CH, Dalhus B. Acta Crystallogr C. (2004), 60(10), 771.

117)   Görbitz CH, Acta Crystallogr B. (2004), 60(5), 569.

118)   Moen A, Frøseth M, Görbitz CH, Dalhus B, Acta Crystallogr C. (2004), 60(8), 564.

119)   Görbitz CH, Acta Crystallogr C. (2004), 60(5), 371.

120)   Görbitz CH, Acta Crystallogr C. (2003), 59(12), 730.

121)   Görbitz CH, Acta Crystallogr C. (2003), 59(10), 589.

122)   Görbitz CH, Acta Crystallogr B. (2002), 58(5), 849.

123)   Görbitz CH, Acta Crystallogr C. (2002), 58(8), 533.

124)   Görbitz CH, Acta Crystallogr B. (2002), 58(3), 512.

125) Görbitz CH, Chemistry. (2001), 3, 7(23), 5153.

126) Görbitz CH. Acta Crystallogr C. (2001), 57(5), 575.

127) Görbitz CH, Acta Crystallogr C. (2000), 56(12), 1496.

128) Görbitz CH, Torgersen E, Acta Crystallogr B. (1999), 1, 55(1), 104.

129) Gorbitz CH, Hersleth HP, Acta Crystallogr B. (2000), 56(3), 526.

130) Görbitz CH, Acta Crystallogr C. (2000), 56(4), 500.

131) Dalhus B, Görbitz CH. Acta Crystallogr C. (1996), 15, 52(8), 2087.

132) Görbitz CH, Gunderson E, Acta Crystallogr (1996), 52, 1764.

133) Görbitz CH, Etter MC. Acta Crystallogr C. (1993), 15, 49(9), 673.

134) Görbitz CH, Etter MC. Acta Crystallogr C. (1992), 15, 48(7), 1317.

135) Görbitz CH, Etter MC, Int J Pept Protein Res. (1992), 39(2), 93.

136) Jain RM, Chauhan VS, Peptide Science (1996), 40, 105.

137) Singh TP, Kaur P, Prog. Biophys. Molec. Biol. (1996), 66, 141.

138) Karle IL, Balaram P, Biochemistry (1990), 29, 6747.

139) Balaram P, J. Peptide Res. (1999), 54, 195.

140) Karle IL, Awasthi SK, Balaram P, Proc. Natl. Acad. Sci. USA (1996), 93, 8189.

141) Benedetti E, Biopolymers (1996), 40, 3.

142) Toniolo C, Crisma M, Formaggio F, Peggion C, Biopolymers (2001), 60, 396.

143) Gross E, Morell JL, Craig GT, Proc. Natl. Acad. Sci. USA. (1969), 62, 952.

144) Gross E, Morell JL, FEBS Lett. (1968), 2, 61.

145) Aydin M, Lucht N, Koenig W A, Lupp R, Jung G, Winkelmann G, Liebigs Ann. Chem. (1985), 2285.

146) Allagier H, Jung G, Werner RG, Schneider U and Zahner H, Eur. J. Biochem. (1986), 160, 9.

147) Noda K, Shimohigashi Y, Izumiya N, a, b -dehydroamino acids and peptides. In The Peptides 5Eds., Gross E, Meienhofer J, Academic Press, (1983), New York, pp. 285.

148) Jung G, Angew. Chem. Int. Ed. Engl. (1991), 30, 1051.

149) Breukink E, Viedemann I, Karaaij CV, Kuipers OP, Shal HG, de Kruijff B, Science (1999), 286, 2361.

150) Komatsubara S, Kisumi M, Chibata I, Gregario MMV, Miller VS, Crout0 DHG, J. Chem. Soc. Chem. Commun. (1977), 839.

151) Stammer CH, In Chemistry and Biochemistry of amino acid, peptides and proteins , Weinstein, B., Ed., Marcel Dekker, (1982), New York, pp.33-74.

152) Tsutsui M, Ichikawa M, Vohwinkel F, Susuki K, J. Am. Chem. Soc. (1966), 88, 852.

153) Dossena A, Marchelli R, Pochini J, J. Chem. Soc. Chem. Commun. (1974), 771.

154) Meyer WL, Templeton GE, Grable CI, Siegel CW, Jones R, Woodhead SH, Sauer C, Tetrahedron Lett. (1971), 12, 2357.

155) Langer M, Pauling A, Retey J, Angew. Chem. Int. Ed. Engl. (1995), 34, 1464.

156) English ML, Stammer CH, Biochem. Biophys. Res. Comm. (1978), 83, 1464.

157) Shimohigashi Y, Costa T, Stammer CH, FEBS Letts. (1981), 133, 269.

158) Shimohigashi Y, Dunning JW, Kolar Jr. AJ, Stammer CH, Int. J. Peptide Protein Res. (1983), 21, 202..

159) Shimohigashi Y, English ML, Stammer CH, Costa T, Biochem. Biophys. Res. Comm. (1982), 104, 583.

160) Shimohigashi Y, Kodama H, Imazu S, Horimoto H, Sakaguchi K, Waki M, Uchida H, Kondo M, Kato T, Izumiya N, FEBS Letts. (197), 222, 251.

161) Shimohigashi Y, Stammer CH, Costa T, Vonvoigtlander PF, Int. J. Peptide Protein Res. (1983), 22, 489.

162) Salvadori S, Marastoni M, Balboni G, Marzola G, Tomatis R, Int. J. Peptide Protein Res. (1986), 28, 254.

163) Salvadori S, Marastoni M, Balboni G, Marzola G, Tomatis R, Int. J. Peptide Protein Res. (1986), 28, 262.

164) Nitz TJ, Shimohigashi Y, Costa T, Chen H, Stammer CH, Int. J. Peptide Protein Res. (1986), 27, 522.

165) Hallinan EA, Mazur RH, In peptides: Structure and biological function. Gross E. & Meienhofer Eds. Pierce Chemical Xo, Rochford, (1997), Illinois.

166) Wong TW, Goldberg AR, J. Biol. Chem. (1984), 259, 3127.

167) Fisher GH, Berryer P, Ryan JW, Chauhan VS, Stammer CH, Arch. Biochem. Biophys. (1981), 211, 269.

168) Salvadori S, Marastoni M, Balboni G, Marzola G, Tomatis R, Int. J. Peptide Protein Res. (1986), 28, 254.

169) Salvadori S, Marastoni M, Balboni G, Marzola G, Tomatis R, Int. J. Peptide Protein Res. (1986), 28, 262.

170) Pieroni O, Fissi A, Salvadori S, Balboni G, Tomatis R, Int. J. Peptide protein Res. (1986), 28, 91.

171) Morelli MAC, Saviano G, Temussi PA, Balboni G, Salvadori S, Tomatis R, Bioploymers (1989), 28, 129.

172) Brady SF, Cochran DW, Nutt RF, Holly FW, Benett CD, Palevada WJ, Curley PE, Arison BH, Saperstein R, Veber DF, Int. J. Peptide Protein Res. (1984), 23, 212.

173) Kaur P, Patnaik GK, Raghubir R, Chauhan VS, Bull. Chem. Soc. Jpn. (1992), 65, 3412.

174) Benedetti E, Peptides, Proceedings of the fifth American Peptide Symposium. Eds. M. Goodman and J. Meienhofer, pp. 257. John Wiley (1997), New York.

175) Singh TP, Narula P, Patel HC, Acta Cryst. B46, (1990), 539.

176) Thormann M, Hofmann HG, Journal of Molecular structure (Theochem) (1998), 431, 79.

177) Broda MA, Rzeszotarska B, Smelka L, Pietrzynski GJ. Peptide Res. (1998), 52, 72.

178) Alagona G, Ghio C, Pratesi C, J. Comp. Chem. (1991), 12, 934.

179) Ajo D, Casarin M, Granozzi G, J. Mol. Struc. (1982), 86, 297.

180) Ajo D, Granozzi G, Tondello E, Del Pra A and Zanotti, G, J. Chem. Soc. Perkin II (1979), 927.

181) Rzeszotarska B, Siodlak D, Broda MA, Dybala I, Koziol AE, J. Pep. Res. (2002), 59, 79.

182) Aleman C, Biopolymers, (1994), 34, 841.

183) Aleman C, Perez JJ, Biopolymers (1993), 33, 1811.

184) Glowka ML, Acta Cryst. C44 (1988), 1639.

185) Glowka ML, Gilli G, Bertolasi V, Makowski M, Acta Cryst. C43 (1987), 1403.

186) Singh TP, Haridas M, Chauhan VS, Kumar A, Viterbo D, Biopolymers (1987), 26, 819.

187) Singh TP, Narula P, Chauhan VS, Kaur P, Biopolymers (1989), 28, 1287.

188) Aubry A, Pietrzynski G, Rzeszotarska B, Boussard G, Marraud M, Int. J. Peptide Protein Res. (1991), 37, 39.

189) Busetti V, Crisma M, Toniolo C, Salvadori S, Balboni G, Int. J. Biol. Macromol. (1992), 14, 23.

190) Bussetti V, Ajo D, Casarin M, Acta Cryst. C40 (1984), 1245.

191) Aubry A, Allier F, Boussard G, Marraud M, Biopolymers (1985), 24, 639.

192) Narula P, Khandelwal B, Singh TP, Biopolymers (1991), 31, 987.

193) Dey S, Mitra SN, Singh TP, Int. J. Peptide Protein Res. (1996), 48, 123.

194) Vijayaraghavan R, Kumar P, Dey S, Singh TP, J. Peptide Res. (1998), 52, 89.

195) Chauhan VS, Bhandary KK, Int. J. Peptide Protein Research (1992), 39, 223.

196) Rajashankar KR, Ramakumar S, Mal TK, Chauhan VS, Biopolymers (1995), 35, 141.

197) Soman KV, Karimi A, Case DA, Biopolymers (1991), 31, 1351.

198) Karle IL, Acta. Cryst. B48 (1992), 341.

199) Ciajolo MR, Tuzi A, Pratesi CR, Fissi A, Pieroni O, Biopolymers (1990), 30, 911.

200) Ciajolo MR, Tuzi A, Pratesi CR, Fissi A, Pieroni O, Int. J. Peptide Protein Res. (1991), 38, 539.

201) Ciajolo MR, Tuzi A, Pratesi CR, Fissi A, Pieroni O, Biopolymers (1992), 32, 717.

202) Bhandary KK, Chauhan VS, Biopolymers (1993), 33, 209.

203) Padyana AK, Ramakumar S, Mathur P, Jagannathan NR, Chauhan VS, Journal of Peptide Science, (2003), 9, 54.

204) Ramagopal UA, Ramakumar S, Sahal D, Chauhan VS, Proc. Natl. Acad. Sci. USA (2001), 98, 870..

205) Rajashankar KR, Ramakumar S, Chauhan VS, J. Am. Chem. Soc. (1992), 114, 9225.

206) Pieroni O, Montagnoli G, Fissi A, Merlino S, Ciardelli F, J. Am. Chem. Soc. (1975), 97, 6820.

207) Pieroni, O, Fissi A, Merlino S., Ciardelli F, Isr. J. Chem. (1977), 15: 22.

208) Tuzi A, Ciajolo MR, Guarino G, Temussi PA, Fissi A, Pieroni O, Biopolymers (1993), 33, 1111.

209) Mitra SN, Dey S, Karthikeyan S, Singh TP, Biopolymers (1997), 41, 97.

210) Rajashankar KR, Ramakumar S, Jain RM, Chauhan VS, Biopolymers (1997), 42, 373.

211) Jain RM, Rajashankar KR, Ramakumar S, Chauhan VS, J. Am. Chem. Soc. (1997), 119, 3205.

212) Ramagopal UA, Ramakumar S, Joshi RM, Chauhan VS, J. Peptide Res. (1998), 52, 208.

213) Ramagopal UA, Ramakumar S, Mathur P, Joshi RM, Chauhan VS, Protein Engineering (2002), 15, 331.

214) Rajashankar KR, Ramakumar S, Mal TK, Chauhan VS, Angew Chem Int. Ed. Engl. (1994), 33, 970.

215) Rajashankar KR, Ramakumar S, Jain RM, Chauhan VS, J. Biomol. Struct. Dynamics. (1996), 13, 641.

216) Rajashankar KR, Ramakumar S, Jain RM, Chauhan VS, J. Am. Chem. Soc. (1995), 117, 11773.

217) Rajashankar KR, Ramakumar S, Protein Science (1996), 5, 932.

218) Lisowski M, Pietrzynski G, Rzeszotarsks B, Int. J. Peptide Protein Res. (1993), 42, 466.

219) Pieroni O, Fissi A, Pratesi C, Temussi PA, Ciardelli F, Biopolymers (1993), 33, 1.

220) Inai Y, Ito T, Hirabayashi T, Yokoto K, Biopolymers (1993), 33, 1173.

221) Barlow DJ, Thornton JM, J. Mol. Biol. (1988), 201, 601.

222) Pieroni O, Fissi A, Pratesi C, Temussi PA, Ciardelli F, J. Am. Chem. Soc. (1991), 113, 6338.

223) Piazessi Am, Bardi R, Crisma M, Bonora GM, Toniolo C, Chauhan VS, Kaur P, Uma K, Balaram P, Gazetta Chimica Italiana (1991), 121, 1.

224) Chauhan VS, Uma K, Kaur P, Balaram P, Biopolymers (1989), 28, 763.

225) Uma K, Balaram P, Kaur P, Sharma AK, Chauhan VS, Int. J. Biol. Macromol. (1989), 11, 169.

226) Kaur P, Uma K, Balaram P, Chauhan VS, Int. J. Peptide Protein Res. (1989), 33, 103.

227) Wuthrich K, NMR of proteins and nucleic acids, John Wiley & Sons (1986).

228) Bach II AC, Gierasch LM, J. Am. Chem. Soc. (1985), 107, 3349.

229) Bach II AC, Gierasch LM, Biopolymers (1986), 25, S175.

230) Bharadwaj A, Jaiswal A, Chauhan VS, Tetrahedron (1992), 48, 2691.

231) Gupta A, Bharadwaj A, Chauhan VS, J. Chem. Soc. Perkin Trans. (1990), 2, 1911.

232) Vijayaraghavan R, Kumar P, Dey S, Singh TP, J. Peptide Res. (1998), 52, 89.

233) Supramolecular Chemistry: Concepts and Perspectives (Ed: J. M. Lehn) Wiley-VCH (1995), Weinheim, Germany.

234) Self-organizing Systems (Ed: F. E. Yates) Plenum (1987), New York.

235) Iijima S, Nature (1991), 354, 56.

236) Ajayan PM, Ebbeson TW, Rep. Prog. Phys. (1997), 60, 1025.

237) Chopra NG, Luyken RJ, Cherrey K, Crespi VH, Cohen ML, Louie SG, Zettl A, Science (1995), 269, 966.

238) Meier WM, Olson DH, Atlas of Zeolite Structure Types, Butterworths (1988), London.

239) Dessau RM, Schlenker JL, Higgins JB, Zeolites (1990), 10, 522.

240) Harada A, Li J, Kamachi M, Nature (1993), 364, 516.

241) Ghadiri MR, Granja JR, Buehler LK, Nature (1994), 369, 301.

242) Granja JR, Ghadiri MR, J. Am. Chem. Soc. (1994), 116, 10785.

243) Engels M, Bashford D, Ghadiri MR, J. Am. Chem. Soc. (1995), 117, 9151.

244) Kim HS, Hartgerink JD, Ghadiri MR, J. Am. Chem. Soc. (1998), 120, 4417.

245) Akazome M, Ueno Y, Ooiso H, Ogura K, J. Org. Chem. (2000), 65, 68.

246) Akazome M, Senda K, Ogura K, J. Org. Chem. (2002), 67, 8885.

247) Akazome M, Yanagita Y, Sonobe R, Ogura K, Bull. Chem. Soc. Jpn. (1997), 70, 2823.

248) Akazome M, Takahashi T, Sonobe R, Ogura K, Tetrahedron. (2002), 58, 8857.

249) Tinker DA, Krebs EA, Feltham IC, Attah-Poku SK, Ananthanarayanan VS, J. Biol. Chem. (1988), 263, 5024.

250) Surewicz WK, Mantsch HH, Biochem. Biophys. Acta (1988), 952, 115.

251) Surewicz WK, Mantsch HH, Chapman D, Biochemistry (1993), 32, 389.

252) Krimm S, Bandekar J, Adv. Protein Chem. (1986), 38, 181.

253) Byler DM, Susi H, Biopolymers (1986), 25, 469.

254) Goormaghtight E, Cabiaux V, Ruysachaert JM, Subcellular Biochem. (1994), 23, 363.

255) Hvidt A, Nielson SO, Adv.Protein Chem. (1966), 21, 287.

256) Hennessey JP, Johnson WC, Biochemistry (1981), 20, 1085.

257) Kukula H, Schlaad H, Antonietti M, Forster S, J.Am.Chem.Soc. (2002), 124, 1658.

258) Reches M, Gazit E, Nano Lett. (2004), 4, 581.

259) Santoso S, Hwang W, Hartman H, Zhang S, Nano Lett. (2002), 2, 687.

260) Medical Applications of Liposomes , Lasic DD, Papahadjopoulos D, Ed. Elsevier Science (1998), Amsterdam.

261) Antonietti M, Förster S, Adv. Mater. (2003), 15, 1323.

262) Chen X, Ding X, Zheng Z, Peng Y, Macromol.Rapid Commun. (2004), 25, 1575.

263) Merden T, Kopecek J, Kissel T, Adv. Drug Deliv. Rev. (2002), 54, 715.

264)   Förster S, Schmidt M, Adv. Polym.Sci. (1995), 120, 51.

265)   Hermsdorf N, Ph.D. Thesis, University of Potsdam, Germany, 1999.

266)   Förster S, Abetz V, Muller HE, Advances in Polymer Science, Springer, Berlin, (2004), 173.

267)   Jenekhe SA, Chen XL, Science (1999), 283, 372.

268)   Jenekhe SA, Chen XL, Science (1998), 279, 1903.

269)   Holder SJ, Hiorns RC, Sommerdijk N, Williams SJ, Jones RG, Nolte RJM, Chem. Commun. (1998), 1445.

270)   Noda, I.; Ozaki, Y. Two-Dimensional Correlation Spectroscopy: Application in Vibrational and Optical Spectroscopy; John Wiley & Sons: 2004; pp 119.

271)   Dewar MJS, Zoebisch EG, Healy EF, Stewart JJP, J. Am. Chem. Soc. (1985), 107, 3902.

272)   Klamt A, Schüümann G, J. Chem. Soc. Perkin Transactions 2 (1993), 799.

273)   Kurth DG, Fromm KM, Lehn JM, Eur. J. of Inorg. Chem. (2001), 6, 1523.

274)   Lee SK, Yun DS, Belcher AM, Biomacromolecules (2006), 7(1), 14.

275)   Lu Y, Yang J, Sega E, The AAPS Journal (2006), 8, E466.

276)   Lalitha PV, Malhotra P, Chattopadhyay R, Chauhan VS, Exp. Parasitology (1999), 92, 12.

277)   Das P, Grewal JS, Chauhan VS, Parasitol Res. (2006), 100, 39.

278)   Dalhaimer P, Bates FS, Discher DE, Macromolecules (2003), 36, 6873.

279)   Donaldson K, Stone V, Tran CL, Kreyling W, Borm PJJ, Nanosci. Nanotech. (2004), 7, 3048.

280)   Gordon JC, Myers JB, Folta T, Shoja V, Heath LS, Onufriev A; Nucleic Acids Res. (2005), 33, W368.

281)   Anandakrishnan R, Onufriev A, J. Comp. Biol. (2004) 15, 165.

282)   Bashford D, Karplus M, Biochemistry, (1990), 29, 10219.

283)   Gsponer J, Haberthür U, Caflisch A, PNAS (2003), 100(9), 5154.

284)   Ferrara P, Caflisch A, PNAS (2000), 97(20), 10780.

285) Kammerer RA, Kostrewa D, Zurdo J, Detken A, García-Echeverría C, Green JD, Müller SA, Meier BH, Winkler FK, Dobson CM, Steinmetz MO, PNAS (2004), 101(13), 4435.

286) Selkoe DJ, Annu. Rev. Cell Biol. (1994), 10, 373.

287) Selkoe DJ, Trends Neurosci. (1993), 16, 403.

288) Haass C, Hung AY, Citron M, Teplow DB, Selkoe DJ Arzneim. Forsch. (1995), 45, 398.

289) Higaki J, Quon D, Zhong ZY, Cordell B, Neuron (1995), 14, 651.

290) Seubert P, Vigo-Pelfrey C, Esch F, Lee M, Dovey H, Davis D, Sinha S, Schlossmacher MG, Whaley J, Swindlehurst C, McCormack R, Wolfert R, Selkoe DJ, Lieberburg I, Schenk D, Nature (1992), 359, 325.

291) Shoji M, Golde TE, Ghiso J, Cheung TT, Estus S, Shaffer LM, Cai X, McKay DM, Tintner R, Frangione B, Younkin SG, Science (1992), 258, 126.

292) Haass C, Schlossmacher MG, Hung AY, Vigo-Pelfrey C, Mellon A, Ostaszewski BL, Lieberburg I, Koo EH, Schenk D, Teplow DB, Selkoe DJ Nature (1992), 359, 322.

293) Busciglio J, Gabuzda DH, Matsudaira P, Yankner BA, Proc. Natl. Acad. Sci. USA (1993), 90, 2092.

294) Narang HK, J. Neuropathol. Exp. Neurol.(1980), 39, 621.

295) Merz PA, Wisniewski HM, Somerville RA, Bobin SA, Masters CL, Iqbal K, Acta Neuropathol. (1983), 60, 113.

296) Kirschner DA, Abraham C, Selkoe DJ, Proc. Natl. Acad. Sci. USA (1986), 83, 503.

297) Kirschner DA, Inouye Y, Duffy LK, Sinclair A, Lind M, Selkoe DJ, Proc. Natl. Acad. Sci. USA (1987), 84, 6953.

298) Hiramatsu H, Kitagawa T, Biochim Biophys Acta. (2005), 1753(1), 100.

299) Nilsson MR, Methods (2004), 34(1), 151.

300) Sipe JD, Cohen AS, J Struct Biol. (2000), 130(2-3), 88.

301) Hilbich C, Kisters-Woike B, Reed J, Masters C, Beyreuther K, J. Mol. Biol. (1991), 218, 149.

302) Barrow CJ, Yasuda A, Kenny PTM, Zagorski M, J. Mol. Biol. (1992), 225, 1075.

303) Fraser PE, Nguyen JT, Inouye H, Surewicz WK, Selkoe DJ, Podlisny MB, Kirschner DA, Biochemistry (1992), 31, 10716.

304) Burdick D, Soreghan B, Kwon M, Kosmoski J, Knauer M, Henschen A, Yates J, Cotman C, Glabe C, J. Biol.Chem. (1992), 267, 546.

305) Hilbich C, Kisters-Woike B, Reed J, Masters CL, Beyreuther K, J. Mol. Biol. (1992), 228, 1.

306) Soto C, Kindy MS, Baumann M, Frangione B, Biochem. Biophys. Res. Commun. (1996), 226, 672.

307) Soto C, Sigurdsson EM, Morelli L, Kumar A, Castaño EM, Frangione B, Nat. Med. (1998), 4, 822.

308) Soto C, Kascsak RJ, Saborio GP, Aucouturier P, Wisniewski T, Prelli F, Kascsak R, Mendez E, Harris DA, Ironside J, Tagliavini F, Carp RI, Frangione B, Lancet (2000), 355, 192.

309) Azriel R, Gazit E, J. Biol. Chem. (2001), 276, 34156.

310) Shoval H, Lichtenberg D, Gazit E, Amyloid (2007), 14, 73.

311) Porat Y, Abramowitz A, Gazit E, Chem. Biol. Drug Des.(2006), 67, 27.

312) Pharmacological Mechanisms in Alzheimer's Therapeutics, Ed.A. Claudio Cuello, Springer (2008), New York.

313) Wang SSS, Chen YT, Chou SW, Biochimica et Biophysica Acta (BBA) - Molecular Basis of Disease (2005), 1741(3), 307.

314) Lomakin A, Chung DS, Benedek GB, Kirschner DA, Teplow DB, Proc. Natl. Acad. Sci. USA (1996), 93,1125.

315) Camus MS, Santos SD, Chandravarkar A, Mandal B, Schmid AW, Tuchscherer G, Mutter M, Lashuel HA, ChemBioChem (2008),9(13),2104.

316) Kammerer RA, Kostrewa D, Zurdo J, Detken A, Echeverría CG, Green JD, Meier BH, Winkler FK, Dobson CM, Steinmetz MO, PNAS (2004), 101(13), 4435.

317) Hortschansky P, Schroeckh V, Christopeit T, Zandomeneghi G, Fändrich M, Protein Science (2005), 14, 1753.

318) Kim JR, Murphy RM, Biophys J. (2004), 86(5), 3194.

319) Moss MA, Nichols MR, Reed DK, Hoh JH, Rosenberry TL, Mol Pharmacol. (2003), 64(5),1160.

320) Tjernberg LO, Naslund J, Lindqvist F, Johansson J, Karlstrom AR, Thyberg J, Terenius L, Nordstedt C, J. Biol. Chem. (1996), 271, 8545.

321) Zanuy D, Porat Y, Gazit E, Nussinov R, Structure (2004), 12, 439

322) Miravalle L, Tokuda T, Chiarle R, Giaccone G, Bugiani O, Tagliavini F, Frangione B, Ghiso J, J. Biol. Chem. (2000), 275, 27110.

323) Gupta M, Acharya R, Mishra A, Ramakumar S, Ahmed F, Chauhan VS, Chembiochem. (2008), 9(9), 1375.

324) Balbach J, Ishii Y, Antzutkin O, Leapman R, Rizzo N, Dyda F, Reed J, Tycko R, Biochemistry 2000, 39, 13748.

325) Ma BY, Nussinov R, PNAS (2002), 99, 14126.

326) Klimov DK, Thirumalai D, Structure (2003), 11, 295.

327) Favrin G, Irback A, Mohanty S, Biophys. J. (2004), 87, 3657.

328) Santini S, Mousseau N, Derreumaux P, J. Am. Chem. Soc. (2004), 126, 11509.

329) Wei GH,Mousseau N,Derreumaux P, Biophys. J. (2004), 87, 3648.

330) Santini S,Wei GH, Mousseau N, Derreumaux P, Structure (2004), 12, 1245.

331) Cecchini M, Rao F, Seeber M, Caflisch AJ, Chem. Phys. (2004), 121, 10748.

332) Morimoto A, Irie K, Murakami K, Masuda Y, Ohigashi H, Nagao M, Fukuda H, Shimizu T, Shirasawa T, J. Biol. Chem. (2004), 279, 52781.

333) Lashuel HA, Hartley DM, Balakhaneh D, Aggarwal A, Teichberg S, Callaway D, J Biol Chem (2002), 277, 42881.

334) Ono K, Hasegawa K, Naiki H, Yamada M, Biochim Biophys Acta (2004),1690, 193.

335) Yang F, Lim GP, Begum AN, Ubeda OJ, Simmons MR, Ambegaokar SS, Chen PP, Kayed R, Glabe CG, Frautschy SA, Cole GM, J Biol Chem (2005), 280, 5892.

336) Perutz MF, Finch JT, Berriman J, Lesk A, PNAS (2002), 99(8), 5591.

337) Bnhold H, Muenchen.Med.Wochenschr.(1922), 69, 1537

338) Divry P, J.Neurol.Psychiatr.(1927), 27, 643

339) Khurana R, Uversky VN, Nielsen L, Fink AL, J. Biol. Chem. (2001), 276(25), 22715.

340) Khurana R, Coleman C, Ionescu-Zanetti C, Carter SA, Krishna V, Grover RK, Roy R, Singh S, J Struct Biol. (2005), 151(3), 229.

341) Bourhim M, Kruzel M, Srikrishnan T, Nicotera T, J. Neurosci. Methods (2007), 160(2), 264.

342) Tauro S, Coutinho E, Srivastava S, Mag. Reson. Chem. (2002), 40(3), 211.

343) Baumketner A, Shea JE, J.Mol. Biol. (2006), 362 (3), 567.